Integrated Design of Electrical Machines for Wave Energy Converters

Lewis Chambers
B.Eng., M.Sc.

A thesis submitted for the degree of
Doctor of Philosophy

School of Engineering

Newcastle University
United Kingdom

November, 2024

Abstract

This is a thesis on co-design in wave energy, focused on exploring the importance of designing the wave energy converter in conjunction with the applied power take-off device, such that a connection between each field may come together in a mutual benefit to the resultant product. The need arises from a disconnect in industry that leads to the device and power take-off to be researched or developed independently, with the two connected later.

This thesis explores the problem space with a strong focus on directly driven generators as the power take-off technology selected. A case study is undertaken wherein a marinized IPS buoy topology is developed to include a fully integrated direct drive generator in a real wave resource location, with a methodology for the iterative design of a co-designed direct drive IPS Buoy developed to aid in this task.

The case study is conducted with both parts of the wave energy converter in mind and from a multiphysics perspective to include the wave resource, hydrodynamics, and hydrostatics of the IPS Buoy, and the electrical performance of the generator.

Novel topologies of direct drive generators are compared for application into the device with geometric constraints applied for their comparison, and two levels of generator integration into the converter are assessed.

This thesis attempts to showcase the challenges and benefits of co-design in wave energy converters, and it is hoped that being mindful of co-design may assist researchers and developers to fail faster, and narrow their focus toward the most promising technologies in the field so that wave energy can become commercially feasible sooner.

Acknowledgements

I would like to thank my supervisor Dr. Nick Baker who in the past four years has been my guide to academia, tirelessly giving advice and guidance. I am grateful to him for his commitment to mentorship and for pushing me to take on industrial projects and research papers. I consider myself lucky to have him as a supervisor and wish him luck in the future.

I am grateful to Mocean Energy who gave me to opportunity to get my first experience in an industrial research environment and to develop as a machine designer.

Many thanks to the CDT team who helped me navigate through daily university life; particularly Amanda Lane who was always available with a friendly face, ready to tackle any problem.

Special thanks to my wonderful wife Xinya, the one person who has always been by my side keeping me steady in tough times, giving academic advice, and patiently motivating me to keep going. She is the strongest person I know and this thesis truly would not be possible without her. I am eternally grateful to her for giving birth to our precious daughter Isabella, who came to us when we needed her most. I would also like to give thanks to my parents-in-law who helped us to survive those first few months of being new parents.

This work was supported by the Engineering and Physical Sciences Research Council (grant number EP/S024069/1). Simulation work was conducted within the Centre for Doctoral Training in Sustainable Electric Propulsion. The practical work was part funded by an InnovateUK smart award, reference 56808.

Nomenclature

Abbreviations

AC Alternating Current

ACF Airgap Closing Force

DC Direct Current

DD Direct Drive / Directly Driven

EFM Electro-Motive Force

FEA Finite Element Analysis

FRM Flux Reversal Machine

GHG Greenhouse Gases

HRS Hydraulics Research Station

IPS Interproject Service

LCOE Levelized Cost of Energy

MMF Magnetomotive Force

NdFeB Neodymium Iron Boron

NNRCMP National Network of Regional Coastal Monitoring Programmes

OWC Oscillating Water Column

PF Power Factor

PM Permanent Magnet

PTO Power Take Off

RMSE Root Mean Squared Error

TFM Transverse Flux Machine

UK United Kingdom

VHM Vernier Hybrid Machine

VRM Vernier Reluctance Machine

VRPM Variable Reluctance Permanent Magnet

WEC Wave Energy Converter

Symbols

$\ddot{y}$	Vertical acceleration
δ	Displacement
$\dot{y}$	Vertical velocity
λ	Wavelength
μ_0	Permeability of free space
ω	Angular frequency
ϕ	Phase angle
Ψ	Flux linkage
ρ	Density
σ	Shear stress
τ	Pitch width
τ	Torque
A	Area
B	Flux density
C	Damping coefficient
c_g	Wave group velocity
c_p	Wave phase velocity
C_w	Radiation damping coefficient
E	Energy
F	Force
f	Frequency
g	Gravitational constant
H_d	Water depth

H_s	Significant wave height
I	Current
J	Current density
K	Spring constant / electrical load
L	Length
L_s	Inductance
m	Mass
m_e	Effective mass
P	Power
p_c	Number of coil poles
p_m	Number of magnet poles
p_r	Number of rotor poles
R	Reluctance
r	Radius
T	Period
T_e	Energy period
V	Voltage
v	Volume
X	Inductance
y	Vertical displacement
Z	Impedance

Contents

List of Figures

List of Tables

Chapter 1. Introduction

1.1 Problem Statement and Motivation

In the current time, it is wholly uncontroversial to state that the climate is at an unprecedented state. Extreme weather events of all types are steadily becoming more commonplace and governments across the world are driving changes to reverse climate damage. Legislation such as the Climate Change Act [1] and the Paris Agreement [2] set the stage for meaningful changes to be adopted.

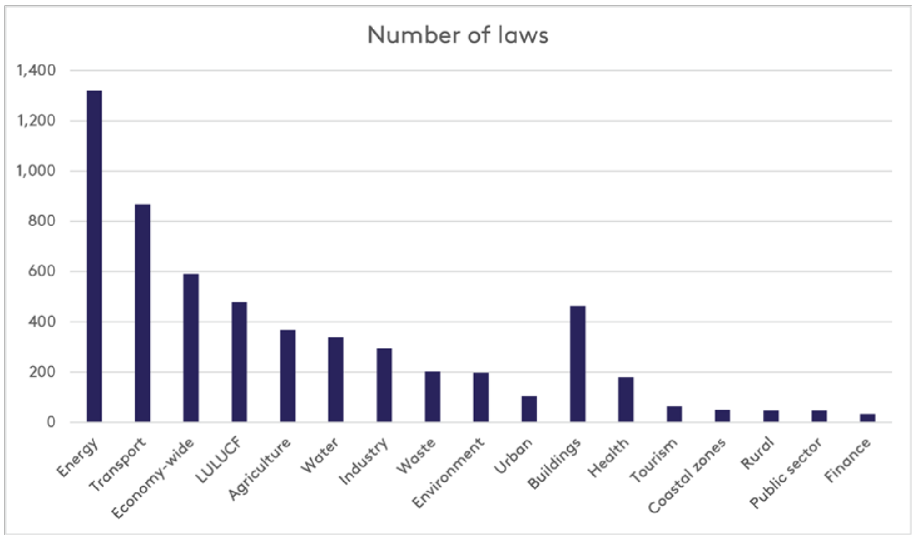

Figure 1.1: Worldwide climate change laws per sector [3].

There are currently thousands of climate change laws and legislature across the world as can be seen in figure 1.1. What stands out is that the most heavily regulated sectors are energy and transport. These two are the largest contributors of greenhouse gas (GHG) emissions worldwide, as can be seen in figure 1.2.

Because transportation and energy represent such a large share of GHG emissions, they represent an excellent target for reduction through renewable energy resources. Great efforts are being made towards electrification of the transport sector, although case studies [4] have shown that full electrification has a net positive effect on costs and emissions, the success is dependent on the availability of renewable energy sources. It is essential that local energy production can support the need of electric vehicles without impacting decarbonisation of energy.

Traditional sources of renewable energies have become well-established and commonplace. As can be seen in figure 1.3, wind energy accounts for a significant portion of the energy mix at 25%. However, except for nuclear, other low carbon resources have such a small share at 6% that they don't even warrant a section on the chart.

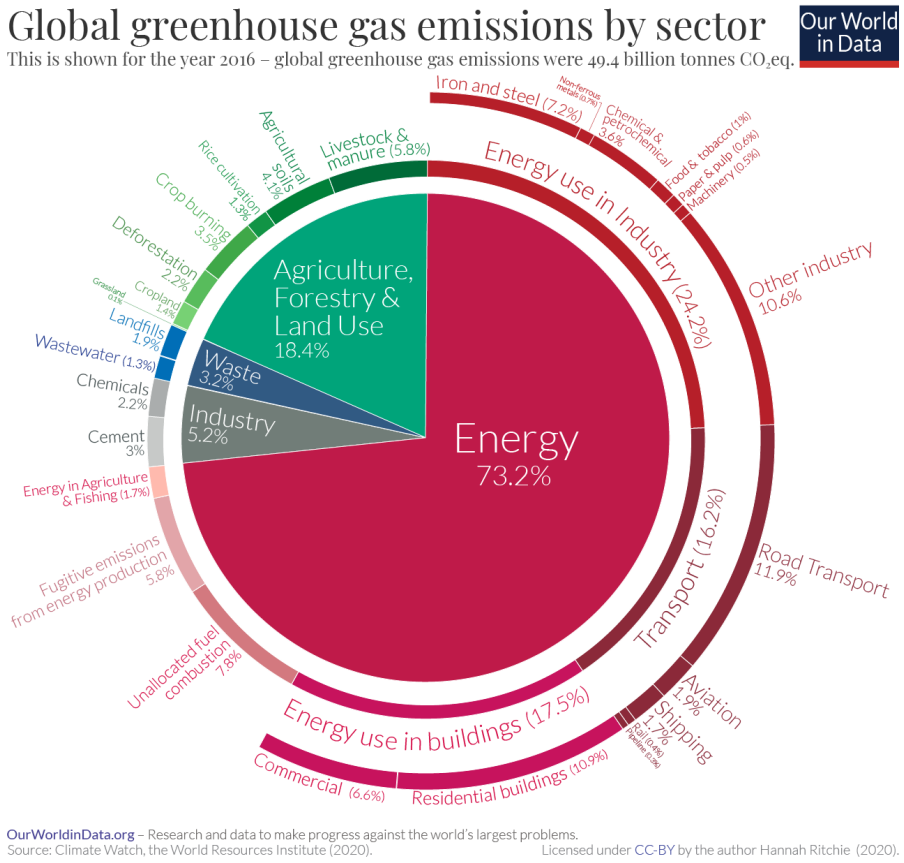

Figure 1.2: Worldwide emissions per sector [5].

The UK is uniquely placed in its ability to adopt marine-based renewable energies. As a narrow island, there is no point within the nation more than 85 miles from the sea, minimizing the distance from energy source to usage location. Furthermore, the position of the island means it is influenced by both the Atlantic Ocean and the highly energetic North Sea, placing it in multiple sea systems, yielding one of the highest wave energy resources worldwide. Moreover, due to numerous water channels around the UK, these areas have particularly high tidal-stream energy resources.

Due to its location, the UK has access to 50% of Europe's tidal energy resource and a technical potential of 16 TWh/year [7], enabling up to 20% of the UK's energy to be supplied by the sea.

Since the 1970s many researchers and industrialists have attempted to capture energy from the sea waves and apply it as electrical power. However, many of the historical wave energy ventures have ended without success, and contemporary devices exist on a grant-to-grant basis. It remains this way after such a long time of research because of fluctuating interest from governing bodies, and the challenge of manufacturing a device that is economically viable and capable of surviving the hostile marine environment.

Current Wave Energy Converter (WEC) devices are found to be more successful in their point absorber topology wherein the device dimensions are relatively small compared to the wavelength, resembling a typical navigation buoy. However, it remains challenging to convert the slow reciprocating energy of sea waves into electrical energy. The Power

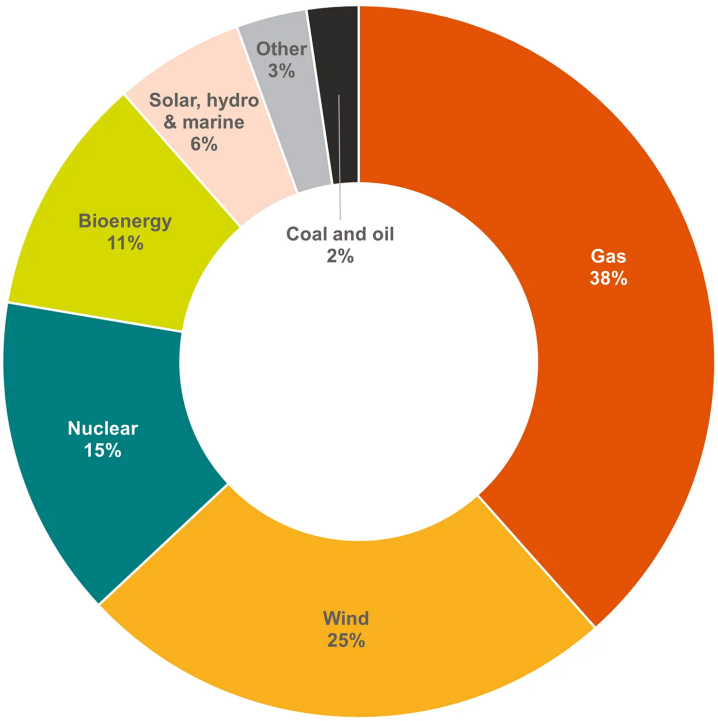

Figure 1.3: Energy mix in the UK during 2022 [6].

Take Off (PTO) is often fulfilled by gearing, hydraulic circuits, pumped storage, pneumatic turbines, or various others; each effectively forming the role of intermediary and enabling an interface with a conventional high-speed generator [8, 9, 10, 11]. But many of these PTOs are formed of complex systems with high capital or operational costs; offshore repair events must be kept to a minimum to maintain an acceptable levelized cost of energy.

A simple solution to the problem is to move away from the concept of high-speed generators and adopt high-force and slow-speed generators that can be Directly Driven (DD) by the wave and generate power without the need for intermediate power conversion. In doing so, the power conversion steps from wave to wire are reduced to the bare minimum, theoretically enabling a simpler drive train with fewer failure modes and loss mechanisms.

DD machines have been successfully proposed for electric propulsion and wind turbines; however, for wave energy they are uniquely challenging to design due to the extremely low velocity of oscillation requiring a proportionally large force to be reacted for the same power output.

In a fully realised DD WEC system, the WEC and the DD generator are closely and irrevocably linked, but due to the interdisciplinary nature of the two, they are rarely studied as one. The two must be researched together from the perspective of how the PTO may be integrated into the WEC. This thesis seeks to bridge the gap between the two fields through a series of case studies linked together to propose a fully designed WEC by asking the question:

"Why is it important to co-design the generator and wave energy device?"

1.2 Aims and Objectives

The principal aim of this research project is to design and develop a fully marinized wave energy converter with a co-designed all-electric direct drive power take-off and propose a design specification for deployment in a real sea location.

The objectives of this research are to:

- Develop a multidisciplinary approach to WEC design.
- Fully integrate an all-electric direct drive power take-off into a marinized wave energy converter.
- Propose a fully designed and rated WEC, aimed for real sea deployment.
- Analyse variable reluctance permanent magnet machines for wave energy converters.
- Develop a mathematical model of a WEC and optimise it for peak power.
- Perform a comparative study between a Vernier Hybrid Machine (VHM) and a Permanent Magnet Synchronous Machine (PMSM).

1.3 Thesis Overview

This thesis comprises various research areas split across several chapters. This section provides a brief abstract of each chapter for the convenience of the reader. The chapters are:

Chapter 2 This chapter provides a literature review of wave energy research, focusing on WEC topologies, their power take-off options, and the driving wave energy theory behind them. In this review, the environmental, social, and material costs are explored, and the challenges to wave energy are presented.

Chapter 3 The literature review is extended into this chapter, focusing instead on DD machines, and is split into a separate chapter due to the multidisciplinary nature of this thesis and the reasonable size constraints of a chapter. Here DD machine concepts are introduced, and their unique considerations for wave energy are laid out. Afterwards, topologies of DD machines appropriate for wave energy are introduced, and the research surrounding them is explored. Finally, particular interest is given to research into the structural mass of DD machines for wave energy.

Chapter 4 A rotary Vernier Hybrid Machine (VHM) and Flux Reversal Machine (FRM) are compared for application into a real WEC. This chapter is resulting from a project in partnership with Mocean Energy and funded by an Innovate UK Smart Award. First, the deeper theory behind the VHM and FRM topologies is presented, including valid configurations of the two machines. After, the process of constructing

a modular VHM prototype is documented, and the challenges of modular machines are discussed. Finite Element Analysis (FEA) models of the VHM and FRM are then validated using prototype experimental data and compared for their suitability as a PTO in the WEC. In the FEA comparison care is also given to understand the impact of rotor teeth on the harmonic content of the airgap and its impact on machine properties.

Chapter 5 A topology of WEC is selected, and a mathematical model is developed. The chapter opens with the selection of a sea location wherein a proposed WEC will be deployed. The wave resource at the selected location is analysed with real-time and historical data from the site, and a target wave state is chosen for further investigation. A mechanical model is developed for the WEC, and a hydrostatic model is developed for a neutrally buoyant electric machine translator. An optimisation of the mechanical model and PTO parameters is then performed.

Chapter 6 A design for a WEC with integrated PTO is proposed in this chapter, bringing together findings from chapters 4 and 5 in the form of a case study. First, the specifications and requirements of the case study are compiled from the conclusions of chapter 5, while also giving some insight into the challenges of WEC co-design. After, several variants of a linear tubular synchronous machine are compared, subject to the case study constraints. Next, the best-performing variant is used as a baseline to consider the suitability of a VHM as the PTO topology in the WEC. Lastly, the final WEC converter with fully integrated PTO is proposed.

Chapter 7 The thesis is concluded with a summary of the findings and proposals made for the continuation of this research.

1.4 Published Works

- Lewis Chambers et al. "Comparison of the Flux Reversal and Vernier Hybrid Machine for a Hinged Wave Energy Converter". In: *2021 IEEE Energy Conversion Congress and Exposition (ECCE)*. IEEE. 2021, pp. 4016–4023

- NJ Baker et al. "Developing a direct drive power take off for the mocean wave energy converter". In: *11th International Conference on Power Electronics, Machines and Drives*. IET, 2022

- Lewis Chambers and Nick J Baker. "Developing a direct drive generator for a heaving IPS buoy". In: *11th International Conference on Renewable Power Generation - Meeting net zero carbon*. IET, 2022

- Nick J Baker et al. "Development of a direct drive power take off system for a hinged wave energy converter". In: *11th International Conference on Renewable*

Power Generation-Meeting net zero carbon (RPG 2022). Vol. 2022. IET. 2022, pp. 28–32

- Nick Baker, Lewis Chambers, and Serkan Turkmen. "Design of an integrated generator and heaving buoy". In: *Proceedings of the European Wave and Tidal Energy Conference*. Vol. 15. 2023

- Lewis Chambers and Nick J Baker. "Designing an Integrated Generator for a Wave Energy Converter". In: *2023 IEEE International Electric Machines & Drives Conference (IEMDC)*. IEEE. 2023, pp. 1–7

Chapter 2. Wave Energy

2.1 Introduction

2.1.1 Scope

The purpose of this chapter is to provide a thorough review of wave energy, its current state of the art, and where it may be heading in the future. As wave energy is a relatively recent field of study and development; it is also important to understand its history and the social, political, and environmental factors that have shaped it to this day.

Some effort is also given in this chapter to provide a fundamental understanding of wave theory, how wave energy converters are designed around it, and why so many have failed.

2.2 Wave Theory

The importance of having a sound understanding of a wave's physical properties cannot be understated. A poor understanding in the early days of wave energy development enabled the avoidably poor performance aboard the Kaimei barge [12]; arguably one of the biggest blows to wave energy at the time.

During the first big push towards wave energy converters, researchers, mathematicians, and marine engineers made great efforts to understand the properties of sea waves and their application to energy generation [13, 14]. It is thanks to them that we understand the sea and hydrodynamics in general to the extent we do today.

This section seeks to lay out what a wave is, and how it applies to the design of wave energy converters.

2.2.1 What is a Wave?

If one were to look at the sea, particularly during a storm, it would be easily noticed that the motion of water in the sea is extremely complicated and almost random. It is important to consider how waves are formed before considering their behaviour.

Waves can be created through various mediums of energy interactions, but the two main mechanisms of wave production are the wind and gravitational pull. Wind waves create sea waves as we think of them, and gravitational waves are responsible for tides. The wind produces a wave via friction between air and water. Over long durations and distances, the continued disturbance creates wave crests that travel across the water body [15].

When a wave travels across a fluid, it is energy moving across the medium, not fluid [16]. The water particles travel in small circular patterns, transmitting the energy over a

short distance and returning to their origin [17]. The energy transfer is extremely efficient and allows waves to propagate for hundreds or thousands of miles and collect enormous energy along the way.

Because sea waves are created by winds, which in turn are driven by solar radiation of the sun, it can be considered that their true source is solar energy. Each step from solar to wind to wave concentrates the energy into denser fluids, and by extension increases the energy density per square metre.

The formation of a sea wave is mainly dependent on two factors, the wind speed, and the fetch, otherwise known as the uninterrupted distance across which the wind blows. Given a wind speed and sufficiently long fetch, the waves reach their maximum height and a fully developed state that propagates the energy over long distances. It is thanks to the expansive Atlantic and North Seas, and favourable winds that provide Western Europe with energetic waves. It is also why coasts around the Mediterranean Sea have much lower wave energy resources in comparison [18].

2.2.2 Physical Behaviour of a Wave

During wave events, water particles do not travel across the sea, but rather orbit their current position, as can be seen in figure 2.1. The orbits are circular for deep water waves, and as the water becomes shallower, the orbits flatten; they are elliptical for intermediate depth, and horizontal in shallow water. The orbits are largest at the surface and become exponentially smaller with depth. This is a manifestation of the fact that most of a wave's energy is concentrated at the water surface [19]. It should however be noted that WECs have also found success by utilizing the pressure difference of a passing wave to absorb energy from the seabed.

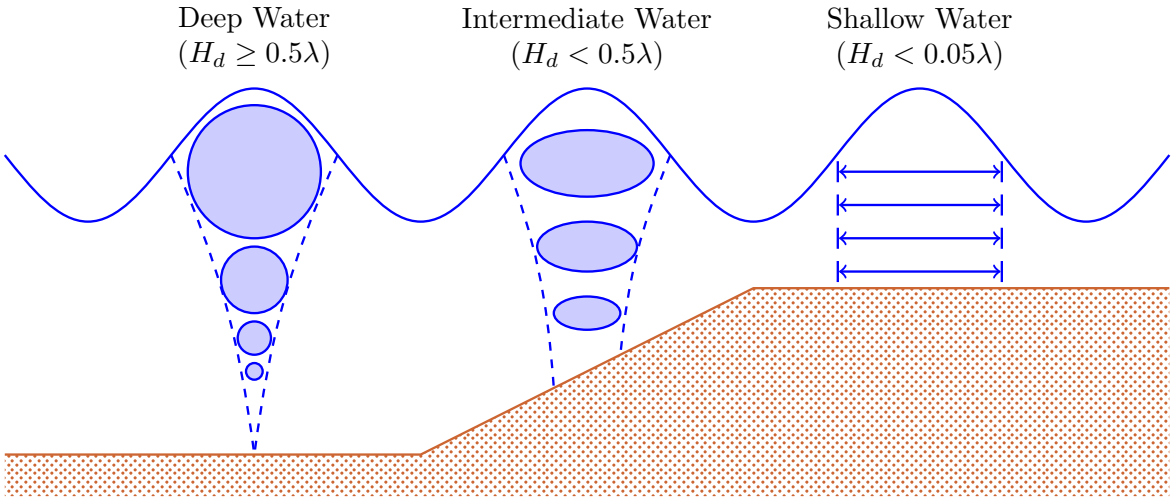

Figure 2.1: Motion of water particles during a wave event dependent on water depth.

Ocean waves, similar to energy waves, follow the principals of superposition [20] when two waves meet, their amplitudes are combined. Waves in phase are additive, while out-

of-phase waves are subtractive. This is partly the reason that seas look so random, it is the unpredictable combination of waves combining and subtracting.

Because of the semi-random nature of wave combinations, it has inspired an area of probability that is important to marine structures. It is a statistical fact that every 50 and 100 years, waves will combine in such a way that waves large as 25 m can form with little warning [21]. Likewise, even in ordinary conditions, waves can combine into large waves without warning, known as rogue waves.

Two distinct types of waves are of interest. Deep waves where the depth is more than half the wavelength ($H_d > 0.5\lambda$) and shallow waves wherein the depth is significantly smaller than the wavelength ($H_d < 0.05\lambda$). Both wave depths follow Airy wave theory [16], meaning that the following assumptions stand true:

- Fluid motion is irrotational.
- Pressure is constant at the water surface
- Water depth is constant.

The phase and group velocities of each wave type are:

$$c_p = \begin{cases} \frac{g}{2\pi}T & \text{if} \quad H_d > 0.5\lambda \\ \sqrt{gH_d} & \text{if} \quad H_d < 0.05\lambda \end{cases} \tag{2.1}$$

$$c_g = \begin{cases} \frac{g}{4\pi}T & \text{if} \quad H_d > 0.5\lambda \\ \sqrt{gH_d} & \text{if} \quad H_d < 0.05\lambda \end{cases} \tag{2.2}$$

And the wavelength is:

$$\lambda = \begin{cases} \frac{g}{2\pi}T^2 & \text{if} \quad H_d > 0.5\lambda \\ T\sqrt{gH_d} & \text{if} \quad H_d < 0.05\lambda \end{cases} \tag{2.3}$$

Where T is the period, H_d is the water depth, and g is the gravitational constant.

These equations describe that deep water waves are naturally dispersive, and their propagation velocity is dependent on their period and thereby their wavelength. Therefore, longer deep waves tend to overtake shorter and slower ones, adding to the unpredictability. On the other hand, in shallow waves, the phase and group velocities are equal and dependent on the water depth, not the wave period. Generally, shallow waves are shorter and travel at slower velocities.

2.2.3 Power & Application to Wave Energy

The energy density of a wave for any given sea state is given by:

$$E = \frac{1}{16}\rho g H_s^2 \tag{2.4}$$

The power per metre of wavefront is proportional to the group velocity [19]:

$$P = Ec_g \tag{2.5}$$

Combining with equation (2.2), the power for each wave type is then:

$$P = \begin{cases} \frac{\rho g^2}{64\pi} H_m^2 T_e & \text{if} \quad H_d > 0.5\lambda \\ \frac{\rho g}{16} H_s^2 \sqrt{gh} & \text{if} \quad H_d < 0.05\lambda \end{cases} \tag{2.6}$$

Where ρ, H_s, and T_e are the water density, significant wave height, and energy period of the wave. Both types of waves are proportional to the square of the significant height. The deep-sea wave however is additionally proportional to the wave period, while the shallow wave is fixed at a static depth. Although it is more difficult to operate in the deep sea, the power available there is higher.

For a deep-sea wave of 2 m high and 10 second long, there is 20 kW of power in every metre of wavefront. Under a 100-year wave scenario, a 25 m wave with the same energy period would transmit 3.1 MW/m over just 10 seconds.

Practically speaking for a wave energy converter, it can be desirable to capture energy across the most wavefront length as is possible. Some WECs have even been designed with the ability to capture energy across a wavelength larger than their physical dimensions [22].

2.3 A Brief History of Wave Energy

Throughout history, people have often looked upon the sea with a sense of awe and fear. The raw power contained within has inspired generations of poetry, literature, and mythology. Many have stood by the shore and dreamt about turning the destructive power of the sea into usable power. The first recorded instance is attributed to one Pierre-Simon Girard and his son [23], who filed a patent in 1799 describing a device using floating beams to drive pumps and mills. Little is known about the inventors aside from the patent and there were few mentions of gathering energy from the sea until electricity started becoming more widespread.

The theory of rotational sea was first put to paper in 1864 [24] to explain the propagation of the waves. This was extended into practical applications by Stahl who presented possibly the first paper on wave energy to a group of mechanical engineers in 1892 [25]. One of these devices, using water to displace a column of air would later be adopted to power the home of M. Bochaux-Praceique in 1910. This was done by adapting a vertical bore in the cliff-face to drive an air turbine and provide 1 kW of power, in what is thought to be the first application of meaningful power output [26]. The next great innovation of the air column technology came in the 1940s when Yoshio Masuda, inspired by Stahl and Bochaux-Praceique began experimenting with self-powered navigation buoys [27] and the

concept garnered its name of the Oscillating Water Column (OWC).

Through the decades Masuda continued to be an industry leader, gradually improving his OWC navigation buoys, commercializing them in 1965 with some still operational decades later [28]. His work culminated in a 1.25 MW floating barge dubbed "Kaimei" as part of an international collaboration in 1976. However, due to the extremely immature knowledge at the time, the project performed poorly [12]. This failure caused a massive blow to wave energy confidence internationally.

Outside of Japan, the real first interest in wave energy began shortly after the energy crisis of 1973 started. In 1974, the Central Policy Review Staff in the UK proposed a technological and economical appraisal of wave energy [29]. This marked the first big push for wave energy and indeed any other energy that could solve the crisis.

After several years and influential conferences, Stephen Salter of Edinburgh University set a major milestone in 1974 when he proposed his 'Edinburgh Duck' [30]. His design was a long machine, set perpendicular to the wave direction with an egg-shaped cross-section, designed to bob up and down about its axis. The device claimed to have very high efficiency, capturing the imagination of the academic community.

After Salter's landmark paper, wave energy received a significant boost in popularity, and historic designs such as Masuda's oscillating water column [26] and the Russell Rectifier [31], as well as a new design from inventor Sir Christopher Cockerell for a floating raft, were proposed [32].

Ultimately, except for the OWC, none of the devices made it out of the prototype stage. At the time, they were competing to be the next big energy provider and were hence very large. The diameter of Salter's Duck was 15 metres and expected to stretch tens of kilometres of coastline. Although these hypothetical giants never saw any real service, they each founded their own category of wave energy converters, and the Duck grew Edinburgh University into a world leader in wave energy.

After this boom of interest in wave energy, the oil crisis began to wane in the early 1980s, taking the demand for renewables with it.

Wave energy research funds were cut significantly [33], but with the looming crisis over, smaller-scale projects and prototypes consistently continued to appear worldwide; the second and current wave of renewable energy interest. Climate change mitigation policies and a general drive towards sustainable practices ensure the continuation of wave energy and other renewable power.

In more recent decades, the ambitions of wave energy have reduced with a stronger focus on smaller scale devices and seeking a market niche for commercial success. Several developers have come forward with promising proposals [34, 10], although many were unable to maintain investor interest [9, 35, 36].

2.4 The Wave Energy Converter

A Wave Energy Converter (WEC) is a machine designed to convert the energy contained within sea waves into a regular and predictable energy flow. The regulated energy can be manifested as relative motion between mechanical bodies [37, 38, 39], piezoelectric activation [40], or motion of fluids [41, 42, 10]. Ignoring the power take off, the WEC is considered effective if it can capture and convert energy into regulated energy with high efficiency. WECs have been considered to provide energy input for applications such as water pumping, desalination, and electrical power generation [43, 44]

Onshore/nearshore, they can be electrical grid energy providers, capable of providing power to isolated populations who rely on diesel generators for power. Around coastlines, WECs can be integrated into navigation and other informational buoys to create self-powered devices, which was one of the first wave energy developments [28].

Far from the shore, on sites such as research stations and oil rigs, power supplies are much more difficult and are often supplied by diesel generators. In these areas, the sea is a convenient source of energy, making a WEC and battery a desirable choice for power supply. Recent developers have made this their business model [45, 46]. Additionally, unmanned stations in the sea are often too small or too far below the surface for diesel to be an option. Floating/Seabed research equipment and remotely operated vehicles are uniquely suited to be supplied by WECs [47].

2.4.1 Costs

Wave energy converters are not without their drawbacks. One of the biggest historical issues for adoption has been the cost. The first generation of WEC proposals were enormous, monolithic structures, designed for powering the grid; due to competing against nuclear energy to capture interest and become the new big power provider. In modern WECs, this is no longer the case, and the scale of WECs has scaled back significantly.

The cost issue stems back to the relative infancy of the technology. Wind energy is a mature technology and has converged onto the 3-blade horizontal axis machine, as developers iterate, the LCOE reduces over time [48]. Although wind turbines have not fully converged in all countries, the sharing of knowledge and component availability aids in reducing the cost. The wave energy field is in a much more divergent phase wherein there are many exiting development paths to pursue, and less part availability and investor confidence [49].

Furthermore, WECs, although easily compared to wind turbines, do not scale well for power behaviour or performance. It is not always possible to make a small powered WEC with low cost, and gradually increase the size as the technology develops. In the past, they were proposed at a large scale from the start [38, 31], creating a high barrier for entry and requiring developers to build a strong interest and investment before true development can even begin. Constructing a WEC location with meaningful power output

is, therefore, a significant task, and is challenging to succeed without strong financial backing. The development of sophisticated wave tanks for testing has made great steps towards addressing this challenge. Furthermore, (O&M) costs in WECs can become a significant factor in the overall Levelized Cost of Energy (LCOE) [50].

The coastline and the sea particularly are among the harshest environments a machine can operate. Any device placed in the seawater is under constant attack from the salt water and will rust away and break down unless countermeasures are used wherever possible. Because of this, the most sensitive components must be shielded from the water. However, because WECs are devices of movement, watertight seals are applied. This means that routine maintenance is essential to keep the seals in good order and replace any failing parts.

When a WEC has scheduled maintenance, repairs cannot necessarily be made immediately. A repair crew must be shipped out during an acceptable weather window. If the weather is not suitable, maintenance must wait for acceptable weather conditions, incurring higher costs as the vessel waits for deployment. Moreover, if the repairs needed are below water, it may be necessary to also bring divers, further increasing costs [51]. The only alternative is towing the WEC back to shore for repairs and redeploying afterwards. If the device has been towed or was sufficiently damaged to go offline, there is a loss in operation time until back in deployment.

2.4.2 Environmental & Social Impact

WECs are quite mixed in their environmental and social impact. The environmental impact is strongly dependent on the type of WEC and its distance from the shore. It has in in the past been claimed that WEC deployments may impact animal life in the ocean through presence, physical motion, acoustics, and vibration. However, many of these studies are based on literature reviews as the field is severely lacking in data and there are many uncertainties [52]. Moreover, some have been found that sea life congregates around large subsea structures for shelter and resources [53]. The issue still stands though, that developers should take care not to cause undue harm to marine environments, and there is a great need for further research in this area.

In the 80s, when WECs were proposed for grid energy production at a major scale, the proposals were set to take up a significant portion of the coastline; potentially causing issues for the local people and environment.

When a large quantity of coastline is occupied by WECs, it can reduce the sea's energy level between the WEC and the coast, hugely impacting the natural flow of sediment deposition. Coastlines are constantly changing and evolving and are maintained by a steady flow of sediment displaced and supplied by the sea waves. If the energy levels near the coast are changed too drastically, it can erode treasured coastlines to erode or excessive deposits elsewhere [54].

Similar to wind turbines, WECs are not immune to the politics of their local areas.

Onshore wind farm proposals have long received pushback from those who live in the proposed area based on complaints of noise and visual pollution [55]. For onshore wave energy devices care should be taken to ensure devices are integrated in such a way that they cannot become an eyesore or otherwise offend residents. Deep water WEC topologies are beneficial is this regard as they cannot be seem from the coast.

2.4.3 Materials & Resources

WECs that are designed with large power production in mind, are required to span miles of coast. In the first big push towards wave energy, the only feasible and sufficiently buoyant material was concrete. However, at the time, concrete was expensive, difficult to work with, and "needlessly strong" [56].

Since then, material science has made significant improvements. There is a wide range of materials suitable for use in WECs, but challenges to materials remain. In recent years, researchers have begun to develop mechanically simpler Power Take Off (PTO) via high-force, low-speed electric machines, placing increasing the strain and dependency on silicon and powerful rare earth permanent magnets [57, 58]. This comes at a time of unprecedented electrification in the transport industry that is already suffering from silicon and rare earth magnet supply chain issues.

Using the "Nodding Duck" as an example. Allowing the duck's claimed efficiency 80% [59], assuming deep water, and that linear wave theory applies, the wave resource has a significant height of 3 m and energy period of 10 s, equation (2.6) yields a power of 35.15 kW/m. For an installation to provide 500 MW of electrical power, it would require approximately 14 km of coastline.

2.5 Wave Energy Converter Topologies

Other renewable power generation technologies have reached some level of convergence on a topological level, such as the horizontal axis wind turbine. Wave energy converters are much less mature and remain in a divergent stage wherein there is not yet a clear optimal topology.

This is partially due to the nature of wave energy transfer. Because the energy in a wave travels near the wave surface, but the fluid moves in small orbits near the surface. Effective kinetic energy converting WECs must be near the surface and capable of moving in multiple modes to achieve a high capture efficiency. For example, a cylinder operating in a single mode is limited to 50% efficiency [14].

For this reason, wave energy converters are an exciting research area with a broad range of potentially viable topologies for many power applications.

2.5.1 Terminator

The terminator is positioned parallel to the oncoming wavefront and tends to cover great lengths of wavefront. It is named a terminator due to it existing like something of a wall, to capture the entirety of the wave's energy, leaving near still water behind it. The topology be floating, or shore mounted.

The most notable example is the Edinburgh Duck [38], which gained significant interest due to it appearing to leave almost completely still water in its wake, as is shown in figure 2.2. It was so efficient because it captured all modes of incoming motion. The duck however had the critical flaw of not having a viable PTO mechanism or sufficient energy storage. The team behind it went to great lengths to design flywheels and gyroscopes into the device; considering numerous PTO topologies, but the technology simply wasn't ready at the time.

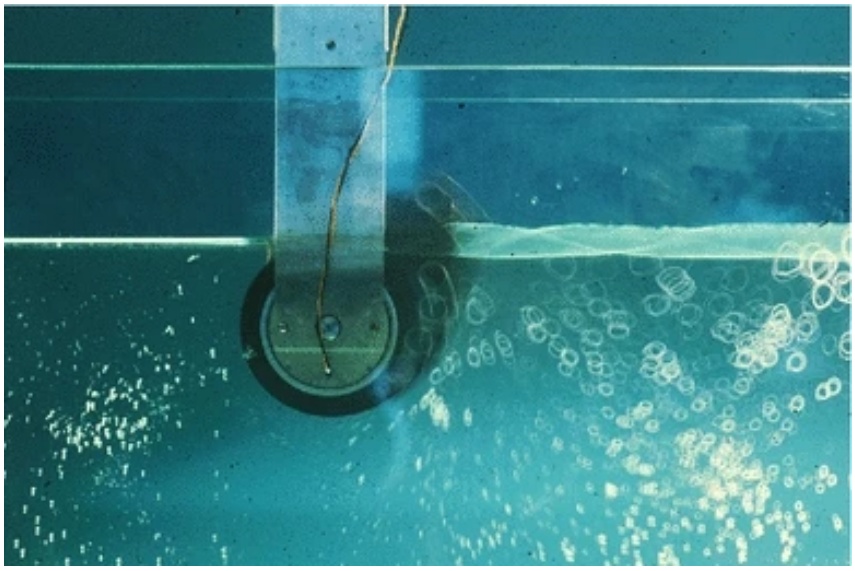

Figure 2.2: The famous "Salter's Duck" photograph [60].

Terminators, due to their extreme lengths additionally attract difficulties in politics and ecology. Constructing a terminator across a length of coast effectively forms a wall around it, troubling other sea users. Additionally, because the device intends to extract the maximum power from the sea, it can cause serious changes in material deposition.

Their main weakness however is survivability. Few, if any, terminators have any reasonable method of avoiding storms. Because of a maximum energy absorption design, they are at higher risk of damage during storms and damage mitigation must be considered in their design.

2.5.2 Attenuator

Attenuators are of similar proportions to the terminator but rotated perpendicular to the oncoming wave. They extract power by being built up of two or more segments attached by a joint. As a wave passes along the length of the device, each segment is angled in

turn by the wave crest, and power is produced from the relative motion, typically by a hydraulic ram. They are by their design, floating, deep-water devices.

They were one of the first WECs considered, put forward by Sir Christopher Cockerell [32]. Through the years they have retained a decent popularity and several enterprises have attempted to commercialize attenuators [9, 39]. A well-publicised device in recent decades was the Pelamis[9], pictured in figure 2.3. The Pelamis reached a technology readiness level (TRL) of approximately 7 but ran into financial difficulties and ceased operations. In recent years a standout attenuator has been developed by Mocean Energy, who are currently developing a robust direct drive PTO system [61] and have a strong focus on reliable simplicity in their WEC.

Figure 2.3: "Pelamis" WEC on site in Portugal [9].

The attenuators stand out from terminators in that they ride across the wave, only absorbing a moderate amount of energy, reducing environmental and sea-sharing concerns.

2.5.3 Oscillating Water Column

The oscillating water column is one of the first WECs to be conceived and has been developed for many years [26, 12], and has received great interest in many countries [8, 62].

Any WEC that converts energy from the waves to a contained column of air can be labelled as an oscillating water column. Figure 2.4a shows the basic operating principle on a fixed OWC. As a wave approaches, the water level rises, forcing the contained air through a pneumatic turbine, driving a generator. Near the start of its conception, it required rectification valves to ensure the turbine was always driven in the same direction, at the cost of increasing system complexity. However, the invention of self-rectifying turbines allowed the OWC system to be further simplified [63].

Besides being one of the first commercially successful WEC concepts, the 500 kW LIMPET was the first WEC to contribute energy to a grid [64]. The LIMPET then directly inspired the creation of the Spanish 296 kW Mutriku Plant, which has been producing energy since 2011; making it the longest-serving WEC with the most energy produced [65]. The massive 2 MW OSPREY device in Scotland had the misfortune of

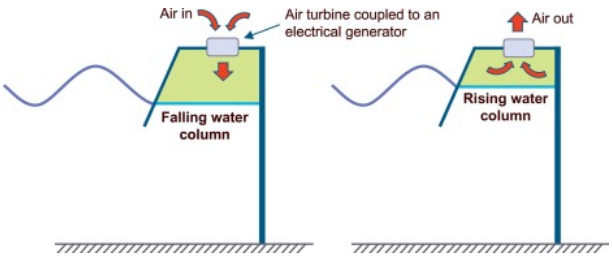

(a) Concept [62]

(b) Self powered navigation buoy [8].

Figure 2.4: Oscillating water column concepts.

being one of the most publicised failures in wave energy when it was written off by the back end of a hurricane [35].

2.5.4 Pressure Differential

Pressure differential devices can be considered as somewhat passive devices similar to an OWC. They are usually placed such that the crest and/or trough of a wave creates a pressure difference within the system; usually to displace air or water through the system.

Travelling waves do not produce pressure differences at the seabed, only less common standing waves do [66]. Therefore, they must be placed at or very near the surface and can require very specific wave heights to be fully excited.

They are usually formed of flexible tubes or compartments like the Lancaster Bag [67], or one-way gates and valves like the HRS Rectifier [31]. They can also exist in any form, terminator, or attenuator. Some pressure differential WECs have been presented as structurally challenging [68].

Pressure differential devices have received continued development in recent years. The Archimedes Wave Swing (AWS) is a two-part rigid pressure vessel that uses the pressure of wave to compress and extend (figure 2.5) [34]. The developers are continuing to improve the device and recently achieved 80 kW peak power at the EMEC testing ground [46].

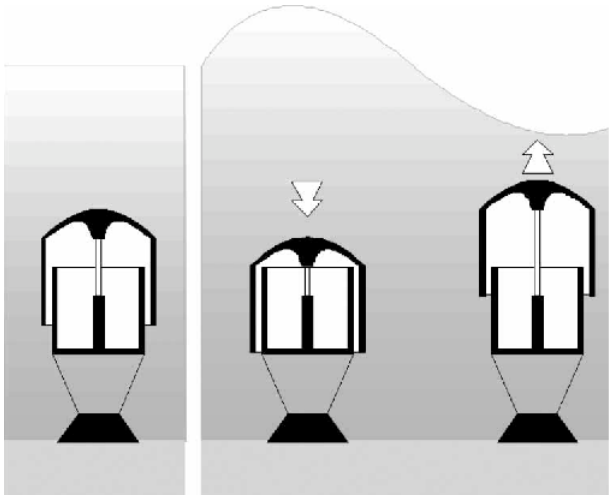

Figure 2.5: Archimedes Wave Swing concept [34].

2.5.5 Overtopping

Overtopping WECs are an interesting topology in that it is the most similar to existing power generation technologies. They are self-contained reservoirs with low-head turbines and can be shore-mounted like the TAPCHAN [42], or floating like the Wavedragon [10]. These WECs quite effectively solve the problem of intermittent power output as the turbine is dependent on the water inside the reservoir, not the current wave. Provided that the reservoir does not run dry, steady power is produced as water flows out.

Alongside the usual power restrictions of low head turbines [69] and construction costs, overtopping WECs introduce unique challenges. They are reliant on vertically displacing wave crests over a barrier and into the reservoir. In calmer conditions, the wave height may be insufficient to enter the reservoir; a compromise must be made between reservoir volume and turbine head.

The wave height problem is mitigated by implementing concentration techniques such as tapered channels and reflector arms for raising water to larger heights. Some devices have also implemented multi-level slotted structures to enable ingress from several heights [11]. In addition, the floating varieties benefit from adjustable ballast to maximise water ingress.

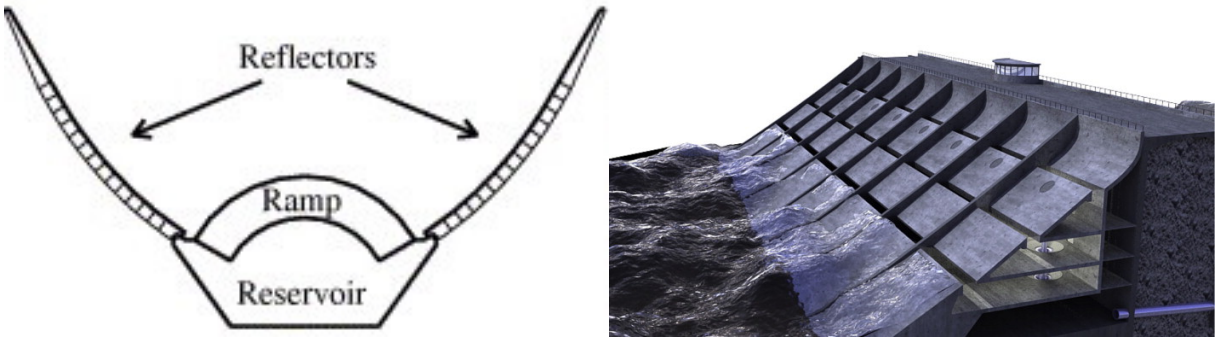

(a) Overtopping concept [10] (b) Seawave Slot-Cone Generator [11]

Figure 2.6: Overtopping WECs

These devices are both helped and hindered by their concept. Hydropower is well established, and parts are readily available, additionally, shoreline devices can save costs by integrating into existing structures. Floating designs often include long concentration reflectors (figure 2.6a) introducing a new failure mode during large waves.

2.5.6 Oscillating Wave Surge

Surge devices are nearshore WECs that consist of a flap and pump. They are generally affixed to the seabed, with a buoyant flap attached to the base via a hinge. As wave crests and troughs pass, the flap oscillates back and forth, and useful work can be generated from the motion [36]. The Oyster was fitted with a water-pumping piston useful for a high-pressure hydraulic system or water desalinisation (figure 2.7). However, the parent company of Oyster closed in 2015.

Figure 2.7: Oyster wave energy converter [36]

Because they operate in shallow water, all plant can often be displaced onto land, eliminating water ingress concerns and ease of maintenance. Like many WECs, they suffer from being optimised for a specific wave profile, but unlike other topologies, they are generally passive devices capable of fine-tuning into different wave inputs. Additionally, because they are fixed, they are less capable of avoiding dangerous wave conditions; although this could be mitigated by controlling the device to lay flat on the sea floor during storm conditions.

2.5.7 Point Absorber

A point absorber figure 2.8 is characterised as having a short width relative to the length of an oncoming wave. They are extremely broad in location, number of bodies, and power take-off. In general, they resemble a typical sea buoy with one or more axisymmetric bodies floating at or near the surface.

Point absorbers have gained significant attention in recent years and are currently the most prevalent WEC topology worldwide [70]. They are highly dynamic, requiring only a semi-stable reference point to react force against. The reference point can be the seabed, a structure built into the water such as an oil rig, a more massive body, or a drag plate. Their resemblance to regular buoys affords them the benefit of having an established product at their back and makes it simple to convert existing buoys into WECs.

This topology of WEC has been there from the start of wave energy research, and many landmark papers in hydrodynamics were conducted with them. Breakthroughs in latching, reactive control [71], and resonant effects [13] were first discovered with or applied to point absorbers. They are so prolific in literature [71, 13, 72, 73, 22, 34], that even devices such as the Archimedes Wave Swing, and some OWC concepts could share this classification.

The core benefit of the point absorber their axisymmetric construction, this makes them insensitive to the direction of the oncoming wave, unlike the attenuator or termi-

nator which would likely not perform well if the oncoming wave were approaching from an unfavourable angle. The point absorber gains the additional benefit of capturing the equivalent energy of a device larger than its physical dimensions, giving them good economic potential [74].

(a) AquaBuOY [72]

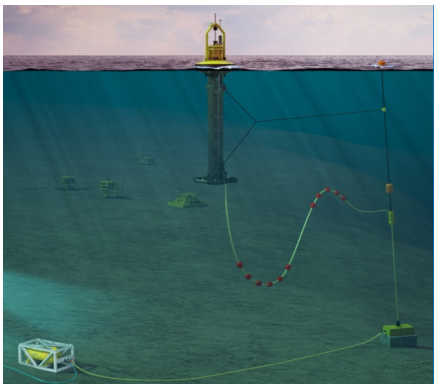

(b) PowerBuoy [73]

Figure 2.8: Point absorbers

Because point absorbers have a small size relative to the wave, they tend to track waves and can absorb power in any degree of freedom. Their dynamic customisation allows designs to be tweaked to operate well in any wave climate or mode of operation. Elongating the WEC into a spar for example concentrates the motion into heave only.

The greatest challenge to the point absorber is the power take-off. Although point absorbers can take many forms, the relative motion usually ends up as vertical, or otherwise linear displacement. Converting slow linear motion into consistent and high-frequency electrical energy is not a simple task. In the early days of wave energy research this was prohibitively so and remained so until powerful rare earth magnets were conceived [75] enabling the expansion of directly driven generators.

Due to their small size and fairly solid structure, they may be less prone to sinking when compared to larger hollow WECs [35]. It is more likely that the failure mode of a point absorber in deep water could be the mooring lines breaking and the device going adrift [76].

2.5.7.1 The IPS Buoy

The IPS Buoy is a floating, two-body device that operates in heave along its axis. It was first proposed by Interproject Services (IPS) [37], and has received consistent research through the years [77, 78, 61, 79].

The upper body is a floatation buoy and serves only to provide sufficient buoyancy to the system. It is upon this body that all other components must be supported; the buoyancy force provided here then, informs the ultimate size of the system. A hollow vertical tube, open at both ends is rigidly connected to the buoy some distance below the water.

Mounted to the inside of the tube is the 'cylinder'. Further inwards is a piston, which forms a watertight seal with the cylinder. Further to this, the piston has an energy transfer connection to the cylinder and/or float via the PTO. The layout of these components with an internal stator is presented in figure 2.9.

Additionally, the tube is closed off at both ends with a structure that allows water to flow freely but impedes the egress of the piston.

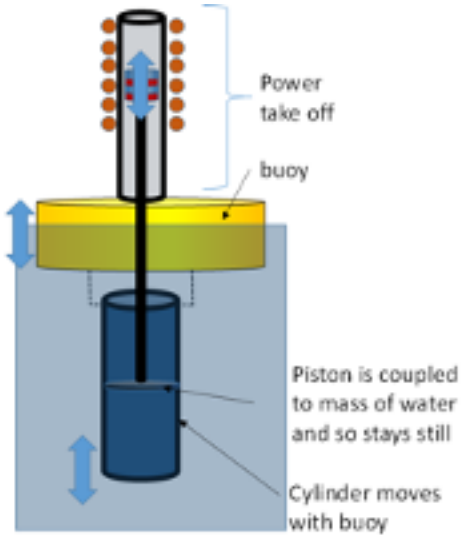

Figure 2.9: IPS buoy layout [61].

During normal operation, the float closely tracks the sea motion. It would be expected that the piston follows due to the PTO connection. However, because the tube is filled with water, the PTO must develop sufficient force to overcome the inertial mass of the internal water. There is hence a phase difference between float and piston upon which power can be extracted.

The IPS effectively tackles the end-stop problem [80]. Whilst still in nominal conditions, the piston follows behind the buoy, oscillating with an amplitude less than the cylinder length. When more extreme waves are encountered, the piston may be forced beyond the cylinder length. But because the cylinder has a smaller diameter than the tube; once the piston exits the cylinder loses the watertight seal and decouples from the water mass.

During a decoupling event, the piston is assumed to behave as a drag plate with its own inertia - albeit at a much lower value. Because the effective piston mass is greatly reduced it approaches the tube's end stops with greatly reduced force. Furthermore, because the mass is so reduced, it becomes feasible to control the piston position via the PTO, either to aid in slowing down or for cylinder reinsertion.

2.6 Power Take Off Technologies

Many technologies of WEC operate in varied modes of movement. The selected power take-off used in a wave energy converter is vitally important to the feasibility and success

of a wave energy topology. Many WEC concepts have failed to reach the prototyping stage due to not addressing the PTO needs from the start.

Maintenance is a major challenge to WECs; all components aboard the device have a lifespan and must be replaced or repaired eventually. It is important then, to ensure any PTO is simple and robust, with minimal components to fail and high mean time between failures.

What makes the PTO for WECs so difficult and costly is due to how different the generator requirements of wave energy are compared to conventional power generation. A traditional four-pole synchronous generator for grid energy usually operates at 1500 rpm to produce 50 Hz electrical power. On the other hand, WECs are often designed to capture energy periods around 10 s (6 rpm). Mechanical power is generally described as the product of force and velocity, implying that the electric machine must have an intermediate velocity conversion stage, or react to a higher force. The conversion stage is often achieved with gears, hydraulics, or bypassing the problem via magnetic gearing.

2.6.1 Traditional Machines and Gearing

One of the most traditional and simplistic approaches to the rotational velocity problem is to simply add additional energy conversion via mechanical gearing [81], an example of this is shown in figure 2.10. Ignoring for a moment the direction of motion, gears fulfil their role effectively, increasing the speed by the specified ratio and allowing the electrical power output to be much closer to the 50 Hz standard.

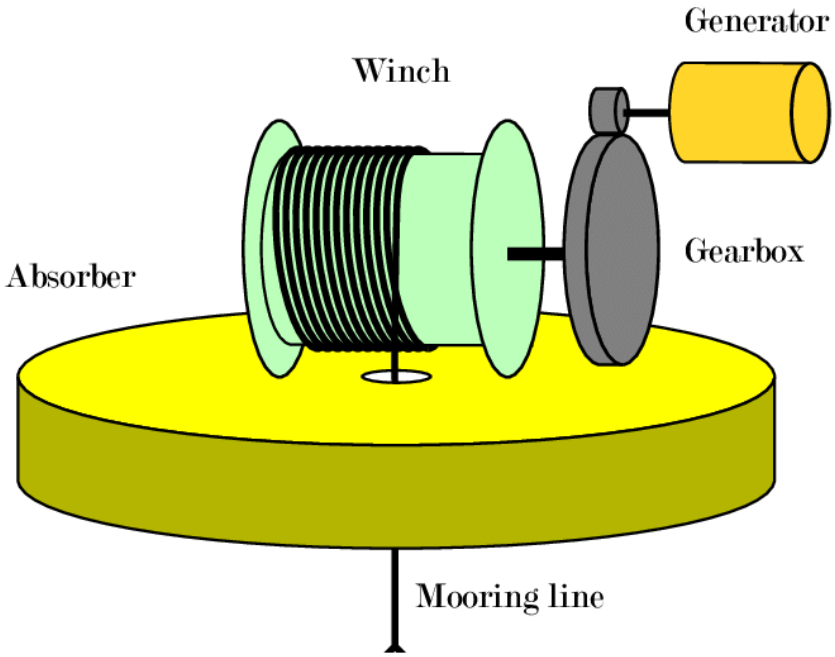

Figure 2.10: Geared power take-off [82].

Any additional power conversion introduces losses, reducing the efficiency of the system. Moreover, more moving parts may cause a higher number of breakdowns; especially for sensitive components and mechanically interacting parts. Additionally, if the device

is intended to drive a 50 Hz at fairly consistent speed, it could be necessary to include a smoothing mechanism such as a flywheel.

In wave energy, even the concept of a gearbox becomes more complicated. In conventional fossil fuel power generation, or wind turbines the motion is rotary, and implementing a gearbox is as simple as attaching it between the power source and electric machine. On the other hand, the goal of wave energy is usually to convert the slow sea swell into usable energy.

In many WECs, the PTO motion is often linear, or rotary with reciprocating oscillatory rotation across a few degrees. Under this scheme, the gearing scheme must be specially adapted to translate linear motion or restricted displacement into consistent rotary energy.

In recent years, some WEC developers have been phasing out gearboxes in favour of other PTOs [61], however, some have produced sound designs with gearing integrated [81]. Others have taken mechanical concepts and applied them in novel ways. One such example is the "Manchester Bobber", which uses a counterbalanced buoy and winch to drive a ratcheting flywheel and gearbox; enabling smoothed rotational motion at a high speed, utilising off-the-shelf components [83].

2.6.2 Hydraulic

A more common topology employs high-pressure hydraulics to achieve power conversion. With a piston being operated from the WEC displacement, common hydraulic components can be used to drive a high-speed hydraulic motor and thereby an electric machine (figure 2.11). Because hydraulics is a very mature field, off-the-shelf components can be used to construct a WEC at low cost. Moreover, the addition of an accumulator allows for power smoothing between oscillations.

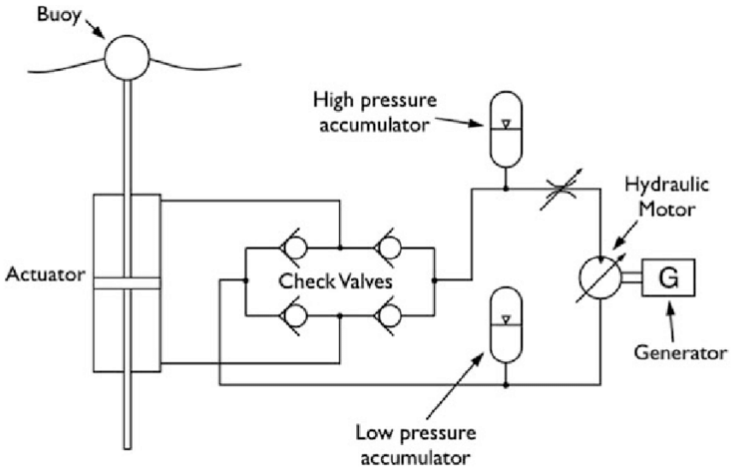

Figure 2.11: Hydraulic power take-off [84].

They have retained popularity over the years with numerous prototypes deployed to the sea [9, 85]. The major weakness of hydraulic PTO is that they are built up of many

components, requiring much stricter monitoring and maintenance plans, and potentially higher O&M costs. Furthermore, because hydraulic systems have poor efficiency at part load it is challenging for a hydraulic PTO to produce electrical power without high losses. Moreover, because they commonly use hydraulic oil as an operating fluid, the seals require periodic replacement, and a rupture of the system can cause ecological damage.

2.6.3 Pneumatic Turbine

Pneumatic PTO is most commonly seen in OWCs (figure 2.4), but some other configurations of pneumatic WECs adopt them [41]. They also utilise well-understood and readily accessible components to form their system. The PTO part of a pneumatic system is the most similar to conventional power generation. With the application of a flywheel to smooth out ripples and the potential addition of a gearbox, an OWC device can be joined to a conventional generator directly. Their similarity is likely the reason they are the earliest successful topologies of WEC.

PTO with pneumatic power is typically quite low risk, especially if located on the shore, with the only real risks being lower performance, and water splashing into the machinery.

2.6.4 Hydro Turbine

Hydro turbines in wave energy are well known for low-head turbines used in overtopping WECs (figure 2.12) [42, 10, 11]. However, it is also possible to utilize reservoir fed high-head turbines by applying wind or wave energy devices to pump water into the reservoir while renewable resources are present and releasing it back to the ocean through a conventional turbine to fulfil electrical power demand [86].

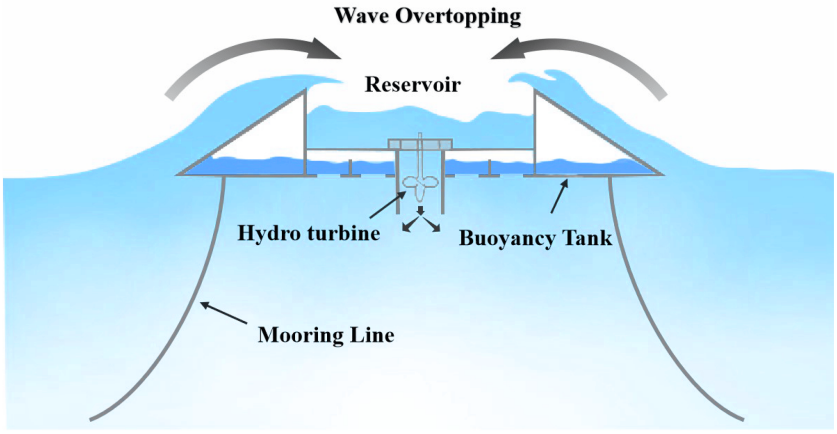

Figure 2.12: Low head turbine power take-off [87].

High head pumped storage effectively solves some wave energy challenges by providing a mechanism of energy storage, enabling electrical power production matching consumer demand, not renewable resource availability. Additionally, because the plant is located

on/near shore, the operation & maintenance challenges of wave energy are somewhat reduced [50, 51].

2.6.5 Directly Driven

Directly driven (DD) topologie s bypass the gearboxes by replacing them with novel electrical machines that use magnetic gearing to produce electrical power at a higher frequency than the mechanical displacement (figure 2.13) [88, 89, 90]. An electric machine such as a flux reversal machine (FRM) [91, 92, 93] or vernier hybrid machine (VHM) [94, 95] has powerful permanent magnets and many pole pairs and completes a full electrical cycle across a very short displacement, effectively functioning as its own fixed gearing. They are extremely dynamic in design and can be adapted into linear or rotary devices as needed by the application. These machines are presented in rotary from in chapter 4, and linear in chapter 6.

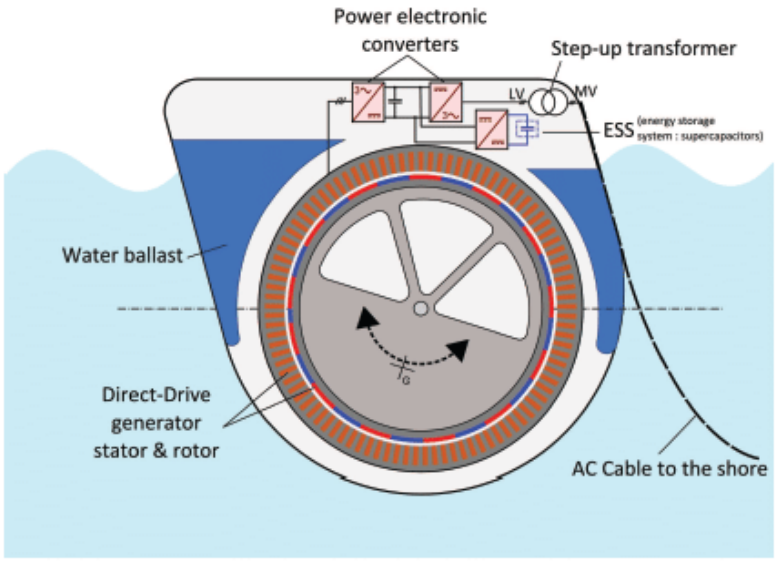

Figure 2.13: Directly driven power take-off [96].

DD drive machines have become more commonplace in wind energy in recent decades [97, 98, 88]. Because they lack standardisation in wave energy applications, DD machines are usually built bespoke, and the cost-saving parts are simply not available.

Due to their nature of being linked directly to the wave force, the output of DD machines varies in a doubly sinusoidal fashion; once from the angular velocity of the wave, and once from the magnetic position of the device [99]. As there are no traditional means of physically smoothing the power, the DD topology is entirely reliant on power electric converters to condition the output power, leading to a higher dependence on power conditioning.

Despite their difficulties, DD machines remain a very interesting research topic and are a promising PTO for application into point absorbers [34, 100].

2.7 Challenges and Commercialisation

Achieving commercial success in wave energy is no easy feat. There have been few devices to demonstrate technical readiness, and those that have, struggle to find a market position and make the switch from research to retail. Numerous reasons for this have been touched upon in previous sections, but not fully explored.

2.7.1 Extreme Weather

One outstanding challenge to development is the sea itself. Because waves contain so much energy, and are semi-random and wave-like, conditions vary from a slow swell with low amplitude, to storm conditions, with the chance of a rogue wave at any time [21]. It is difficult to propose and design a device that is capable of surviving rate events which also provides a competitive LCOE.

This problem is not unique to wave energy. Wind turbines faced the same challenge in the early days of their commercialisation; during storm events, high wind speeds forced the turbines to rotate at a velocity much higher than rated. Brakes were employed to restrict the velocity, but in some cases, the brakes failed allowing the electric machine to accelerate until the resistive heat burned out the generator, causing catastrophic failure of the turbine. The solution in this case was the development of controllable blades, allowing the turbine to stall, providing a backup stopping mechanism, and preventing this type of failure [101].

There is a great deal of similarity between wind turbines and WECs. Both are driven by their operating fluid and are incapable of removing themselves from it during times of extreme activity. The most survivable strategy with a low LCOE is to take inspiration from wind turbines and develop methods of energy shedding. It is well understood that wave energy exists mainly near the water surface, and some WECs like the AWS [46] take advantage of this by sinking the device during storms; mitigating the need to overrate mechanical components to survive weather events.

2.7.2 Corrosion & Fouling

The secondary factors that make the ocean uniquely challenging are the corrosive and fouling impact it has on materials [102]. The high sodium content of the oceans has a strong impact even on coastal constructions that are near the water; accelerating oxidation of metals and stripping protective coatings.

In the context of a WEC, if corrosion is left unchecked, it can damage to the material, weakening the structure and eventually allowing water ingress, possibly damaging the PTO inside. The impact of corrosion is well understood in material science and is controlled by metal plating, inhibiting chemicals, and sacrificial coatings.

Sea life tends to congregate around subsea objects for resources and shelter, causing a build-up of biofouling on the WEC [103]. When any surface is submerged in water it is

coated in organic polymers in a matter of minutes. One day later bacteria and diatoms form a biofilm, or "slime". The biofilm provides a nutrient-dense attachment surface for the better-known biofoulers. First, soft biofouling such as algae and seaweed within a few days. Lastly, the hard biofouling such as molluscs and other calcareous organisms [104].

Biofouling has a serious impact on any applications involving contact with water and impacts industries from medical to shipping [105]. Antifouling techniques have been established for hundreds, if not thousands of years, and are still being researched today [106]. The key functionality of antifouling is to prevent the formation of biofilm, through non-stick coatings, ultrasonic waves, and UV light treatment. Once biofouling has taken hold of an object, methods such as heating, high-voltage treatment, and chemicals are often applied to remove it.

2.8 Conclusions

This chapter has explored the history of wave energy converters, and the physics that drive them have been established. Topologies of WEC and PTO have been broken down, their feasibility assessed, and the challenges faced by the industry established.

2.8.1 Research Gaps

By the lack of its maturity, wave energy struggles not with small research gaps, but rather too many research gaps, and an unclear way forward. Wave energy is well suited to take a significant market share of energy production and niche energy supply applications. However, the two major parts of wave energy - WEC and PTO - remain too isolated from one another. It is insufficient for each to continue being researched in isolation without considering the other. Some promising wave energy proposals have failed due to having no feasible PTO such as Salter's Duck [38], or due to the selected PTO having too high maintenance costs [9].

There must be further efforts committed to combined design studies, bringing both parts together, even if it requires that the hydrodynamic complexity be reduced to accommodate joint studies. Furthermore, an additional understanding of how PTOs can be integrated into a WEC in a stable and maintainable way must be expanded upon before wave energy can become commercially viable.

2.8.2 Consensus & Controversy

Due to the early state of wave energy development, there is a lack of topological convergence. There is some agreement that large monolithic devices like the "Edinburgh Duck" are challenging to achieve economic feasibility due to their high operation and maintenance costs [51]. This is backed up by the trend to focus on smaller point absorber designs [23]. The option to simply remove a smaller-scale device or module from a network or

energy farm simply cannot be understated, and it could become the driving force behind a competitive LCOE in the future.

It is not clear what the most common use of wave energy will be, but it is somewhat likely that research continues to drive forwards on electrical power generation applications, such that it can claim its fair share of the energy mix.

2.8.3 Integration Into Thesis

This thesis aims to expand upon the existing literature by addressing the current gap of lacking integrated design studied. This thesis tackles this by selecting a topology of WEC and assessing it with a combination of hydro and electromagnetic design models. Furthermore, it employs the due diligence of addressing how a relevant PTO can and should be integrated into the structure of the WEC selected.

Chapter 3. Direct Drive Machines for Wave Energy

3.1 Introduction

Electric machines have long provided the world with a mechanism of locomotion and power generation. Electric machines are of course, not restricted to just high-speed power generation or driving electric vehicles. The advent of rare earth permanent magnets [75] has allowed machine sizes and topologies to be tailored to the application it fills [107, 108, 109, 110].

The directly driven (DD) machine is a more recent and much more extreme example of topology adaption for niche applications, especially the linear configuration [91, 111]. DD machines are fairly recent developments because, before the invention of rare earth permanent magnets (PMs), the only option for constructing machines was with either electrical windings or weaker ferrite magnets. In low-speed DD applications, the ferrite magnets have poor low-speed voltage and can often be outperformed by alternatives but are still considered for some applications [112, 113].

In DD applications, an electric machine is coupled directly to the prime mover without any intermediate mechanical interaction. By removing the need for intermediate gearing, the power train is greatly simplified, offering potential savings in cost and mass, while increasing system reliability.

The gearing serves an important role, and its removal from the system introduces unique requirements and challenges to the electric machine. Conventional machines operate at high speeds and low torques which is incompatible with some applications. When an application requires or produces low speed with high torque, a gearbox can be utilised to transpose the speed and force to that of the load. In practice, this allows for a range of standardised electric machines and gearboxes to fulfil the needs of many applications.

With the gearbox removed, the DD machine must be designed such that it can provide the requisite speed and torque directly, making it very bespoke to the application they are designed for.

When proposed for use in a wave energy converter (WEC), there are further challenges introduced. Because the electric machine is coupled directly to the prime mover, there is no mechanical power smoothing or consistency. The incoming power is converted from mechanical to electrical indiscriminately. Because of this, the electrical conditioning needs can be displaced to the electrical system; leading to challenges in electric converter design [99]. Although, the cost of power electronic systems has reduced at a high rate in recent decades. Additionally, because the motion of WECs is often oscillatory, so is the motion of the electric machine, resulting in a waveform that varies in both frequency and magnitude, exacerbating the electrical converter needs.

The adoption of DD has become much more widespread in renewable energy applications, with multi-MW wind turbines seeing significant development [114, 88, 109, 115]. Wave energy is slower in the adoption, but sees many proposals [89, 110, 116]. However, despite their high level of academic interest, they are yet to be commercially adopted; DD has not yet received the same standardisation and over-the-counter accessibility of conventional electric machines. Because of this, DD devices are usually designed bespoke to the application, with the costs and lack of robustness that comes with it; it is not uncommon for experimental machines to combust during tests, or have magnets detach.

3.1.1 Scope and Objectives

This chapter intends to take a close look into directly driven machines and the current state of the technology. This thesis however is somewhat split between electrical machines and hydrodynamics. Therefore, it is insufficient to only address DD topologies in isolation; but rather address them from the perspective of wave energy, taking into consideration how the ideal machine is impacted by the unique design challenges imposed by it.

It is important here to outline the scope that this requirement imposes on the chapter. Ordinarily, a thesis focused on electric machines for wave energy touches upon the importance of wave energy and makes clear that it is the target application, but stays focused on machine improvements, giving thorough details of the physical phenomena that drive them. This thesis on the other hand, although applying the same principles, does not repeat them here for the sake of brevity.

3.2 About Direct Drive Machines

Electric machines are a method of converting mechanical energy into electrical energy (generating), or electrical into mechanical energy (motoring).

For a long time, the status quo of conventional machines has been to operate at high speeds and relatively low forces with semi-constant load for maximal efficiency. Usually, this comes in the form of a synchronous machine for generating and an induction machine for motoring. These have each become standards unto themselves because they are very efficient and mechanically stable, requiring little maintenance; the induction motor particularly is legendary for its life span, lasting decades [117].

In applications that have different operating requirements, such as low speed with high torque, or high speed, or high precision, it can be more desirable to adopt other machine topologies, such as direct drive machines as is the case of wave energy.

3.2.1 What is Direct Drive

Direct drive machines aim to replace the gearbox stage of the chain from primary mover to usable electrical power. It does so by dropping conventional design principles entirely, instead reacting to the large and slow forces directly. By having a small enough pole

length, the magnetic flux can be rapidly cycled, allowing for high electrical speeds relative to the mechanical displacement. In such machines, they effectively work as a generator and gearbox as one.

High-force electric machines received their first serious proposal as a Transverse Flux Machine (TFM) aimed at improving the power density of linear motors [118]; achieving a high force density at low current density. This proposal was a fully wound topology and suffered from high end-winding losses.

Several years after the conception of rare earth PMs [75], the application of gear-less machines was fully realised [119]. Although the TFM is regarded to have an extremely high force density, their utilisation of a three-dimensional flux path demands a highly complex structure that is difficult and costly to manufacture [120]. Moreover, in [121], the authors claim that surface-mounted PM machines are better suited for high overload torque.

DD machines have thus far been described as high-force and low-speed devices; however, this is not exactly the case. More accurate is the replacement of gearboxes with intrinsic machine properties. They are suitably designed for any force/torque and speed application, not only slow renewable energies. In the transportation sector there are promising developments for electric car motors [107], and shipping propulsion [108, 122].

3.2.2 Direct Drive for Renewables

In the context of renewable energies such as wind and wave power, the concept is functionally the same but has a few added requirements and constraints attached. A 10 MW wind turbine rotating at 10 rpm reacts 8.5 MN m of torque, significantly higher than the < 1 kN m produced by an electric car and operated at a lower speed. DD for renewables is the most extreme form of the technology and the furthest away from conventional topologies that it reaches.

For wind turbines, DD machines have received commercial success in the form of a direct drive synchronous generator. However, this topology is revealed as the most expensive and heaviest alternative to conventional wind turbine power take-off [88].

Advances in flux modulation topologies have enabled electric machines with inherent magnetic gearing. Topologies such as the vernier hybrid machine (VHM) and flux reversal machine (FRM) have long been proposed in academia [94, 123] and have recently been adopted by WEC developer Mocean [124]. Both topologies are somewhat descending from the high shear stress TFM but reduce the flux path to a more conventional 2 dimensions; allowing for cheaper machines with simple constructions.

FRMs and VHMs achieve a high shear stress due to their slotted rotors applying introducing a flux concentration effect. Numerous studies have been conducted into flux concentration techniques, revealing mechanisms of voltage/force density optimisation and novel magnet configurations [95]. However, it is well known that modulated machines such as the TFM, FRM, and VHM are dependent on energy exchange in the airgap. This

maintains a large quantity of reactive power, branding the machines with a very low power factor [94], but more recent proposals have allowed for power factor improvements with alternative configurations [125, 126].

Another path to high-speed flux cycling from a low-speed machine is magnetically geared machines. These machines in effect use magnet interactions of multiple rotors to transpose velocity and torque between them. Due to the demands of their design, there are typically multiple layers of moving magnetic materials in close proximity. Their complex design has proven to be the limiting factor of the topology, and it is not currently feasible to produce them commercially. Despite concerns about cost-effectiveness, the magnetically geared topology proves to be a promising replacement for gearboxes with some companies committed to their improvement [127, 128].

3.2.3 Negative Aspects

Renewable energy sources are often variable; for example, the wave energy resource in any given location varies with weather and season. A WEC transmits mechanical energy of variable power and velocity dependent on the current position along the wave, with higher or lower averages dependent on the time and season. Because DD eliminates the gearbox from its system, there is no mechanism to transpose speed or torque to more favourable values and must convert mechanical motion to electrical energy without any inherent power smoothing.

In wind turbines energy transfer is unidirectional in the sense that and power into the turbine contributes to the rotation and at loaded conditions the direction of rotation does not need to change, allowing for some power smoothing from the inertia of the turbine blades [129]. DD WECs on the other hand, often utilize oscillatory motion as the power take-off, precluding them from any inertial power smoothing. When an oscillatory PTO is applied to a DD WEC, the variability of power input is further increased. If the PTO is tracking a sinusoidal wave, the rotor velocity peaks at the sinusoidal origin and slows to a stop at the crest and trough before reversing direction.

This behaviour produces a doubly sinusoidal output during normal operation as can be seen from a VHM in figure 3.1. The high frequency element of the figure is due to the fast flux switching of the topology, which also varies with the linear speed of the rotor - manifested as a low frequency variation in magnitude.

As DD WECs don't have any reliable mechanism of mechanical power smoothing, the electric power output must by conditioned by a power converter before it can contribute to the local energy grid. Depending on the WEC and DD topology, this can require a sizable power electronical converter, driving up the LCOE. However, the converter size and cost are reducing in recent years thanks to the rapid growth of the power electronics field [130, 131].

In [99], the authors proposed that the output of a 100 kW WEC be inverted via an AC/AC conversion with a highly capacitive DC link to smooth out fluctuations [99], with

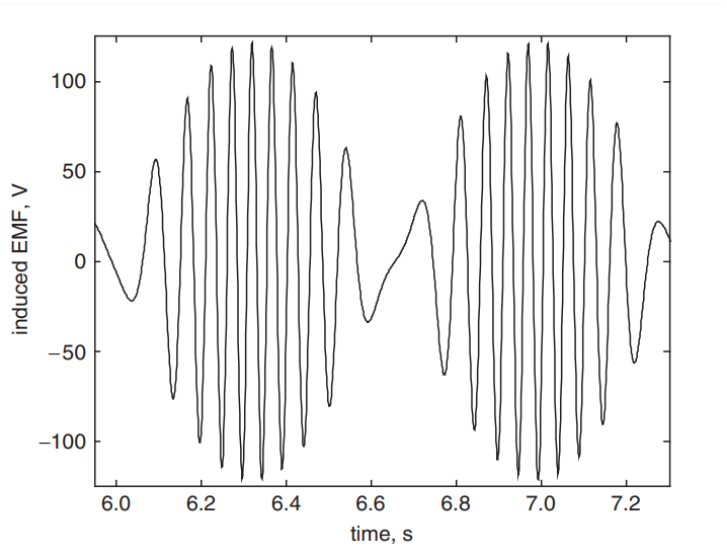

Figure 3.1: No load EMF output from a linear direct drive machine [99].

an estimated cost of £16000 (2005 prices). The authors go on to state that costs can be further reduced by sharing converters across devices in a wave energy farm.

One side effect of the high torque density in DD machines is a high airgap flux density above 0.8 T [93], as opposed to 0.2 T found in an induction machine [132]. The high airgap flux density consequently yields a high normal force which works to close the airgap and contributes no useful torque. Such strong airgap closing forces require significant structural mass to prevent the machine from destructively deforming. A study of MW level wind turbines revealed that the structural mass percentage rises as high as 88% of the total mass for 5 MW axial flux machines.

In three-phase rotary machines, the issue of airgap closing forces is somewhat reduced due to the partial cancellation of the forces around the machine circumference, and the ease of centrally located bearings. Linear machines on the other hand have challenging bearing designs and experience much less force cancellation. This is most apparent in flat topologies; however, some force cancellation can be achieved by tubular or multi-sided topologies [133].

3.3 Machine Considerations for Wave Energy

DD machines are a wide-spanning subject in themselves with many applications not restricted to low speed and high forces. However, to keep the chapter succinct, an effort is made in this section to lay out DD drive topologies from the perspective of their application to wave energy and fields with similar torque/speed requirements.

3.3.1 Wound vs Permanent Magnet

Throughout the years in academia and industry, there has been a debate on using coils or magnets to provide part of the machine magnetomotive force (MMF), whether that

be field, armature, or supplementary MMF. Historically, more attention has been given to wound topologies, however, long before powerful rare earth magnets were developed, there was still a strong hope and interest for the inclusion of permanent magnets into electric machines [134], with some authors suggesting they contributed to an explosion of electric machine topologies in the 1970s [135].

The advent of high-remanence rare earth PMs and cheaper power electronics were extremely disruptive and invited the establishment of numerous novel machine topologies. Rare earth PMs enabled efficiency and performance improvements to existing topologies, whilst cheaper power electronics made it feasible to use magnitude and frequency controllers for PM machines. By replacing a wound field with PMs, no field current is required, and mechanical commutation can be removed. Furthermore, PM inclusion was indispensable in the creation of high-speed motors without suffering as much from copper losses at high frequencies. They also, assist in the application of small motors and high-precision applications.

The vast majority of rare earth material Neodymium is in China, giving the nation a near monopoly on the PM industry from extraction to manufacture. The price and availability of rare earth PMs are highly dependent on the internal policies of China [136]. The concern has such a strong impact on the future stability of electrification that it has spawned branches of research dedicated to magnet reclamation [137, 138] and a revival of ferrite magnet designs.

It is also argued that the use of fully wound machines avoids other PM risks such as demagnetisation from thermal or electrical overload, making them more fault-tolerant overall. It is however hard to deny the applicability of PM machines in the context of renewable energies and most direct drive applications use PM generators.

3.3.2 Core Material

In many applications of electric machines, there is a question of whether air or iron-cored devices are more suitable for the application. In renewables, this is a particularly pertinent topic as the success of a renewable generator may depend on the generator's mass, for example, in a wind turbine the nacelle mass has a direct impact on the structural requirements of the overall turbine [139].

Electric machines often have a rotor and stator constructed from electrical steel or some other form of ferromagnetic material, which must be cut into slices (laminations) to reduce eddy current losses [140]. Electrical steel is highly permeable, allowing magnetic flux to cross the machine airgap with great efficiency. This allows for minimal MMF producing material and higher power density at the cost of a heavier machine. Although power density is an important research topic, it tends to be more relevant in transportation and aerospace applications where any mass saved has great benefit.

Air cored topologies, on the other hand, have the stator and/or rotor embedded into a non-magnetic and non-insulating matrix such as epoxy. By doing so, the machine

mass and cogging force can be dramatically reduced. However, because there is no highly permeable material to assist airgap crossing, a higher quantity of MMF producing material is required for the same rated power.

On the other hand, in high power DD renewable energy applications it has been declared that generators demand a disproportionately high content of structural mass [141]. To expand on this further, the high structural mass is required because the airgap closing force is a function of the airgap flux density; any deflection into the airgap increases the flux density, which can then increase the deflection and collapse the airgap. The acceptable deflection has been described as 10% - 20% of the airgap clearance, which in turn can be small as 5 mm for a 2.5 m radius machine [141], a challenging requirement. There are naturally more forces in the calculation of deflection, but the airgap closing force can be partially avoided by air cored machines. It has been demonstrated that despite requiring a larger active area, air cored machines can still retain a smaller mass overall [141]; although, the saving in structural mass can be offset by the increased PM mass.

3.3.3 Number of Sides in Linear Machines

In electric machines, there is always some level of airgap closing force which serves only to collapse the airgap and provides no useful work. In balanced rotary machines, the force is largely cancelled out around the airgap.

Linear machines on the other hand do not have any mechanism of force balancing between the translator (rotor) and stator. In the simplest form of a linear machine, it is an analogue of its rotational counterpart, with one rotor and one stator, often imagined by cutting a machine on one side and "unrolling" it (figure 3.2). Single-sided machines like that shown in figure 3.2 can develop extreme airgap closing forces making them challenging in practice, with multi-sided topologies preferred [142].

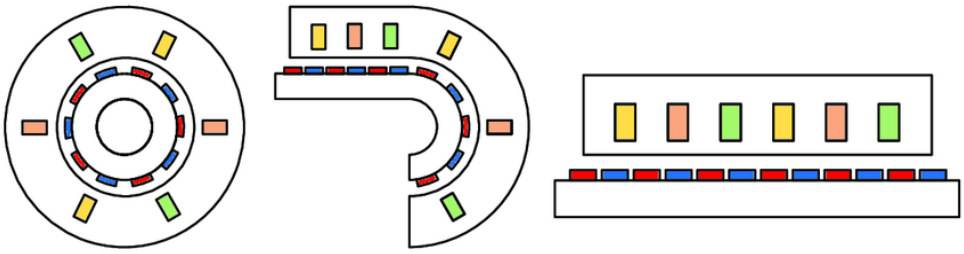

Figure 3.2: Simple concept of creating a linear machine from its rotary counterpart [143].

Modern linear DD machines were quickly updated to feature more stator sides [116]. Due to its relative conceptual and constructional simplicity, novel topologies and flux concentration methods are commonly reported in this configuration. By including a second stator or translator in the design, some force balancing can be achieved. If a translator is moving between two stators, it can be expected that each will have identical

attraction forces inwards or outwards from the translator, greatly reducing the force and making them more viable for real world applications.

Although double-sided topologies achieve some force cancellation, if the translator or a stator side were to deflect into the airgap through active deflection or manufacturing misalignments, the forces could become unbalanced and collapse the airgap. In their current stage of development, linear DD machines are always built bespoke with the lacking manufacturing tolerances of a non-standard product; it is not uncommon for modular machine constructions to have misalignments [124, 144].

Researchers have extended this idea further into the realm of multi-sided machines [145, 146]. By including more sides to the machine, it further increases the number of force balancing directions, and utilises a greater quantity of magnetic material than their flat counterparts. Further, because each side can be magnetically separated, it allows for modular constructions for simple maintenance and replacement. However, an increased number of sides naturally comes with higher edge effects and end winding losses. Furthermore, bearings and airgaps are much more difficult to maintain with more sides [146].

As the number of sides grows, comparisons are inevitably made to tubular machines. The tubular topology is the natural evolution of the multi-sided design, removing some weaknesses and introducing others.

One study compared a tubular and four-sided machine [145], finding that the two had very similar coil flux and induced voltage, but that the airgap flux density in the four-sided design was inconsistent around the corners. They also reported that the four-sided design came with 37.5% longer coils and 32.1% heavier iron than the tubular, yielding a less efficient machine; yet concluding that the four-sided machine is more attractive than the tubular variant due to manufacturability.

Apprehensions towards the manufacturability of tubular machines are not unprecedented, however. The difficulty stems from the laminations and lack of modularity. Tubular machines that utilise axial flux introduce challenges for laminations due to the circular cross section. However, it could be envisioned that the topology be split into magnetically independent units along the axial length, which are split in half and assembled around the translator. However, even in this case, the machine would need to be taken out of service to replace inner sections.

It should also be noted that for application into WECs, the tubular variant comes with a distinct advantage over others, relating to sealing. The current expectation for offshore DD WECs is that the PTO will be located at the WEC or on the seabed, with some mechanical motion between. It is not yet practical for the PTO to run flooded; although work in this area is beginning to see some attention [147]. There must therefore be a sliding seal into a dry housing for the PTO. Such a seal is possible to achieve, but multi-sided translators are likely to pose greater seal engineering challenges, possibly requiring the addition of a cylindrical shaft on the ends of the translator. The tubular machine, on

the other hand, is already cylindrical and needs no special alterations to be compatible with the seal unless a slotted translator is used.

3.3.4 Short Translator or Short Stator

A problem only found in linear machines is the consideration of translator and stator length. Because each part of the machine is linear and finite in length, one must be longer than the other to ensure constant active area. There will be inactive electrical or magnetic material in the longer member.

Which member is made to be the shortened one is wholly dependent on the topological construction of the machine in question. In more conventional topologies with a PM translator, it is argued that the stator should be kept short to ensure all coils are kept active to control ohmic losses in inactive coils [148]. On the other hand, others take a contrary stance that PMs are the most valuable resource and should be kept short, maintaining that ohmic losses from inactive coils can be controlled through power electronics without excessive switching losses [149].

In less conventional machines such as the FRM [91], VHM [150], and some configurations of the TFM [116], the PMs and coils are housed together on the stator. Having a completely iron translator sidesteps the compromise by keeping magnets and coils on the short member, spending mass, but not efficiency on the longer component.

3.4 Direct Drive Topologies

3.4.1 Conventional

In the context of wave energy, conventional topologies are limited by having a shear stress around 20 - 40 kN/m^2, far from the 200 kN/m^2 reported with a TFM [111]. When used in a high-force application such as wave energy, a conventional machine generally must have a larger active area than a TFM.

A comparison of conventional topologies for application as PTO in an Archimedes Wave Swing [116] found that a PM synchronous generator was the most suitable, with lower material costs, and superior efficiency when compared to an induction and switched reluctance machine; proposing that low speed was the cause for its success. However, the authors do go on to claim that a TFM can provide the same performance with much lower losses, albeit with higher construction costs.

3.4.2 Transverse Flux

The transverse flux machine is a historically significant topology that warrants description in any direct drive focused writing for historical context. The TFM is named due to the direction of flux paths within the machine. Unlike the more common longitudinal and axial flux machines, the TFM has a transverse flux path relative to the translator's direction,

creating an inherently three-dimensional flux path. This complex flux path and structure (figure 3.3) completely breaks conventional machine composition; allowing it to achieve both extremely high force density, at the cost of introducing manufacturing challenges.

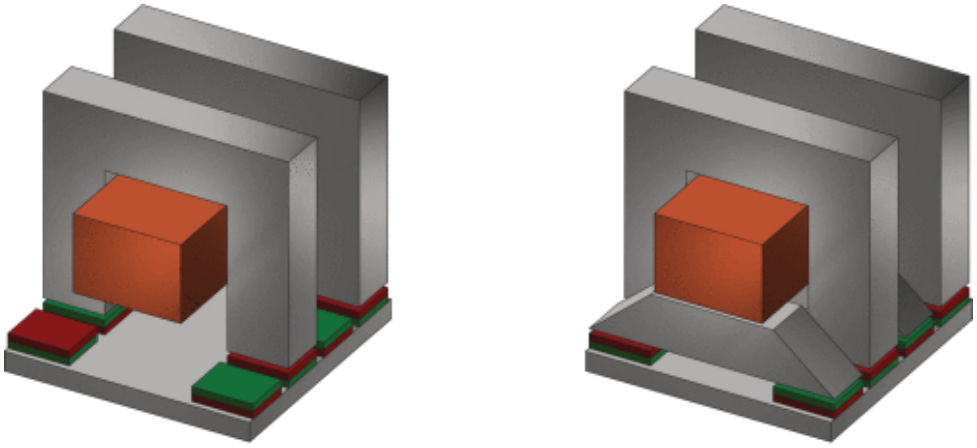

Figure 3.3: Linear transverse flux machine configurations [90].

The general torque equation for synchronous machines is given in [151] as:

$$\tau = \frac{3}{2} p \Psi I \tag{3.1}$$

Where p is the pole pairs, Ψ is the flux linkage of pole pairs, and I is the current.

In a conventional synchronous machine, if the pole pairs are doubled, the flux linkage per pole is halved. A TFM on the other hand has the majority flux path in the transverse direction, thus allowing for the number of pole numbers to increase with minimal impact of the flux linkage.

Additionally, conventional machines are commonly constructed of laminations of two geometries: one for the translator, and one for the stator. The number of geometries can vary and can be simple or complex. However, the number is usually minimal, making for simple manufacture and assembly, whilst providing mechanically robust components. The TFM on the other hand is built up of smaller components with no rigid connection; requiring a more complex support structure to provide the requisite mechanical strength.

Currently, it is considered to be uneconomical and impractical to manufacture TFMs. However, this sentiment is generally reserved for the rotary version of the topology. Moreover, in [152], the authors argue that conventional laminations are not possible in some linear cylindrical and tubular machines regardless, making reservations about 3D flux paths less relevant. Furthermore, academia has recently developed an interest in modular machine construction techniques, and best practices are described in [108, 122, 144]. Further developments in this area may be the disruptive change needed to bring TFMs back to the forefront.

3.4.3 Flux Reversal

The flux reversal machine was developed in a similar timeframe to the TFM but is often considered to be directory related [151]. This is due mostly to the FRM having the closest operational resemblance to the TFM of any flux modulation machine. The resemblance is due to all rotor teeth aligning with small magnetic poles which completely reverse the flux direction over a short distance. Additionally, the FRM has an impressively high shear stress, albeit smaller than the TFM [153]. However, the two topologies are fundamentally different from one another. Unlike the TFM, the FRM topology adopts the conventional longitudinal flux direction, enabling high force density without the high manufacturing costs.

The high force density is achieved through the complete alignment of rotor teeth per phase, combined with small magnet poles. This creates the same high rate of flux reversal and energy exchange seen in the TFM, bringing a low power factor with it. Furthermore, the integration of flux modulation principles enables both the armature and field sources to be located on the stator, allowing a rotor made completely of iron (figure 3.4).

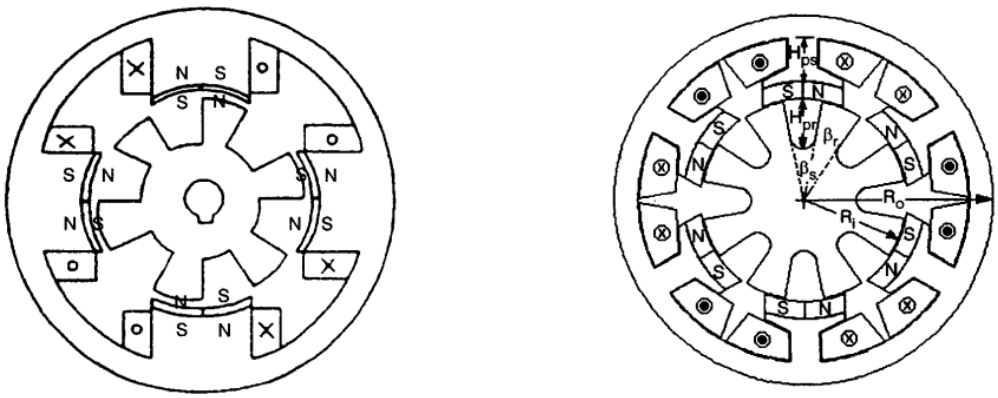

(a) Single Phase (b) Three Phase

Figure 3.4: Rotary flux reversal machines [92]

Such strong alignment of rotor teeth and magnets also provides the topology's greatest weakness. In an unmodified FRM, there is a very strong alignment force between the rotor tooth and magnet, manifesting as cogging torque. For any application, a large cogging force is undesirable; it increases vibrations and noise during operation, impacting the machine's lifespan, and decreasing performance in general. As a renewable source generator, on the other hand, strong cogging forces are particularly undesirable. If the force is too large, the PTO won't move in low sea states, potentially missing out on a wide bandgap of resources.

Fortunately, the mechanisms of cogging forces are well understood and can be reasonably reduced through rotor skewing alone [92].

3.4.4 Vernier Hybrid

Inspired by variable reluctance PM machines, the VHM was proposed to bring together the benefits of the Vernier Reluctance Machine (VRM) and the FRM to produce a machine with very high torque density, but without the high cogging torque [94] - hence the "hybrid" part of the name. An early design is shown in figure 3.5.

The VHM maintains the variable reluctance principles of the VRM but takes the major machine structure from the FRM. By moving the VRM magnets to the stator and adopting the discrete windings of the FRM, a simple structure is achieved, enabling modular designs and easy winding. Unlike the FRM, it has a slightly different number of poles and teeth. This presents a situation where the teeth have mismatched alignment patterns like that of a vernier gauge. Similar to the FRM, the magnetic pole and teeth are small, reversing the flux at a significantly higher frequency than the rotor.

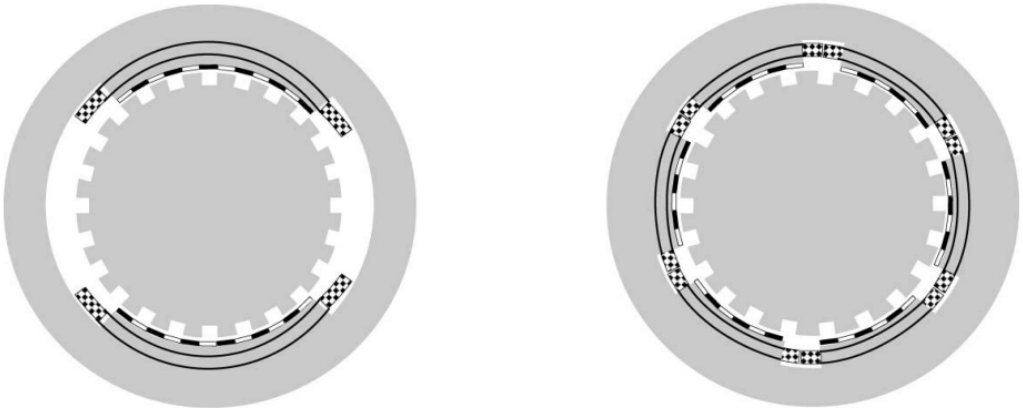

(a) Single Phase (b) Three Phase

Figure 3.5: Rotary vernier hybrid machines [94]

As with the previously mentioned members of the variable reluctance PM family, the VHM too comes with an unfortunately low power factor. In an exploratory paper addressing this, it was found that the low power factor is partially attributed to unusually low flux utilisation, but more specifically due to a low flux ratio IX/E [154]; going on to suggest limiting current to increase power factor. This point was expanded further by [95] who gave a power factor equation:

$$PF = \frac{1}{\sqrt{1 + \left(\frac{L_S I}{\Psi_m}\right)}} \tag{3.2}$$

Where L_s is the synchronous inductance, I is the current, and Ψ_m is the magnet flux linkage.

It is corroborated here that the power factor is negatively impacted by large current and inductance, or small magnetic flux linkage. In this case, the authors do not propose to limit current, but rather, optimise the VHM with alternative magnet and tooth topologies

for flux concentration and magnet mass reduction. By improving flux concentration, the authors increased the power factor from 0.38 to 0.72 without any major machine customisations. Other authors have made similar attempts to increase the power factor, through secondary stators [125], or by adding auxiliary DC windings [155]. Although the latter examples are arguably difficult to implement due to manufacturing or LCOE. It is possible to improve the power factor, and it should not be viewed as an unsolvable problem with the topology.

In toothed rotor machines such as these, force or torque is developed from the tooth edge. Thanks to the misalignment between teeth and magnets in the VHM, an advantage is gained over the FRM by reducing cogging torque. This is achieved because each tooth edge approaches the next magnet pole with differing angles, which when an average is taken, nets a much lower cogging torque.

Furthermore, because the VHM is more flexible in its number of rotor poles, it is possible to customise the flux harmonic components and alter machine performance. Fewer rotor teeth and more misalignments tend to reduce cogging torque, but also EMF [156].

3.5 Structural Mass

Concerns regarding structural mass are extremely important to address such that they can be understood and controlled. In DD wind turbines the machine structural mass raises the foundation costs and LCOE [114]. However, the turbine remains structurally sound and capable of deployment.

Wave energy converters, on the other hand, have an additional layer of difficulty in this area. Unlike most wind turbines, many DD WECs are likely to be either floating or partially floating. Because of this great care must be taken in the design of such WECs as a heavy generator may reduce dynamic performance, or outright sink the device.

WECs are by default fraught with compromises when selecting wave resources, depth and operability, PTO and maintainability, size and LCOE, and generator output vs cogging forces. Any mass saved is highly beneficial to WECs, widely expanding their applicability and changes in commercial uptake.

3.5.1 Structural Mass Sources

Numerous forces impact the structural mass of an electric machine and are described by McDonald [141] for a directly driven wind turbine as:

- Shear stress
- Normal stress
- Gravitational
- Dynamic

- Thermal expansion

3.5.1.1 Shear and Normal Stress

Shear and normal stress are the two critical magnetic forces within the machine. Shear stress is the useful component, enabling the development of force. The normal stress is directed across the airgap and serves only to close the airgap. In force dense or DD machines, due to a high airgap flux density, the airgap closing force is significant, requiring a well-designed bearing and support structure to prevent deflection into the airgap and catastrophic damage.

In the pursuit of force density optimisation, the shear stress is often maximised. Although the direction of shear stress makes it incapable of closing the airgap, most of the high shear stress topologies discussed thus far achieve high shear stress through flux density and flux linkage maximisation, which in turn drives up the normal stress. This relationship can be seen in equations (3.3) and (3.4). Any increase in the flux density yields a linearly proportional increase in shear stress, but a squared increase in normal stress.

The shear stress is given for a radial flux PM machine by [141]:

$$\sigma = \frac{1}{2}\hat{B}\hat{K}\cos\delta \tag{3.3}$$

And the normal stress by [141]:

$$q = \frac{\hat{B}^2}{2\mu_o} \tag{3.4}$$

Where $\hat{B}$ is the peak airgap flux density, $\hat{K}$ is the peak electrical load, δ is the displacement, and μ_0 is the permeability of free space.

There is not a great deal that can be done to reduce the normal stress in machines without impacting the electrical performance. A common solution is to adopt air cored generators [157, 158]. In doing so, the airgap is reduced, lowering structural requirements and providing a lighter machine. Although, it has been found that the cost is still higher [141].

A more interesting technique for structural mass reduction is design for force cancellation. Previously mentioned topologies have achieved this indirectly, such as multi-sided/tubular configurations, and the VHM's misalignment. The former serves to balance the forces between stator sides, and the latter to reduce through average force. One concept manages to take this even further with a C-GEN topology [159], which uses modular design and 3D flux paths to make an encouragingly high-performance machine with minimal structural mass.

3.5.1.2 Thermal Expansion

The thermal behaviour of machines is well understood. All electrical machines have thermal rises associated with each loss component, although this is usually dominated by the I^2R losses in the stator. [141] describes a radial flux machine having higher temperatures in the stator, yielding unequal expansion, and deflection into the airgap.

The thermal expansion of electric machines is inevitable, but management techniques are well understood [160]. Heat can be managed through natural convection, filling material, cooling jackets, sprays, or other systems. However, in the context of wave energy, the number of feasible cooling options is reduced. To remain economically viable WECs must be as robust as possible with minimal maintenance; cooling systems will drive up the costs.

3.6 Co-Design in Wave Energy

This thesis hopes to impress upon the reader that the design processes of WECs and their associated PTO is a complex topic, this much must be clear from the fact that a thesis devoted to co-design felt the need to split the topics across two chapters. Despite this, the co-design of elements in a WEC are a crucially important topic worthy of further research. This section aims to consult existing literature to address where they fit in the co-design model.

In the co-design of DD-WECs there could be defined a range of design elements required to achieve true co-design:

- Wave resource availability
- Hydrodynamic motion of the WEC
- Model of the PTO
- Structural mass of the PTO
- Control of the system
- Cost analysis
- Power conditioning
- Grid integration

Each research contribution towards the topics could be said to fit somewhere on a spectrum depending on how many elements are addressed, with each naturally adding to the challenge of the research and the required skills needed to successfully implement the project. As has been stated already, there are many projects that remain on the fringes having no interoperability with the other field. In DD this is usually research on

generator comparisons or optimization that are clearly driven by the WEC applications, but include no hydrological content except for framing the research as a case study [110, 150, 148, 124]. On the opposite side of the spectrum is research into WECs which are rich in hydrodynamic content, but either do not include PTO at all, or reduce it down to a mechanical spring/damper system [22, 100].

On the DD side of the spectrum there is often research framed as being WEC oriented but focusing on other co-design items, such as the generator structural mass [161, 159, 162], control [157, 133], or cost analysis [116, 95, 149].

Somewhere in the centre there are those contributions that find the co-design region between WEC and DD-PTO [133, 156] that this thesis is focused on. Although, they do not necessarily provide a true framework for full integrated design but appear more as a linear process that moves from hydrodynamic design towards electrical design.

Going past this point leads to what is considered as a "Wave to Wire" framework wherein all stages of the power conversion are modelled from wave hydrodynamics to grid integration. Achieving such a model is a significant challenge that requires strong skills in hydrodynamics, electromechanics, control theory, and power electronics. In [163] a summary is made in which different types of WEC are tabulated on which stages were modelled. It was found that at this time there were no true wave to wire models that include all stages, although some came close [164, 165, 166, 167, 168].

The framework for full wave to wire integration put forward by [163] disqualifies highly integrated models that do not implement non-linear effects of hydrodynamics from being a full wave to wire model [164, 167]. This could be considered as an extreme end of the integration spectrum and may not have been fulfilled yet due to the unique skillset required, and it may not be possible to deliver such a project in a research environment without a large team [166, 167], or being conducted in the context of a PhD thesis [164, 165]. In some applications, value and high-fidelity outputs can still be realised by linearizing some aspects of the design [169].

Although it is not always possible to achieve full co-design depending on the research context, there is still great value found in including several aspects of co-design from an early stage of wave energy converter design to uncover issues sooner.

3.7 Conclusions

In this chapter, a review of the literature on high torque density machines has been conducted with a focus on their applicability to direct drive wave energy converters. A conceptual background was given on what direct drive is, and how a machine can be suitable for direct drive.

Additionally, several machine topologies suitable for direct drive wave energy were introduced and the necessary considerations in the design of direct drive machines expanded upon.

Furthermore, the existing literature on the structural mass needs of directly driven

machines was further detailed along with the challenges faced when integrating the generators into wave energy converters.

Chapter 4. Mocean Case Study

4.1 Introduction

4.1.1 Mocean Energy

Mocean Energy is a wave energy converter (WEC) development company with strong links to research institutions. They are developing multiple ranges of WECs.

The Blue Star (figure 4.1) is intended to supply reliable electrical power to remote subsea applications, such as research equipment, remote control vehicles, and oil & gas infrastructure. To serve these applications, it has been designed to fit inside a 40 ft shipping container for ease of delivery, holds batteries for more consistent power, and is self-powered via solar panels.

The Blue Horizon is similar in concept and much larger in scale. It is purposed to contribute to electrical grids in coastal areas. The design of the WEC has been updated and optimised to reduce costs and improve performance; however, the operational principles are quite similar.

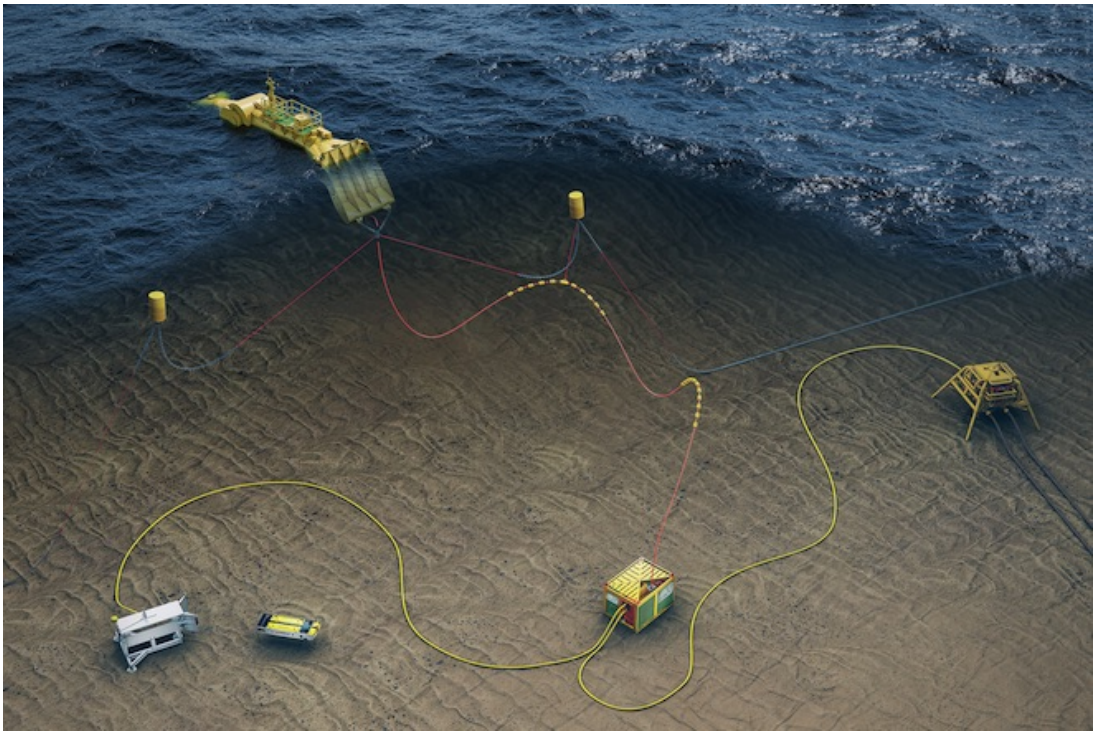

Figure 4.1: Mocean Blue Star concept art [170]

4.1.2 The Mocean Concept

The Mocean concept is a floating, hinged attenuator, comprising two buoyant hulls of differing lengths connected via a hinge. When a wave passes by the WEC, each hull

tracks the wave height at differing rates, allowing for a mechanism of power take-off to extract the mechanical energy from a wave into electrical power.

The attenuator topology of WEC has been proposed and developed by others [9, 39], but the Mocean device stands out by its unique design and optimised geometry that enhances its maximum sweep of motion and helps it to achieve a higher power density.

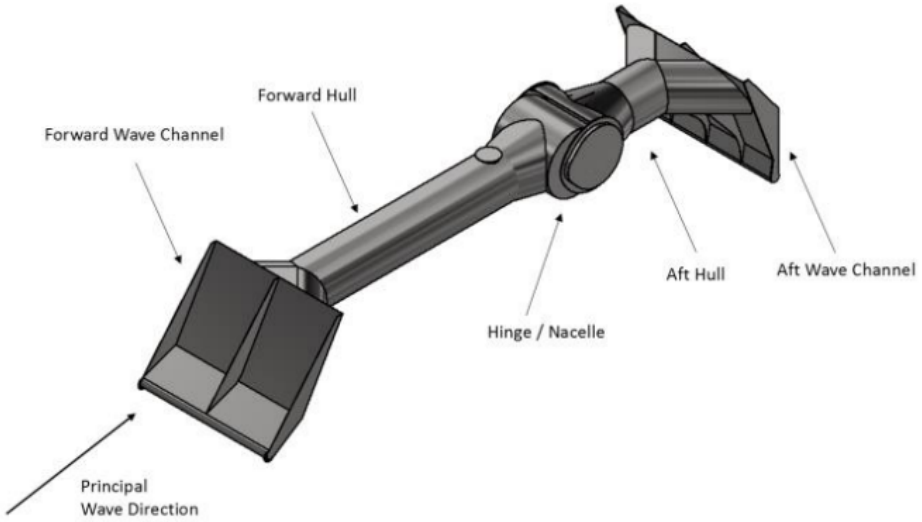

Figure 4.2: Diagram of the Mocean concept [171].

Hinged rafts have a distinct engineering challenge that must be solved; they tend to have a very small angular rotation of 10° or less. Moreover, despite this small angular displacement, one or more of the hulls periodically slams down as the wave falls, resulting in a large impact force. The concept addresses this twofold; the end pieces of each hull are designed such that on the downward slam, it does not simply crash against the water, but dives beneath it, enhancing the degree of angular rotation. Moreover, because the ends are designed like scoops, they entrap seawater, elevating the energy capture.

4.1.3 The Challenge

Figure 4.2 shows an outline of the Mocean architecture, including key structural features. The hinged section functions as the nacelle, within which the Power Take Off (PTO) must be housed.

The PTO requirements are:

1. Housed in nacelle
2. High power density
3. Extract power over small displacement at low speed

Mocean had in the past utilised a gearbox in their power chain but found it to introduce an undesirable inertial load which had to be accommodated by the rest of the chain.

The inertial load allowed the rise of a resonance that complicated control, and reduced reliability and performance. Moreover, the gearbox was not well suited for the abrupt reciprocal motion of the WEC, requiring an overrated gearbox to compensate for the high wear. The gearbox was considered acceptable for a demonstration device but was decided to be unsuitable for long life WECs [124].

In combination, all requirements demand that a directly driven (DD) machine be applied for the PTO; particularly requirements 2 & 3. Mechanical power in a rotational scheme is proportional to angular speed and developed torque. Therefore, because the WEC is limited in angular speed, it further enforces that a DD machine with high shear stress is considered.

4.1.4 Scope and Objectives

In this chapter, a comparison is sought to be made between directly driven machines for their suitability to be deployed in the Mocean "Blue Star" wave energy converter. Using this problem statement and findings from the literature (chapter 3), it is decided that the two most promising candidates for the WEC in terms of power production, torque density, and robustness, are the flux reversal machine (FRM), and vernier hybrid machine (VHM).

Here a case study will be developed as a framing device upon which to compare the two topologies in terms of their application to a specific "Blue Star" construction. The two topologies will be characterised, compared, and analysed concerning their electromagnetic performance, cogging profiles, thrust torque, and harmonic content. It should however be noted that this case study was limited in time and did not afford the capacity to perform an investigation of losses or a cost analysis.

Furthermore, a VHM prototype is constructed and presented for comparison and FEA validation.

4.1.5 Participants

This chapter is the result of collaborative work funded by an Innovate UK Smart Award. Those involved are as follows:

Mocean Energy: Initial electrical and mechanical design

Fountain Design Limited (FDL): Manufacture and testing of prototype

Newcastle University: Characterisation and optimisation for next iteration

Supply Design: Power electronic design

The goal of the project was to increase the technology readiness level and investigate whether the FRM or VHM are suitable machine topologies for the Mocean devices. While

all entities involved in the project were working towards a similar goal, they were each separate and independent in their findings.

Mocean Energy is the product owner and is responsible for the conceptual design of the WEC and provides the initial design electrical and mechanical design. In this project, the prototype was designed, manufactured, and assembled by FDL, with Supply Design providing the power electronic design required for adopting a direct drive PTO. The author is associated with Newcastle University and was responsible for characterising and optimising the proposed electric machine for use in the next phase of the development. This extended further to comparing the FRM and VHM for their suitability for application in the device.

Because the novel research in this chapter builds upon practical work from FDL, the chapter must contain some work from other parties to contextualize the research. For this reason, an effort is made here to clarify the contributions. All physical design, fabrication, and practical testing of the machines in this chapter was conducted by FDL, with CAD models and collected data made accessible. All figures presenting their work state so in the caption. The original work in this chapter begins where FDL's contribution ends. All FEA based research is an original contribution along with figures and results presenting FEA content, and any discussion around them. The connection between FDL and the original research is their experimental data, which was used to calibrate FEA models. CAD drawings developed by FDL are presented to provide a clearer illustration of the electric machine, they were not used directly in the FEA section but were used as a guide to design parametric FEA models.

4.2 The Flux Reversal and Vernier Hybrid Machine

Generally, VRPM machines are characterised by a series of magnets of alternating polarity and short pitch, permeated by toothed iron poles, providing rapid reversal of flux. There is some variation between topologies in terms of orientation and placement of magnets and coils and relative size of rotor tooth pitch and magnet pitch [95, 172]. Figures 4.3a and 4.3b shows a VHM topology with 10 magnets mounted on each stator tooth, encompassed by a single tooth winding. The rotor consists of regular teeth and slots to modulate the field. In this example, 9 stator teeth are formed into 3 phases.

Two topologies in this family are the Flux Reversal Machine (FRM), where the number of magnet and rotor pitches are equal, and the Vernier Hybrid Machine (VHM), where they are not. In an FRM, all magnets in a single phase share the same relative position with the nearest rotor tooth (figure 4.5). This results in a high flux linkage and hence provides good electromagnetic performance. Unfortunately, the high alignment between magnets and rotor teeth produces a strong cogging force. The VHM stems from the Vernier Reluctance Machine (VRM) and integrates the FRM structure by moving PMs to the stator and dropping distributed windings in favour of concentrated. It is from this mixing of topologies that it gets the "Hybrid" designation.

(a) Lab prototype constructed by Fountain Design Limited

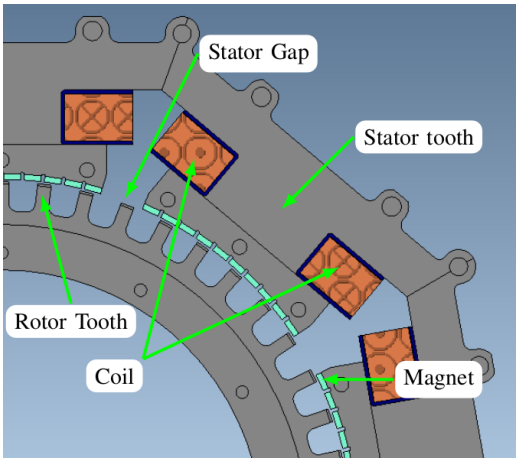

(b) FEA model

Figure 4.3: Vernier hybrid machine used in the case study.

The FRM and VHM are of fairly similar construction and at large pole numbers are quite difficult to tell apart. Both are adapted to place all magnetic material on the stator, leaving the rotor as a simple piece of laminated steel. The stators are split into modular shoes with concentrated windings around the core and a series of alternating magnets on the inner edge. Figure 4.3 shows a VHM with 10 magnets mounted on each stator shoe.

The reluctance variation is achieved in each topology by having slots cut into the outer rotor. As the rotor is displaced, each cycle across North and South polarity magnets over a relatively short mechanical displacement; achieving rapid flux reversal and the apparent magnetic gearing that these machines are known for.

In the VHM, the number of rotor pitches does not equal that of the magnet but instead is defined as:

$$p_r = p_m \pm p_c \tag{4.1}$$

Where p_r is the number of rotor poles, p_m is the number of magnet poles, and p_c is the number of coil poles. This relationship gives two possible designs that will form a part of this study. These are termed VHM(–) and VHM(+), where the symbol signifies the sign taken in equation (4.1) such that VHM(–) has fewer rotor pole pairs than magnet pole pairs, and VHM(+) has more. The VHM(+) has been shown to have a poorer induced voltage and hence loaded torque performance [173], however, it will be included in the study for the sake of fairness and comparison.

Because the pole numbers differ in a VHM and the spacing between stator modules is a non-integer, there appear patterns of misalignment between rotor teeth and stator magnets. Because of this, each tooth within a phase reaches its point of maximum torque at different displacement angles. Thereby creating a blended cogging waveform wherein, a kind of balance is struck between teeth and a smaller cogging torque profile overall. This intra-phase balance is also rotated 120° into the other 2 phases, achieving further

cancellation.

4.2.1 Cogging Torque & Harmonics

Consider a single tooth passing over a magnet pair with no current loading. For each electrical cycle there are 4 positions of zero resultant torque, corresponding to full alignment (d-axis) and full misalignment (q-axis), where the centre of the tooth is aligned with the point where magnets touch, see for example [174]. The first two points are shown in figure 4.4

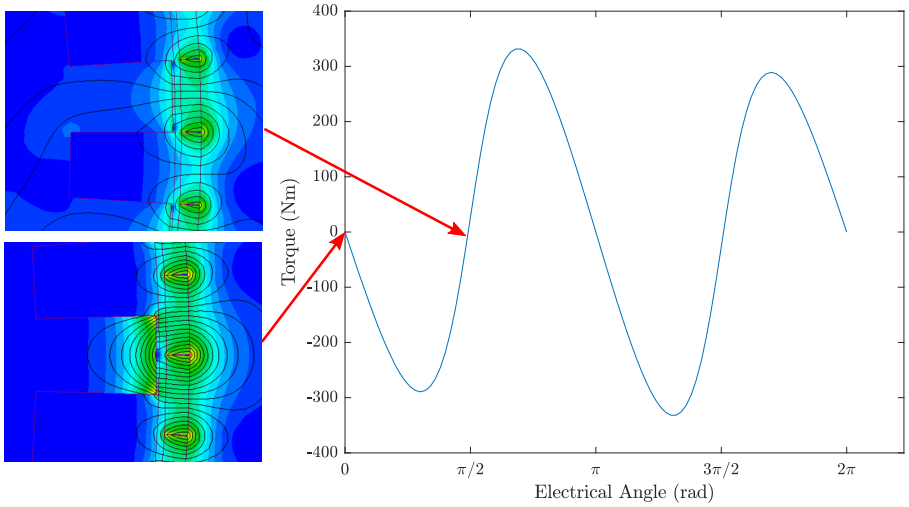

Figure 4.4: Torque waveform for a flux reversal machine with one phase active and the rotor positions marked.

The cogging torque can be approximated to the sum of a fundamental and a second harmonic. For a three-phase FRM, adjacent stator modules are separated by:

$$FRM_{gap} = n\frac{\tau_m}{3} \tag{4.2}$$

Where n is an integer, and τ_m is the magnet pole pitch.

The cogging torque for the full machine is then, the sum of three waveforms shifted by 120 electrical degrees. The fundamental and the second harmonic cancel out and so the idealised cogging waveform would result in a zero cogging force three-phase machine. Unfortunately, in practice, full cancellation is not achieved, and some harmonics remain.

Thanks to having a non-matching number of rotor and stator poles, the VHM can reduce the cogging force experienced. By having misalignment between rotor teeth and stator magnets, there is some cancellation between each phase and each magnet/tooth interaction within each phase. This has the side effect of also reducing the peak magnet flux cutting the coils. This should mean that in selecting an FRM or VHM there is a design trade-off between cogging torque and peak torque capability. However, in practice, the patterns of alignment and misalignment in the VHM introduce additional rotating

harmonics into the air gap, some of which do useful work and improve the performance of the VHM.

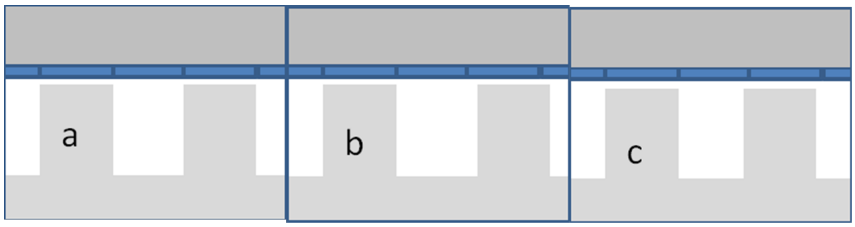

Figure 4.5: Relative tooth and magnet positions for a Flux Reversal (a), and Vernier Hybrid (b & c) variant. In all variants, the left-hand tooth is fully aligned with the magnet. In (c) the rotor pitch is less than the stator pitch, hence there is a higher number of rotor poles and a greater overlap of teeth and the stator pole.

4.3 Methodology

4.3.1 Prototype Details

In this study, it is desired to construct a device matching requirements set in table 4.1. As was described earlier, due to the type of WEC, the maximum speed of the generator is extremely low, operating at a maximum speed of 14.3 rpm.

Parameter	Value
Number of phases	3
Number of rotor pole pairs	51
Peak speed	14.3 rpm
Peak torque	1.85 kN m

Table 4.1: Parameters of case study

Because of the low speed, the generator must have a high number of poles to compensate and output a sufficiently high electrical frequency and avoid unreasonable power converter costs.

The dimensions of the constructed prototype are given in table 4.2 and describe the device with a very wide aspect ratio, having a quite large rotor radius relative to the core depth.

The materials used in the prototype are given in table 4.3.

4.3.2 Prototype Construction

The rotor is constructed out of a single stack of laminations with simple slotted geometry. The stator however is more complex in geometry and assembly. It is split into several discrete modules of identical lamination geometries, which are then assembled first into stacks, and then into a cohesive stator iron.

Parameter	Value
Outer rotor radius (mm)	307.5
Airgap length (mm)	2
Magnet thickness (mm)	5
Rotor slot depth (mm)	3
Lamination thickness (mm)	2
Axial length (mm)	100
Turns per coil	1300

Table 4.2: Prototype dimensions

Component	Material
Rotor Stator core	DD11 steel
Magnets	N42H
Adhesive	Ni Cu black epoxy
Coils	'Magnabond' CAB200 copper
Insulation	Tufnol

Table 4.3: Materials used in machine construction

This modular design of the stator maintains ease of construction regardless of the machine size and keeps costs as low as possible. Additionally, the machine utilises discrete windings, it is convenient to wind each stator module separately before assembly, allowing for simple winding and a higher possible fill factor. A higher fill factor in turn ensures the thermal performance of the stator is at its best.

The winding of a stator module can be seen in figure 4.6 as fabricated by FDL. Here it is shown that the stator coil is wound with a simple rotational winder where the module is rotated while the wire is held in tension. Additionally, the coil is held in place with an insulating guide. It can also be noticed in figure 4.6b that because of the high number of turns, the winding is quite thick relative to the module geometry and may struggle to stay in place if not for the guide. Moreover, as the winding reaches its maximum radius, it deforms the guide outwards. This is unlikely to have much impact on the electrical performance of the generator but seemed worth noting.

The magnets of the machine are designed to be as close to fully pitched as possible. However, it is difficult to assemble a machine where magnets are fully pitched; the strong attraction between them can cause slamming and shattering during insertion. In the prototype, small extrusions are marked out the inner edge of the stator modules to assist in magnet locating during adhesion, reducing the magnets to slightly less than fully pitched. These can be seen in figure 4.7.

The VHM prototype design can be seen in full in figure 4.8. Each subfigure shows a CAD model of the component once assembled. It should be noted that the rotor and stator have spoked support hubs to provide structural strength. The rotor has 6 spokes, and the

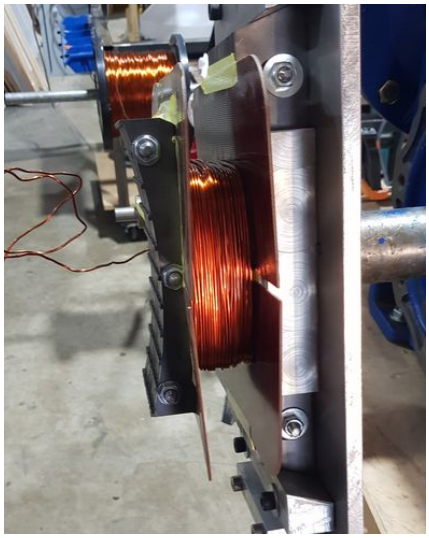

(a) Mid-winding

(b) Post-winding

Figure 4.6: Stator winding process conducted by Fountain Design Limited.

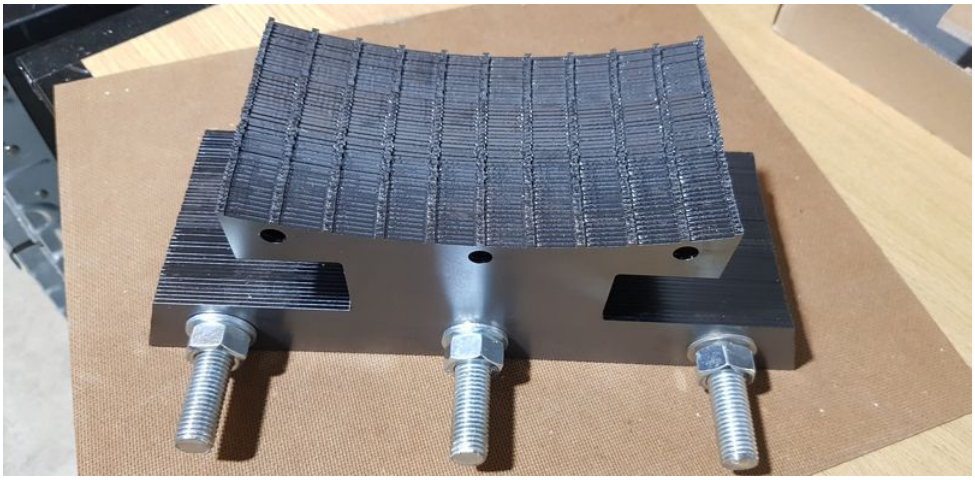

Figure 4.7: Empty stator module showing magnet locating ribs as constructed by Fountain Design Limited.

stator has 9, one for each stator module. It is done so because each stator module holds magnets and marks a point of high attraction force. The stator also has an additional support structure around the intra-module connection areas to prevent modules from slipping out of alignment.

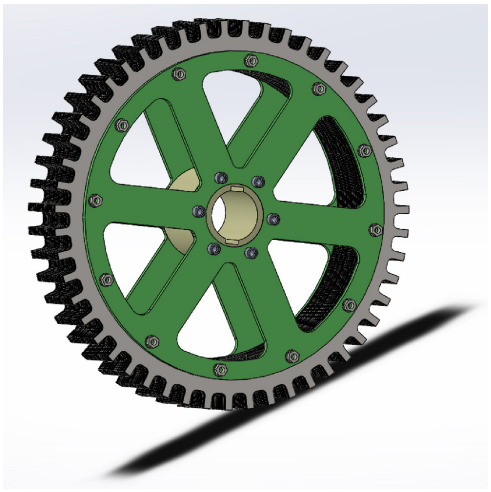

(a) Rotor

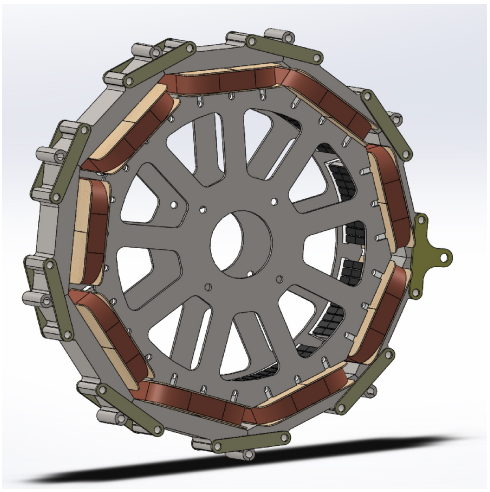

(b) Stator

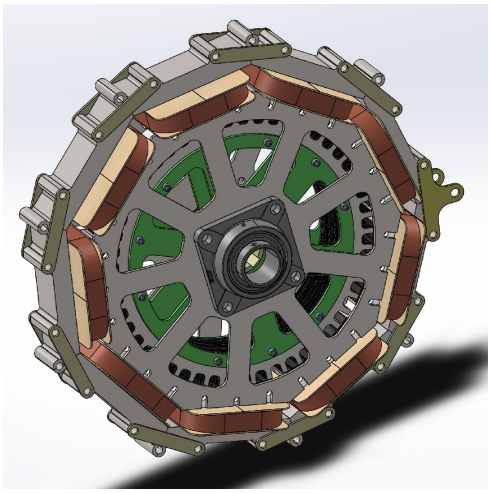

(c) Full assembly

Figure 4.8: CAD models of the VHM prototype produced by Fountain Design Limited.

4.3.3 Prototype Setup

Often, when a machine prototype is constructed, its behaviour is characterised by connecting it to a dynamometer. However, due to an appropriate dynamometer not being available during the project, it was decided to construct two identical prototypes and connect them to a common shaft "back to back" as shown in figure 4.9.

The performance of either machine can be assessed by operating one as a motor, and the other as a generator. This enables simultaneous monitoring of the prototype in both modes and allows efficiency to be calculated from the power input and output of each machine. Operating in this way provides a simple solution to assessment, provided that both machines are identical and without faults.

(a) Isometric (b) Side

Figure 4.9: CAD models of VHM test rig produced by Fountain Design Limited.

4.3.4 Justification of FEA Comparison

This chapter seeks to make a fair and direct comparison between the FRM and VHM topologies using Finite Element Analysis (FEA) and supported by experimental results. All simulation work was done using the software MagNet [175] in 2D mode.

The FRM requires a 120° spacing between phases to function, but the VHM designs do not. Therefore, an FRM cannot operate using a VHM stator, but a VHM can operate using an FRM stator.

If an FRM and VHM were designed using a spacing of $1.\dot{3}$ magnet pitches between the stators, the VHM(–) would not be feasible as the three phases cancel out. For this study, it is necessary to use different stator spacings for the two machine types. There hence will be a slight difference in the number of magnet pole pairs in the air gap circumference. Fixing the stator in this enables the major geometry of all topologies to remain consistent and the quantity of magnetic material to be fixed.

In all topologies, there are 3 coil pole pairs, and the rotor is a slotted and laminated iron structure. The FRM has 57 rotor pole pairs and the VHM rotor pole pairs are found from equation (4.1) to be 51 or 57 for the VHM(–) and VHM(+) respectively, as summarised in table 4.4.

	FRM	VHM(+)	VHM(–)
Stator teeth	9		
Magnets per stator tooth	10		
Magnet pitches between stator teeth	$1.\dot{3}$	1	
Coil pole pairs	3		
Magnet pole pairs	57	54	
Rotor pole pairs	57		51

Table 4.4: Machine configurations

In the FEA study, elements of the machine geometry were parameterised into a series of ratios. For example, the rotor tooth ratio is the rotor tooth width as a fraction of the rotor pitch. For all designs, the ratios were optimised for peak induced voltage.

4.3.4.1 FEA Mesh

The meshing properties used for the models are shown in figure 4.10 highlighting the mesh at varying levels of zoom. Features of the prototype, such as holes, lamination bolts, and coil guides were omitted in the FEA model.

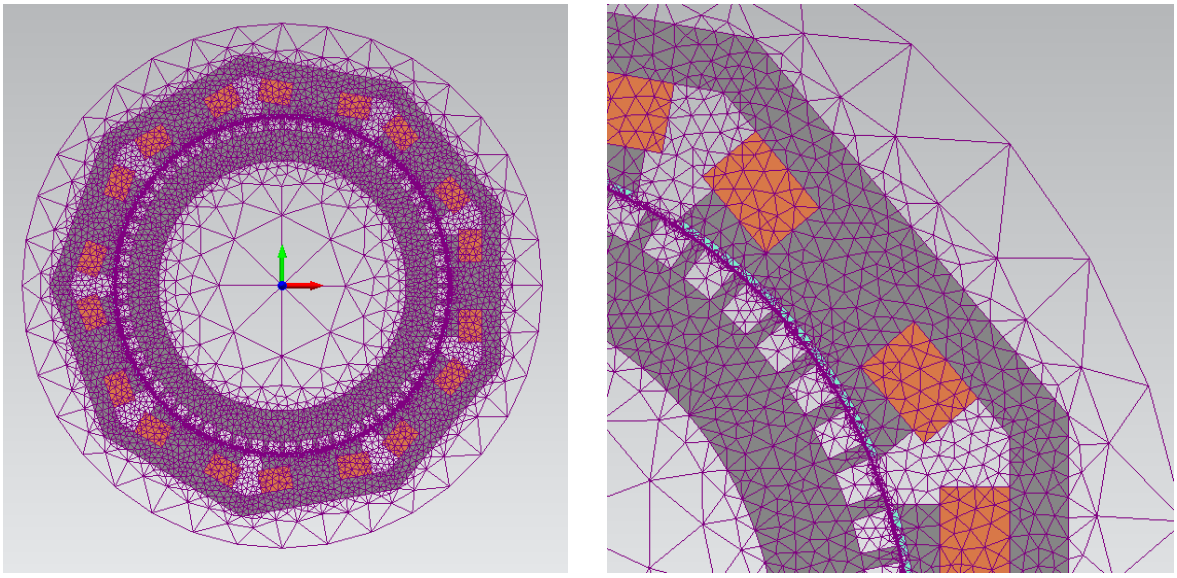

(a) Full model

(b) Single module

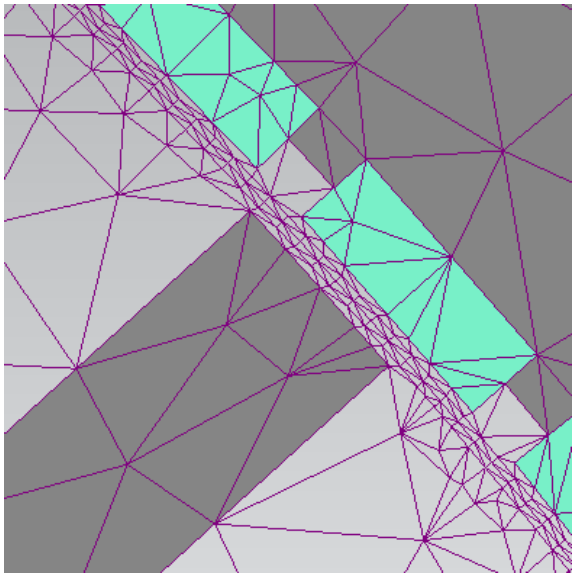

(c) Tooth, airgap, and magnet

Figure 4.10: Mesh used in the FEA validation model for a vernier hybrid machine.

Because the VHM and FRM topologies have a high airgap flux density and high rate of flux reversal, most of the coenergy is stored in the airgap. For this reason, the airgap is a crucially important area and requires a fine mesh. To achieve this, the airgap is split into four regions:

- Rotor remesh
- Inner airgap

- Outer airgap
- Stator remesh

The inner and outer airgap provide the fine mesh and are split into two regions to further refine the mesh into two layers. The rotor and stator remesh regions are separate from the airgap regions to prevent overly dense elements in non-critical areas and minimise solving time. Figure 4.10b shows the remesh regions best. The area between rotor teeth and stator modules is less important and can have a coarser mesh. Meshing can be done with fewer regions and a weighted mesh, but splitting into four regions allows for a tight airgap mesh with well-defined edges.

The remesh regions occupy 25% of the airgap, and the airgap regions cover the central 50% of the airgap, split evenly between them.

4.3.5 Experimental Comparison to FEA

As a means of evaluating both the modular prototype quality and accuracy of FEA models; a comparison between the two is made. There here has been one topology constructed - A VHM with 51 rotor poles and 54 stator poles. This is used to confirm the validity of corresponding FEA models, which are then manipulated to study the VHM topology and two other similar ones.

4.4 Experimental Validation

4.4.1 Notes on Modular Design

The prototype was built modularly to alleviate the common wave energy converter concern of maintenance; if there is a failure, a single module can be swapped out for repair.

Due to imperfections of the stator modules and eccentricity of the rotor, the airgap varied around the circumference and in time. This yielded diverse performance across stator coils and is apparent in the results.

VRPM machines require a small airgap to perform well, 2 mm in the case of this VHM prototype. Because of this, an airgap change of 0.5 mm represents a quarter of the airgap length. This makes the topology and machine family highly susceptible to irregular airgaps and require tight tolerances to succeed in modular form.

4.4.2 Comparison

Experimental and FEA models were driven at 0.5159 rad/s and the result of one electrical cycle is displayed in figure 4.11a including the highest and lowest voltage producing stator coils. The issues during manufacture produce slight deviations in the stator modules from the designed specifications, resulting in a magnitude difference of 13.87% between the highest and lowest modules. One electrical cycle for the maximum and minimum peak amplitude are plotted with the FEA results for comparison.

It should be noted here that the waveforms do not end at the same time in figure 4.11a because the rotor speed was not constant through the experimental measurement. This is problematic because the voltage is proportional to the rotor speed. For fairness in the comparison, all 3 waveforms were scaled to 1 rad/s and plotted against the electrical angle across one cycle, shown in figure 4.11b.

In the unaltered output, there is a Root Mean Squared Error (RMSE) of 14.40 V (19.2 %) and 8.01 V (10.7 %) between the FEA result and the lowest and highest experimental data respectively.

This validates the simulations, which are now used to compare the FRM and VHM topologies.

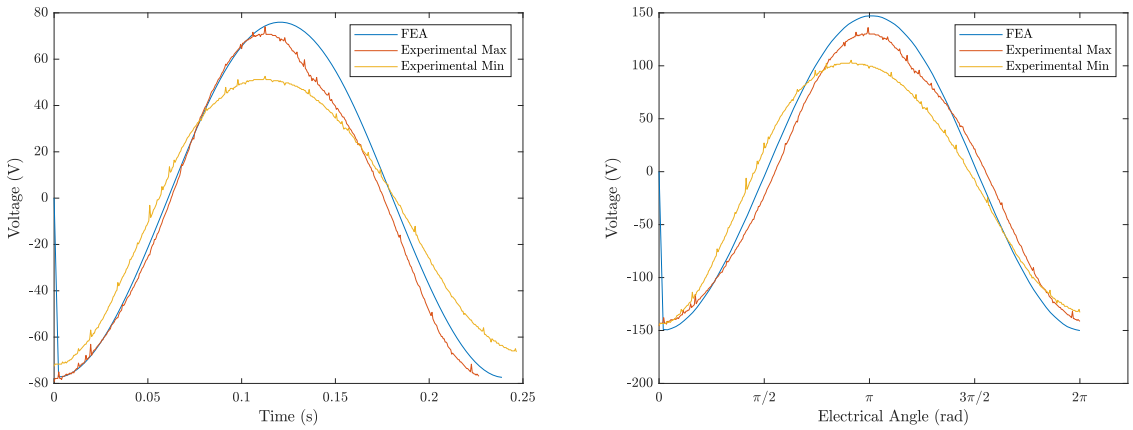

(a) Unaltered output

(b) Scaled to 1 rad/s and normalised to one electrical cycle

Figure 4.11: FEA model compared against the maximum and minimum peak induced voltage from experimental data.

4.5 Simulated Fully Pitched Comparison of FRM and VHM

Three FEA models were used to compare the flux reversal and vernier hybrid machine in terms of induced voltage, cogging torque, and thrust torque.

Before the results are discussed, a brief explanation of the parameterised ratios should be made. Two ratios regularly referred to in the analysis are:

Rotor Fill Ratio mechanical rotor tooth width to rotor pitch width

Magnet Fill Ratio of magnet width to magnet pitch

The magnet fill is set to unity, i.e. fully pitched, and the rotor fill is set such that the rotor tooth width is equal to the width of one magnet.

4.5.1 Unloaded

The three topologies were simulated via FEA at a constant speed of 1 rad/s across one electrical cycle at open circuit.

Figure 4.12a shows the unloaded induced voltage normalised across one electrical cycle.

The VHM(−) achieves the highest induced voltage of 142.83 V and the FRM and VHM(+) are 0.62% and 18.20 % respectively.

As explained in section 4.2, the magnets simultaneously reach complete alignment with the rotor teeth in the FRM, enabling the maximum flux linkage possible without using flux concentration techniques.

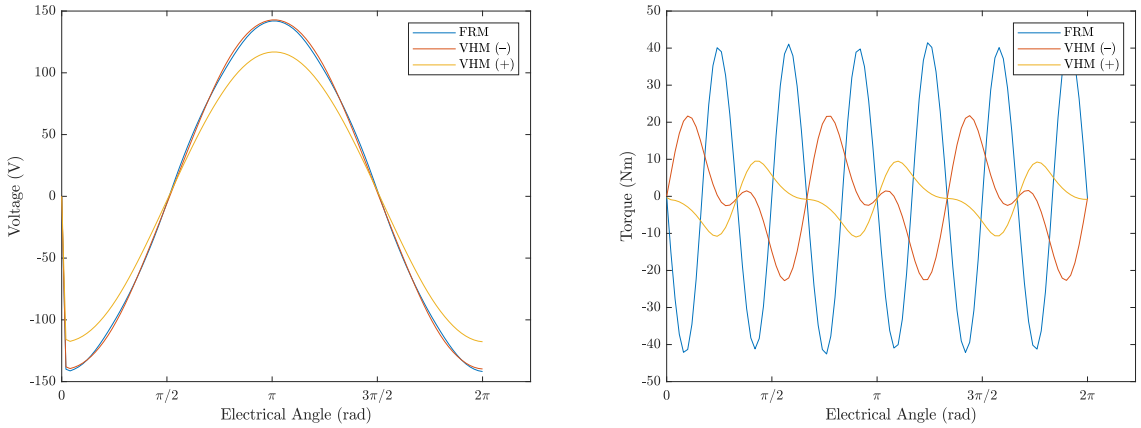

(a) Induced voltage

(b) Cogging torque

Figure 4.12: Electrical performance with no load

Applying only this logic, the VHM designs might be expected to have a lower voltage amplitude as the intra-phase magnets reach the peak flux position in offset patterns, reducing the overall flux linkage by intrinsic operation. In practice, this is partially true, but only for the fundamental harmonic. In the VHM, by having a mismatch between the rotor pole and magnet pole number, there is the additional effect of introducing stationary and rotating harmonics into the air gap [176]. Depending on the specific pairing of poles in the machines, some of these harmonics do not cancel out between phases, impacting induced voltage and torque production positively or negatively. In the case of the VHM(−), it can compensate for alignment flux linkage loss and competes well against the FRM. The VHM(+) however, develops little benefit to the induced voltage.

Because each plot for induced voltage is sinusoidal, the discussion of additional harmonic components adapting the performance of VHMs is not visually clear. Harmonic analysis is out of scope for this section and is expanded upon in section 4.5.4. The impact of harmonics is more visible in the cogging torque of the three machines.

In figure 4.12b, it can be seen that the previous description of the FRM holds. There is a strong 6^{th} harmonic dominating the waveform at a 40.1 N m magnitude and having the appearance of a pure sinusoid. The waveform in this case is simple. Across one electrical

cycle, each phase passes two points of maximum alignment between magnets and teeth, yielding six peaks overall. The reason for such purity in the FRM is due to the fully pitched configuration. If the tooth width were not equal to the magnet width, it would allow for the interaction of other harmonics (section 4.5.4). The integration of further harmonics serves to reduce cogging torque at the cost of a lower induced voltage.

The VHM topologies have lower cogging torques, 45.94% and 76.33% for the VHM(−) and VHM(+) respectively. The misalignment of rotor teeth causes the torque from individual tooth/magnet interactions to partially cancel out, especially in the VHM(+) where the cogging torque is lowest. This leaves behind a mixture of a 3^{rd} and a 6^{th} harmonics. Unlike the FRM, the VHM designs are founded upon misalignment and are free of the ideal of equal tooth/magnet width. For the VHMs, variation of magnet and rotor fill allows for some tuning of harmonics in the airgap. In doing so, a most customisable balance between cogging torque and voltage can be found. However, the optimal tooth and magnet fill tend to yield a compromise between the two.

In the hinged Mocean device, a high cogging torque will prevent motion between the hulls at low wave amplitudes, reducing the energy capture bandwidth.

4.5.2 Constant Current Density Electric Loading

To assess the loaded performance of the three models, they were simulated at 1 rad/s under a fixed current load of 2 A_{rms}/mm^2 for one electrical cycle, and the results presented in figure 4.13. The electrical load was achieved by controlling AC current in each coil to be in phase with the back EMF.

The three topologies achieve similar loaded voltages where the VHM(+) achieves the highest magnitude, and the FRM and VHM(−) are 5.46% and 13.66% lower respectively

Figure 4.13 shows the back emf and torque profile for the three considered designs. The summarised results for torque production are shown in table 4.5. The FRM and VHM(−) are shown to have approximately equal average torque of 2500 N m, with the VHM(+) delivering around 20% less. Despite quite different cogging torque amplitudes in unloaded conditions, all variants have similar cogging torque percentages.

Topology	Average (N m)	Ripple	
		(%)	(N m)
FRM	2548	11.48	292.51
VHM(−)	2519	12.04	303.29
VHM(+)	2034	12.09	245.91

Table 4.5: Summary of loaded torque of three designs

Table 4.5 shows that the VHM(−) maintains the electrical performance of the FRM quite closely. The topology effectively reduces and smooths the cogging torque, without enforcing much compromise upon the rest of the system. It is also clear that not all VHM configurations are created equally; the VHM(+), although initially promising with

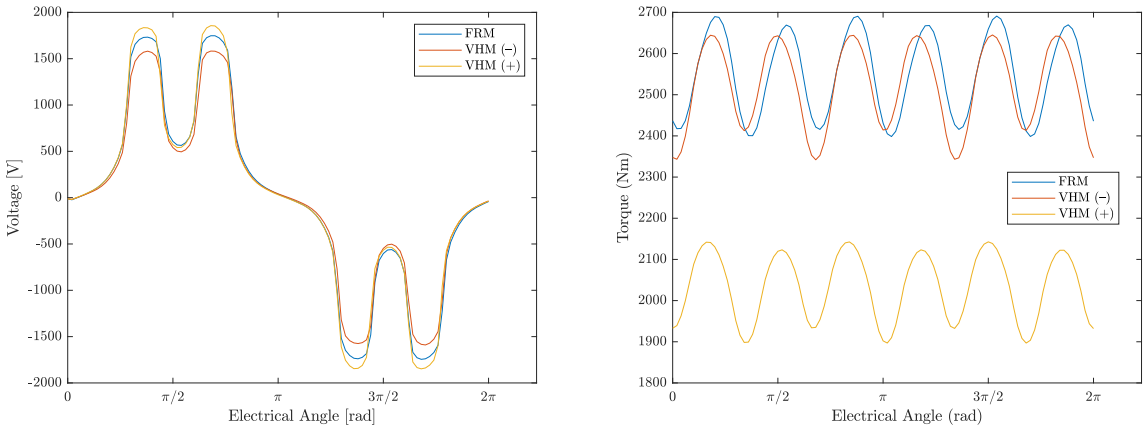

(a) Voltage

(b) Thrust torque

Figure 4.13: Electrical performance at current density 2 A_{rms}/mm^2

the smallest cogging torque, brings upon similar reductions in no load EMF and loaded torque production.

This is the electrical performance at one current loading condition and is a small window into the machine characterisation. This represents the machines in unoptimized and fully pitched tooth/magnet configurations. Performance changes can be made with adaptions to geometry or flux optimisation.

Depending on the deployment location and target wave states of the WEC, the VHM(+) could be seen as a strong candidate. Lower cogging torque would enable the device to capture weaker wave energy states, shifting the capture bandwidth towards lower ranges. However, this is not the case in the case study at hand. For the WEC in question, high power density with acceptable cogging torque is more favourable, making the VHM(–) the preferred configuration. The Mocean WEC is marketed to fit inside a 40 ft shipping container. A tight form factor and high-power density are essential to keep within transportation constraints and ensure the limited buoyant load capacity is not exceeded.

For these reasons, the VHM(+) is henceforth dropped from further consideration in this section such that additional focus and analysis can be placed upon the FRM and VHM(–).

4.5.3 Rotor Tooth Sensitivity

In the previous sections, the rotor fill was set separately to fix the width of rotor teeth to that of a single magnet. In this section, the rotor fill was varied from 0.1 to 0.7 in steps of 0.025 for the FRM and VHM(–), while the magnets remain fully pitched. The simulations were conducted under no-load conditions at a rotational speed of 1 rad/s and the results are presented in Figure 4.14. The voltage magnitude is presented as a smooth line on the right axis, and the cogging torque is shown by bars for the maximum and

minimum values.

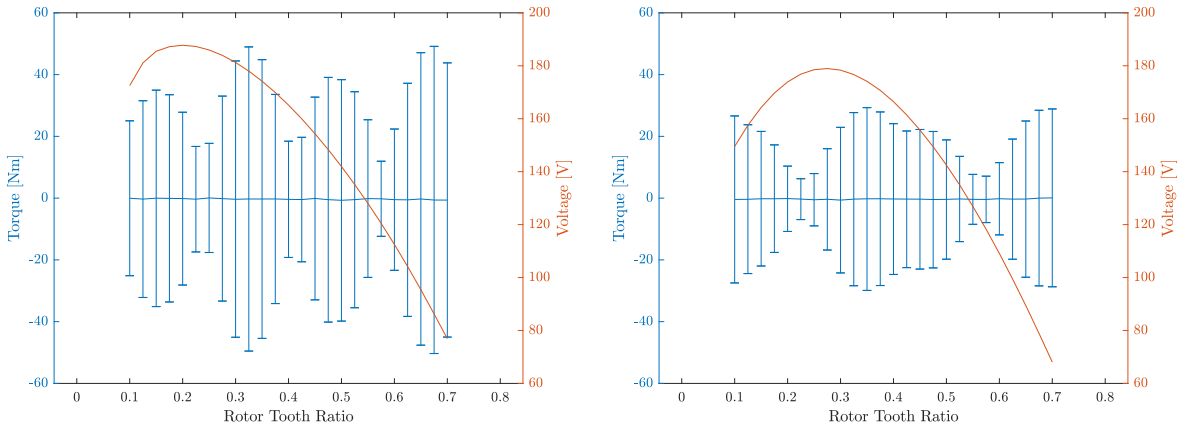

(a) Flux reversal machine

(b) Vernier hybrid machine

Figure 4.14: Cogging torque ranges plotted together with peak voltage across a range of rotor tooth ratios. The cogging torque is on the left axis and uses error bars to represent full waveform in terms of average, and minimum/maximum peak positions. The voltage magnitude on the right axis is presented as a smooth line.

In figures 4.14a and 4.14b the peak voltage increases with rotor fill, reaching a maximum of 187.76 V at 0.2 fill in the FRM (figure 4.14a) and 178.95 V at 0.275 fill in the VHM (figure 4.14b). After this point, the voltage gradually declines as the tooth width approaches and overtakes the width of one magnet.

Although the decision to match rotor tooth width to magnet width has been justified, in both cases, the point of fixed tooth width is far from the optimal point of peak voltage; 0.4755 and 0.5315 for the FRM and VHM(–) respectively. These starting points also bear unfavourable cogging torque for both designs.

The peak voltage follows a simple curve for both machines wherein there is an optimal tooth width and a gradual drop off on either side where the rotor tooth becomes too small or large; both extremes for the VHM are shown in figure 4.15. When the tooth is small, the tooth becomes saturated limiting performance. When too large, the tooth overlaps magnets of alternating polarity, complicating the flux direction, and enhancing leakage paths.

In both models there is a rhythmic rise and fall to the cogging peaks with rotor fill with a fairly significant difference between highs and lows where there is cancellation of harmonics. It can be assumed then that the conclusion of section 4.5.2 is accurate only with some constraints attached. Both topologies have quite some capacity for electrical customisation and are sensitive to changes in rotor tooth width. More importantly, the point of peak voltage for both machines do not necessarily correspond to a point of maximal cogging torque; a particularly useful fact when considering the application of an FRM.

Table 4.6 summarises the findings in figure 4.14. Here it is shown that through optimal

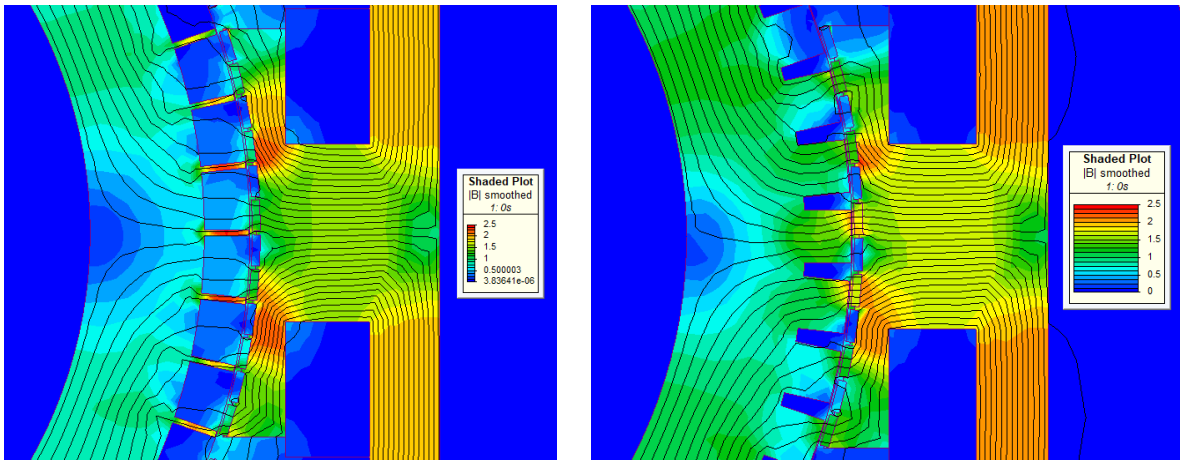

(a) Rotor tooth ratio = 0.1 (b) Rotor tooth ratio = 0.8

Figure 4.15: Comparison of rotor tooth width in a VHM.

rotor tooth width selection, the FRM and VHM achieved 32% and 25% increase in back emf respectively. Moreover, they did so while reducing the cogging torque peaks by 29% and 47%. It can be noted that at the optimal design points, the FRM achieves the best peak voltage at around 5% higher than the VHM. On the other hand, at almost every design point, the VHM has lower cogging peaks. At the optimal point, the VHM cogging is 50% that of the FRM.

Topology	Peak Voltage			Peak Cogging Torque		
	Original (V)	Optimal (V)	Change (%)	Original (N m)	Optimal (N m)	Change (%)
FRM	141.95	187.76	32.27	42	30	-28.57
VHM(–)	142.83	178.95	25.29	22	15	-46.67

Table 4.6: Summary of optimised tooth widths

4.5.4 Cogging Harmonics and Tuning

In three-phase machines, the interaction of magnet fields creates a cogging torque profile which is variable relative to rotor position. This torque profile is not just a singular waveform, but rather, built up of harmonic components which can be used to further explain the developed torque and further optimise it. One of the benefits of three-phase electric machines is that strong harmonics generated from a single phase are partially, or completely cancelled out, greatly reducing the overall waveform. However, this does not apply to the multiple of 3 harmonics in these machines.

This concept can be better demonstrated by assessing the harmonic content of one of the models. Figure 4.16 shows the harmonics for the FRM machine across the range of rotor tooth ratio values given in section 4.5.3. The waveforms across the range can be approximated to a 3^{rd} and 6^{th} harmonic, all other harmonics have either cancelled out or are insignificant.

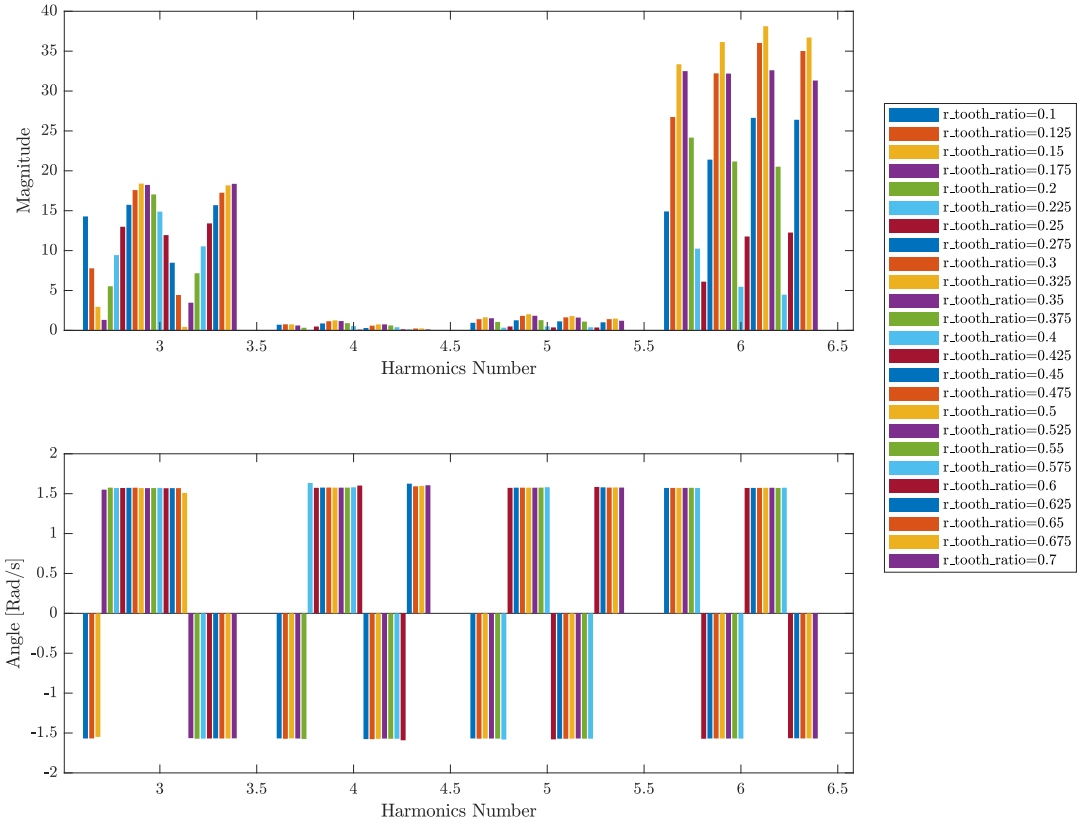

Figure 4.16: Cogging torque harmonics across a range of rotor tooth ratios for the FRM.

Each harmonic is variable in magnitude across the range of values, cycling from zero to the maximum. It should furthermore be noted that as the magnitude crosses the zero line, the polarity of the harmonic phase angle completely reverses. This suggests that the direction of torque application for the harmonic component periodically changes direction due to an interaction between the rotor and stator.

Figure 4.17 shows a third and sixth harmonic waveform with an example rotor tooth drawn on. If that tooth were to move right; the left side will experience an increasingly positive attraction force from the 3rd harmonic, and the right side will experience a negative attraction force of equal magnitude. The two forces on the tooth cancel out completely and the harmonic contributes no cogging torque. This is the case in the 3rd harmonic when the rotor tooth ratio is approximately equal to 0.0175 and 0.5 for the FRM, the harmonic is effectively tuned out and contributes no cogging torque. This was the case in the prior comparison wherein the rotor tooth width was equal to the width of one magnet, which removed the 3rd harmonic, leaving only the 6th harmonic as a near pure sinusoid.

However, in the same figure it can also be seen that when the tooth moves right, both sides of the tooth are subjected to equally positive attraction forces from the 6th harmonic with doubled magnitude. Hence, for this tooth, it is possible to tune out the 3rd harmonics but doing so heightens the contribution of the 6th harmonic. Moreover, the 6th harmonic visibly reaches much larger magnitudes and represents a better candidate for reduction.

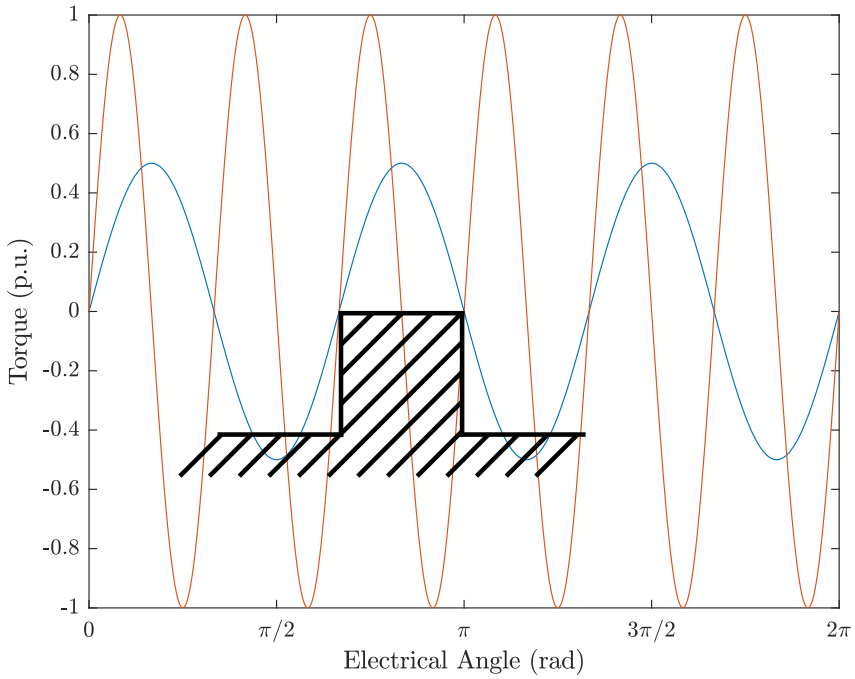

Figure 4.17: Example 3rd and 6th harmonics across one electrical cycle with a single tooth drawn on top.

Cogging torque reduction would be well achieved if tooth width selection could cancel out all harmonics. As was already seen, an attempt to eliminate the 3rd, maximises the

6^{th}; any attempt to cancel out the 6^{th} results in the 3^{rd} being fixed to half its maximum magnitude. As the contributing harmonics are multiples of each other, it precludes a machine with consistent tooth shapes from completely removing cogging torque through conventional means.

Furthermore, this is just a view from a purely harmonic standpoint. Although it is theoretically possible to target or exclude some harmonics it is not necessarily possible to do so. As was addressed prior, at small tooth widths, there is an issue with cogging, and at large ones, an issue with flux leakage. Moreover, small teeth or slots can present an engineering challenge to manufacture, assemble, or maintain the rotor; presuming small teeth can survive regular operation.

4.6 Conclusions

In this chapter, the FRM and VHM topologies have been compared for application in a hinged wave energy converter. The two topologies were compared with the rotor tooth width equal to the width of one magnet.

In open circuit conditions, the VHM(–) achieved the highest back EMF while the FRM and VHM(+) were 0.62% and 18.20% lower. The VHM(+) and VHM(–) had lower cogging torque peaks, 45.94% and 76.33% respectively.

With an AC electrical load applied, the VHM(+) achieved the highest voltage, followed by the FRM and VHM(–) which were 5.46% and 13.66%. Despite producing the highest voltage, the VHM(+) developed 20% lower torque than the others.

It was further revealed that the rotor tooth width in slotted VRPM machines has a high impact on the cogging torque harmonic content, phase, and magnitude. Because of this, it is challenging to select the appropriate geometry at which a fair comparison between the topologies can be made. Often in machine comparisons, authors choose to fix electromagnetic parameters such as magnet mass or active area. In the case of VRPM topologies, it is also important to find a means of setting the tooth width such that fairness in the comparison can be found. With the high sensitivity of voltage and cogging torque to tooth width, it is likely true that there is no singular point representing fairness between the two designs. More likely, it is better to incur the higher cost of a wide simulation sweep to optimise the rotor tooth width for each model and make a fairer comparison therefrom.

More importantly, it has been demonstrated through this chapter that the cogging torque profile, and by extension, the torque ripple for VRPM machines is not an intrinsic property of the topology; but rather, can be customised without resorting to cogging torque reduction techniques. It is therefore decided that the FRM be carried on into the following chapters due to its higher peak voltage.

Chapter 5. Hydrodynamic Design of a Wave Energy Converter

5.1 Introduction

In the design of a Wave Energy Converter (WEC), it is important to use hydrodynamics. This chapter is dedicated to framing the selection of a WEC, selecting, and analysing a deployment, and using an analytical model.

5.1.1 MU-EDRIVE Project

This research in this chapter was conducted as part of a funded Engineering and Physical Sciences Research Council (EPSRC) project. The project is named, "Marinization and Upscaling of an all-Electric Drive" (MU-EDRIVE) [177]; A partnership between Newcastle University, Edinburgh University, and industrial partner Mocean Energy. MU-EDRIVE seeks to upscale and marinize a fully electric wave energy converter.

The goal of the project is to develop a fully electric Power Take Off (PTO) for a WEC at a meaningful power output scale, which will be proven at sea for 12 months. Through the deployment period, operational data will be accrued to assess device performance and build investor confidence in wave energy devices.

Furthermore, the project aims to address a major issue faced by WECs. In WECs, the PTO is generally housed inside the WEC in a water-tight compartment requiring seals to prevent water ingress. This requires regular maintenance to ensure the seals are in good condition, driving up operational costs; the issue is particularly severe in linear PTO, as linear seals have a lower life expectancy. In MU-EDRIVE the goal is to develop a fully marinized PTO by running the machine flooded and removing the need for seals.

A flooded generator benefits natural cooling from the cold water but has many challenges that must be overcome. Because the generator is open to the sea, it is under continuous threat from corrosion, biofouling, and ingress of particulate matter. The project therefore aims to work with industrial partner Mocean, and bio-fouling specialists to protect the PTO.

Corrosion protection of outer bodies is the most simplistic, is achieved through coatings, and has little impact on generator integration. Antifouling measures, on the other hand, have a direct impact on the generator requirements in this project. Ultraviolet LEDs are used as an antifouling measure to prevent biofilms from forming inside the generator. The Ultraviolet lights, in combination with required protective coatings, bearings, and a water gap result in a large 5 mm magnetic airgap.

Newcastle University has a buoy off the coast of Blyth, UK, which is dubbed the "Acoustic Network Gateway Buoy", and was deployed in a previous project (USMART) [178]. It was originally expected that this buoy would be adapted to carry the WEC,

introducing further constraints on how the conversion could be achieved without damaging the buoy or interfering with the USMART project. This design work is however not presented in this thesis as it was found to be too restrictive for an IPS buoy concept, with a bespoke design flow selected instead.

5.1.2 Selection of WEC

Chapter 2 presented a diverse range of WECs. One of these devices is selected here, which can showcase the integrated design of a direct drive power take off. For small-scale devices, linear direct drive PTO is suitable for use in point absorber WECs. The small size of point absorbers is adaptable for any test or deployment location and at any prototype scale; moreover, the similarity of point absorbers to navigation buoys allows for the conversion of existing infrastructure and the reuse of mooring points.

Many point absorbers use vertical oscillatory motion on one or more bodies with an amplitude varying with the sea state. To convert power, the PTO must react a force against this motion, requiring an inertial reference, typically the sea floor or a high inertia body. To demonstrate DD design, a heaving IPS buoy will be investigated, a diagram of the device is shown in figure 5.1.

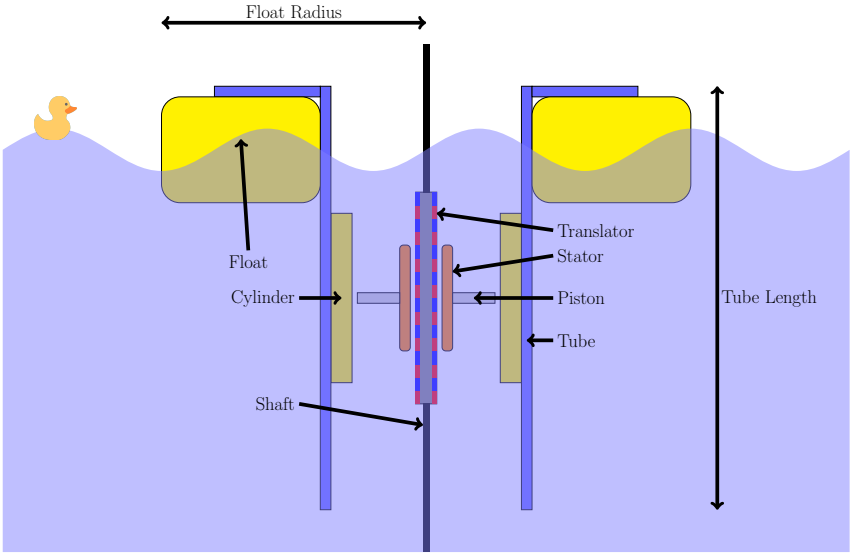

Figure 5.1: Direct drive IPS buoy layout

5.1.3 Scope and Objectives

This chapter is focused on the design process of a wave energy converter, starting from a wave energy resource location, and ending with a well understood search space upon which the WEC can be sized, and the PTO device may be designed and integrated.

The goal is achieved through the development of a hydrodynamic model of a two-body WEC. This model is used to characterise the WEC behaviour, understand the impact of design variables, and optimise the WEC for maximum power output. By necessity,

the model developed relies on simplifications and assumptions to focus on the PTO and system-level design. The inclusion of hydrodynamic mathematics and design techniques of out of scope for this chapter.

A mathematical model of the requisite geometry for a neutrally buoyant piston is also provided in this chapter and used in the next chapter.

5.2 Selected Location

Blyth, UK, is the selected location for deployment from a compromise between wave resource, and local access. Additionally, the university already has resources in the area in the form of a vessel and mooring site. However, a caveat of this is that the size of WEC deployable is constrained to the lifting capacity of the vessel unless another were to be acquired.

5.2.1 Data Resource

The sea state on site must be understood before a WEC or PTO can be sized. There are several coastal monitoring groups around the UK set up to understand the health of our coast and how it changes over time. The National Network of Regional Coastal Monitoring Programmes (NNRCMP) [179] is a collection of regional programmes that collects large quantities of data around England and Wales, made publicly available for research and monitoring purposes. Their datasets contain wave and tidal data both in real time and historically. Additionally, they also perform in-person surveys, track storm thresholds, and provide a wealth of other reports and resources. However, only the sea state data is relevant to this thesis.

The sea data was collected via a 'Datawell Directional WaveRider Mk III' buoy at an approximate water depth of 18metres and is located 1 mile off the coast of Newbiggin-by-the-Sea as shown in figure 5.2. The data buoy records constantly, but in the long-term dataset, these observations are processed in 30-minute intervals.

This model of data collection buoy measures the sea state in the following metrics:

Location: Latitude and Longitude of the buoy.

Significant Wave Height (H_s): Average height from peak to crest from the highest 3rd of waves (m).

Max Height (H_{max}): Maximum height of the largest wave (m).

Peak Period (T_{max}): Period of the wave with the highest energy (s).

Zero Up-Crossing Period (T_z) Average zero up-crossing period (s).

Peak Direction: Dominant wave direction (°).

Spread: Directional spread of waves from peak direction (°).

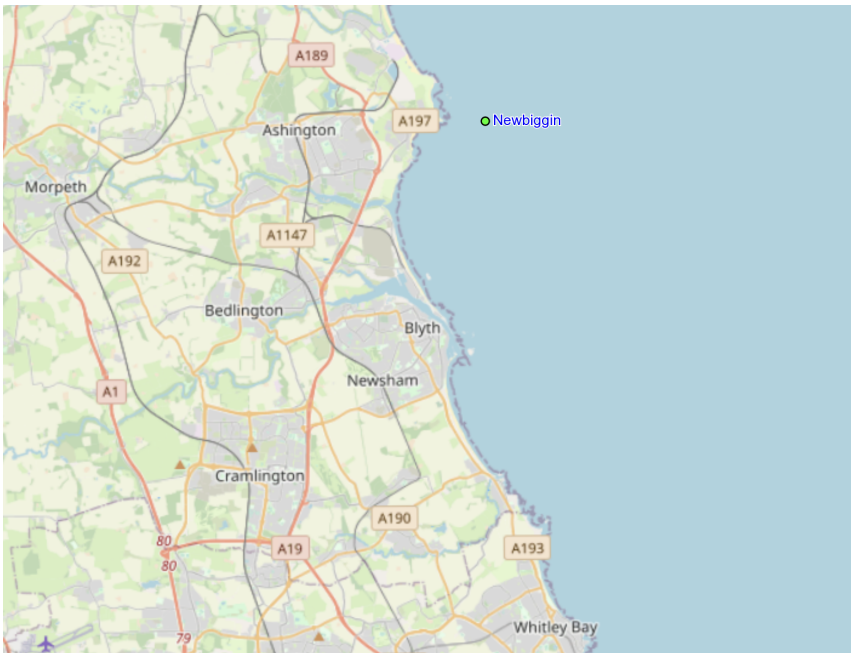

Figure 5.2: Map of Blyth/Newbiggin-by-the-Sea area showing location of data collection buoy marked in green [179].

Temperature: Temperature of the sea (°C).

Energy Period (T_e): Period between zeroth and first negative values in the frequency spectra (s).

Some example from the dataset for the year 2022 is shown in figure 5.3. These radial plots present the frequency that the significant wave height and peak period occur, relative to the wave source direction. For directional WECs such as attenuators, wave rose plots are used for the planning of installations. However, they are used only for demonstrative purposes here as the target WEC is a point absorber and direction agnostic.

It can be seen here the waves experienced are almost exclusively sourced from the North, with the highest concentration of high period waves arriving from the North East direction (figure 5.3b). This is the expected wave resource direction, as Northeastern England is generally impacted by continental polar weather systems.

5.2.1.1 Data Quality

Although the data acquired from NNRCMP is an excellent resource with data spanning almost 10 years, there are some caveats about the data to be noted.

Data collection buoys are under similar challenges as WECs in that they must survive long periods moored in situ regardless of the sea state. The buoy has a scheduled service approximately every 6 months. Even so, there have been times when either the buoy or onshore station has equipment failures, or the buoy gets cut loose and goes adrift.

The buoy drift can be seen best in figure 5.4a. The mooring location is *55° 11.11' N, 001° 28.69' W*, but in some cases, the buoy has drifted as far as 6 minutes South and 8

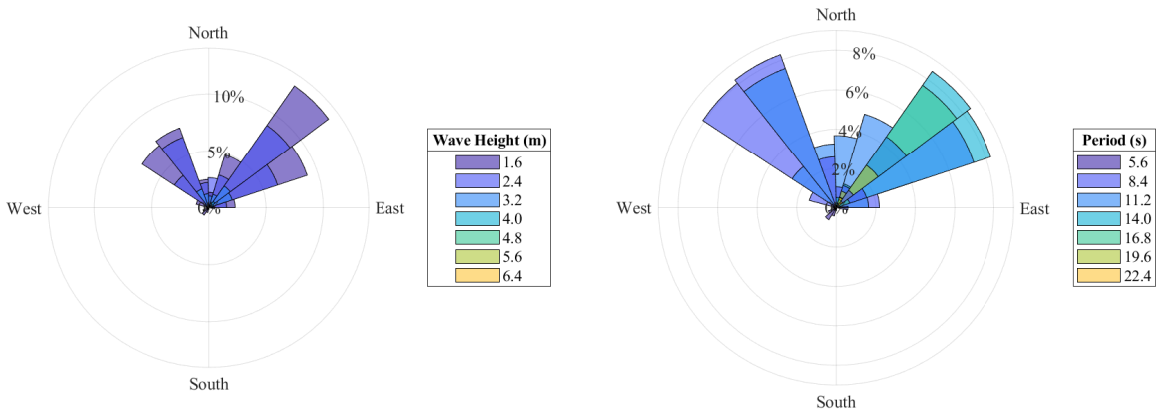

(a) Significant height (b) Peak period

Figure 5.3: Wave rose plots presenting frequency and direction of wave states during 2022 at Newbiggin-by-the-Sea. Data taken from [179].

minutes East of the monitoring location.

In these times of servicing, breakdown, or drifting, the data is either cut off or unreliable depending on how far it drifts. Therefore, there can be large gaps in the dataset when the buoy is offline or data is corrupted, or otherwise removed. During some years the data loss spans several months. This is undesirable and can skew the true sea state, particularly if winter data is missing.

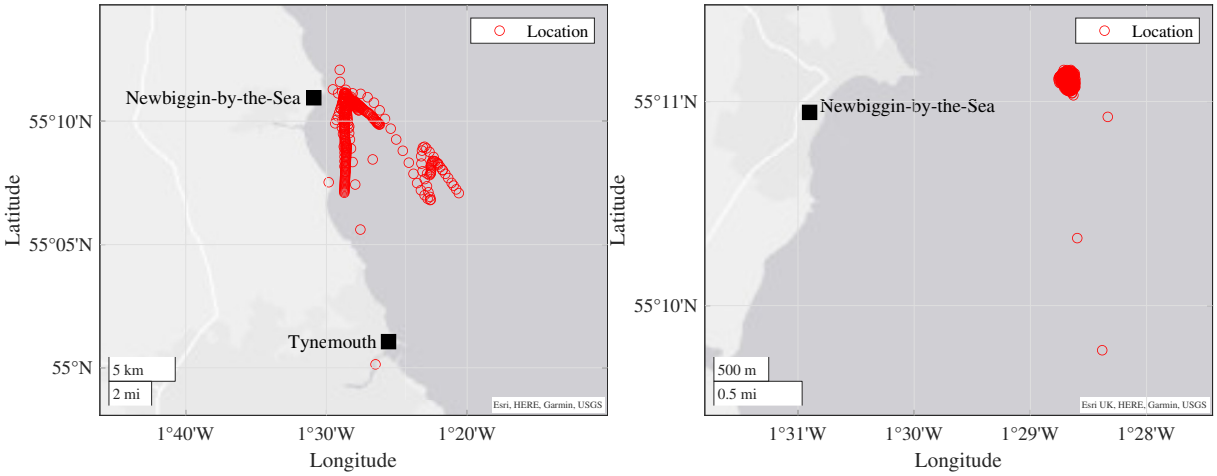

(a) 2013 - 2023 (b) 2022 - 2023

Figure 5.4: GPS location of data collection buoy during at Newbiggin-by-the-Sea. Data taken from [179].

In the following analysis of wave states, only the year 2022 is considered because it has the lowest data loss of 2.8% as compared to 15% in 2019. Furthermore, there are no gaps in the dataset lasting more than 12 hours during this period and there were no incidents of equipment or mooring failure.

5.2.1.2 Data Processing

In the dataset, every 30-minute interval must have valid data associated, otherwise, large gaps may cause misleading statistics, particularly cumulative statistics. Each variable of the dataset was interpolated in a layered approach.

First, a moving average of fixed window width is used to fill gaps smaller than the window width. This is done with a 24-hour window, followed by a 7-day window. Lastly, any remaining gaps are filled with linear interpolation.

Figure 5.5b demonstrates the 24-hour interpolation. The moving average achieves a close fit to the measured data, but the method requires the gap in data to be less than 24 hours and can therefore not interpolate the full dataset.

The interpolation of wider gaps is highlighted in figure 5.5a. The 7-day moving average is used to provide a wider fill range with a modest fit to the dataset. Finally, any gaps larger than 7 days in length are linearly interpolated, because moving averages with larger windows were suspected to give misleading results.

In the select date range of the dataset, only the 24-hour window interpolation was required because the gaps in data are small, but it is important to note how the dataset was prepared for the full dataset.

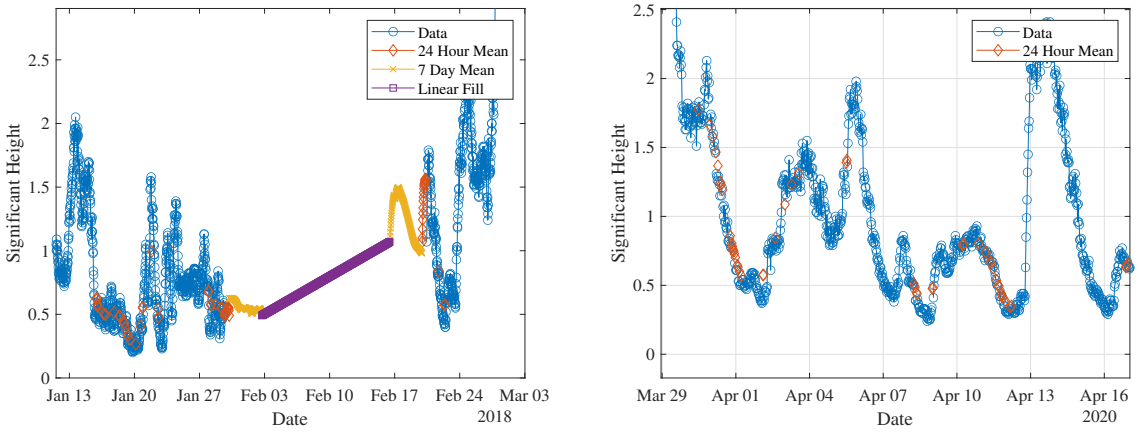

(a) Wide range

(b) Short range

Figure 5.5: Interpolation of sea data

5.2.2 Analysis of Location

The wave resource in terms of peak period and significant height is displayed in figure 5.6. The data has been collected into a 2D histogram viewed from the top and coloured by probability. Because the data is collected into bins, they form a kind of resolution when looking at the data. If too few or too many bins, the data becomes less informative. For this reason, it is presented here with bin quantities from 20 to 50. Additionally, there are some bin numbers wherein no wave periods occur. This is a quirk of statistics and is likely due to the wave period having a wide range.

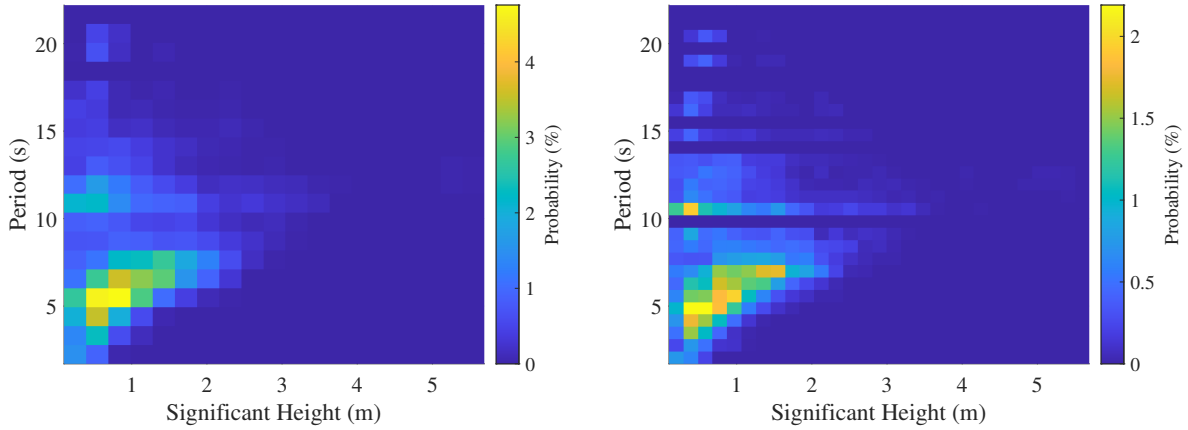

(a) 20 bins per axis

(b) 30 bins per axis

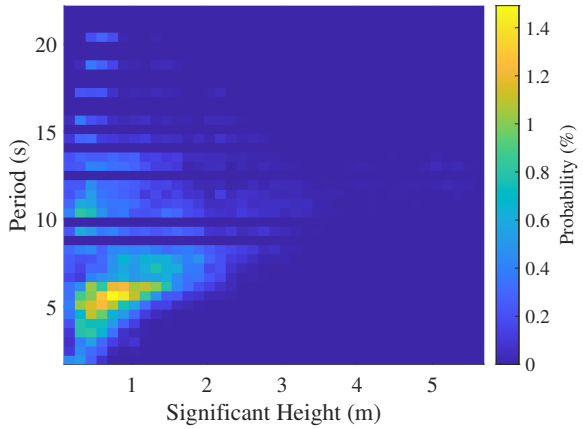

(c) 40 bins per axis

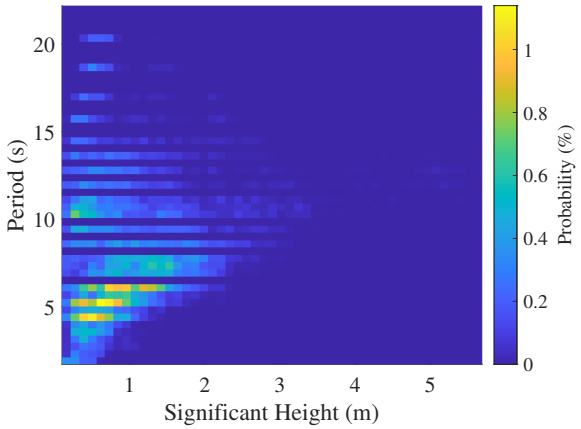

(d) 50 bins per axis

Figure 5.6: Significant wave height and energy period in Newbiggin-by-the-Sea across the year 2022. Data taken from [179].

It can be noted firstly that the sea state is most commonly between 2 - 8 seconds and less than 1.6metres for the peak period and significant height respectively. Where the absolute peak is at 5.38 seconds and 0.67metres respectively. These most common waves are quite some way off the ideal 10-second wave that wave energy developers are often pursuing. With that said, the resource is more than sufficient for a research application.

The wave states shown so far have related only to the probability of occurrence. That is however not the only perspective under which to assess a wave resource. Because the power per metre of wavefront in kW is approximately $P \approx 0.5TH_s^2$, i.e. $P \propto T$, $P \propto H_s^2$. The wave state for the highest annual yield often does not correspond with the most probable wave, this is demonstrated in figure 5.7.

In figure 5.7 can be seen that to achieve a high annual yield; more powerful, but less common waves must be selected. Moreover, some waves containing the highest annual yield occur at rare but extremely large waves. Given that the storm alert threshold is marked by [179] as 3.32 m, these large waves are likely to damage any device not prepared for it.

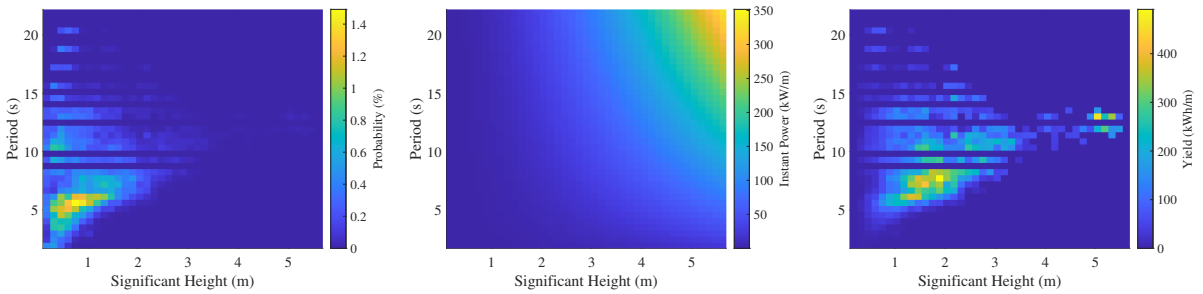

(a) Probability (b) Instant power (c) Annual yield

Figure 5.7: Comparison of probability and annual yield at each wave state.

As point absorbers tend to operate best at a specific wave frequency, it can be argued for a commercial energy production device whether it is better to target powerful infrequent waves for maximal net power, or weaker frequent waves for more consistent generation. The WEC deployment considered in this thesis is for research purposes, it is better to transmit a regular supply of data to shore, and so a wave of 1 m significant height and 6.5 s period is selected going forward.

5.3 Derivation of Hydrodynamic Model

5.3.1 Hydrodynamic Model

To minimise modelling and computational complexity there are some hydrodynamic assumptions made:

- Linear wave theory is applied. Sinusoidal waves are assumed.
- The acceleration tube is placed sufficiently far below both the float and the waves, such that any excitation force from either can be neglected.

- The radiation damping force on the buoy is modelled by a representative damping force.
- The power take off force is represented by a spring-damper system.
- The buoy is a vertical cylinder that oscillates in pure heave.
- The piston is watertight and neutrally buoyant.
- Friction between the piston and cylinder is neglected.
- During piston decoupling, the piston behaves as a drag plate.
- The tube is fully and constantly submerged.

Using these assumptions, a mechanical model for a generic two-body, heaving WEC can be developed. The float is acted upon by gravity due to the material mass of the float, tube, and cylinder. Equally so, the same components are pushed to the surface by a buoyancy force. It can be noted that the buoyancy force is described as a static component from the tube and cylinder, and a variable component from the float, which is dependent on the submerged volume. Additionally, there is a radiation force upon the float; here represented by a damper between float and wave. Finally, there is a force from the power take off with a spring and damping component.

It is assumed that the piston is neutrally buoyant, so the gravitational and buoyant forces cancel out, leaving only the PTO forces acting on the piston body. A free body diagram for this system is shown in figure 5.8.

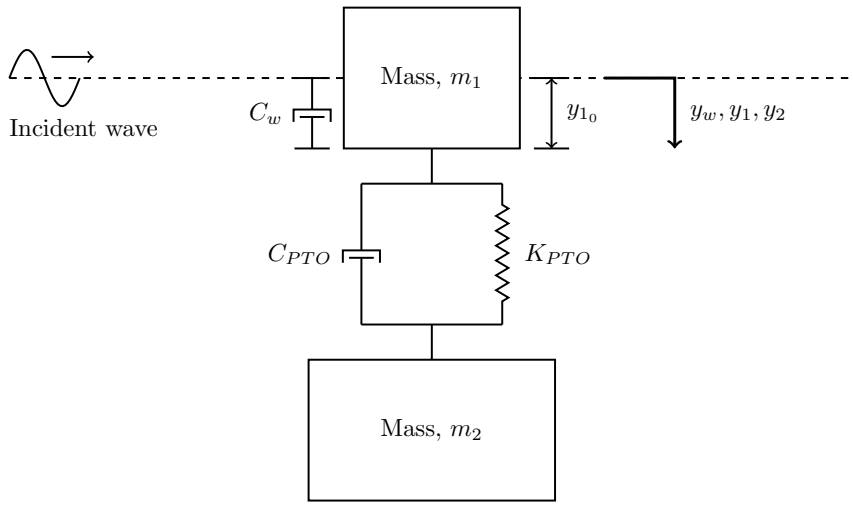

Figure 5.8: Mechanical model of a two-body system operating in heave.

Any mechanical body that is displaced through a fluid must accelerate not only its mass but also the mass of the surrounding fluid. For a vertical cylinder oscillating in heave, the added fluid mass is stated by [180] to be approximated as a hemisphere of equal radius to the cylinder:

$$m_{ac} = \frac{2}{3}\pi r^3 \rho_w \tag{5.1}$$

Where ρ_w is the fluid density, and r is the cylinder radius.

Additionally, it is assumed that the added mass of the tube is approximated as half the volume of a torus:

$$m_{at} = \pi^2 R t^2 \rho_w \tag{5.2}$$

Where R is the central radius of the tube, and t is half of the tube thickness.

The summary of forces is then given in equation (5.3):

$$\begin{cases} m_{e1}\ddot{y}_1 = F_{g1} - F_{b1} - F_r + F_{PTO} \\ m_{e2}\ddot{y}_2 = F_{g2} - F_{b2} - F_{PTO} \end{cases} \tag{5.3}$$

Where m_{eN} is the effective mass of the numerical body $N \in \{1, 2\}$. $\ddot{y}_N$ is the acceleration of the body. F_{gN}, F_{bN}, F_r, and F_{PTO} are the gravitational, buoyancy, radiation damping, and power take off forces respectively.

The effective mass m_{eN} comprises the physical mass of the body with added fluid masses in addition.

For the float/tube body, this equates to the mass of float and tube construction plus the added mass from both float and tube:

$$m_{e1} = m_1 + m_{ac} + m_{at} \tag{5.4}$$

For the piston/water mass, it is the piston mass plus the volume of water inside the tube:

$$m_{e2} = m_2 + m_{aw} \tag{5.5}$$

The buoyancy force is described as the displaced water mass accelerated by gravity, or $F_b = V\rho_w g$. For body 1, the volume is equal to the submerged volume only and varies with the float submersion depth. It is assumed that the tube/cylinder remains constantly underwater, therefore providing a constant buoyancy force. The float submerged volume is variable with depth and is conditionally given by:

$$v_f = \begin{cases} 0 & if \quad y_w \leq y_1 & , \text{ not submerged} \\ \pi r^2 \left| y_w - y_1 \right| & if \quad y_w > y_1 & , \text{ semi-submerged} \\ \pi r^2 L_f & if \quad y_w > y_1 \geq L_f & , \text{ completely submerged} \end{cases} \tag{5.6}$$

Where y_w, and y_1 are the vertical displacements of the wave and float from an undisturbed free surface. Furthermore, the displacement of the float is measured from the bottom face. When the float is above the water surface there is no submerged volume, when semi-submerged, it is a function of float depth and is constrained to the maximum

volume at depths more than the float length L_f.

The complete submerged volume is:

$$v_{sub} = v_f + v_t \tag{5.7}$$

Where v_t is the volume of the tube/cylinder construction.

The power take off force is modelled as a spring and damper system, and is given by constants C_{PTO}, K_{PTO} multiplied by the relative velocity and displacement of the bodies respectively:

$$F_{PTO} = C_{PTO}(\dot{y}_1 - \dot{y}_2) + K_{PTO}(y_1 - y_2) \tag{5.8}$$

Lastly, the radiation damping is modelled as a damping force acting between wave surface and float:

$$F_r = C_w(\ddot{y}_w - \ddot{y}_1) \tag{5.9}$$

Equations (5.1) to (5.9) are then combined into the final mathematical model:

$$\begin{cases} (m_1 + m_{ac} + m_{at})\ddot{y}_1 = m_1 g - \rho_w v_{sub} g - C_{wave}(\dot{y_w} - \dot{y}_1) \dots \\ \qquad\qquad + C_{PTO}(\dot{y}_1 - \dot{y}_2) + K_{PTO}(y_1 - y_2) \\ (m_2 + m_{aw})\ddot{y}_2 = -C_{PTO}(\dot{y}_1 - \dot{y}_2) - K_{PTO}(y_1 - y_2) \end{cases} \tag{5.10}$$

5.4 Derivation of Hydrostatic Model

5.4.1 Basic Model

Because the piston is assumed to be neutrally buoyant, it is necessary to develop a numerical model for the point at which neutral buoyancy is achieved.

The gravitational and buoyant forces are given by:

$$F_g = v_m \rho_m g \tag{5.11}$$

$$F_b = v_w \rho_w g \tag{5.12}$$

Where v_m, v_w are the volume of the material and displaced water, and ρ_m, ρ_w are the density of the material and water. Neutral buoyancy is found when:

$$|F_g| - |F_b| = 0 \tag{5.13}$$

If the piston were a solid, then $v_m = v_w$, and $\rho_m \equiv \rho_w$ to satisfy equation (5.13), preventing the use of high strength materials. The piston must therefore be constructed of a hollow shell cylinder as illustrated in figure 5.9.

Structural strength is provided by marine grade steel or other materials in the wall and endcap, with a hollowed centre and the possible addition of foam on the ends, or ballast in the centre to enhance either force without altering the core geometry.

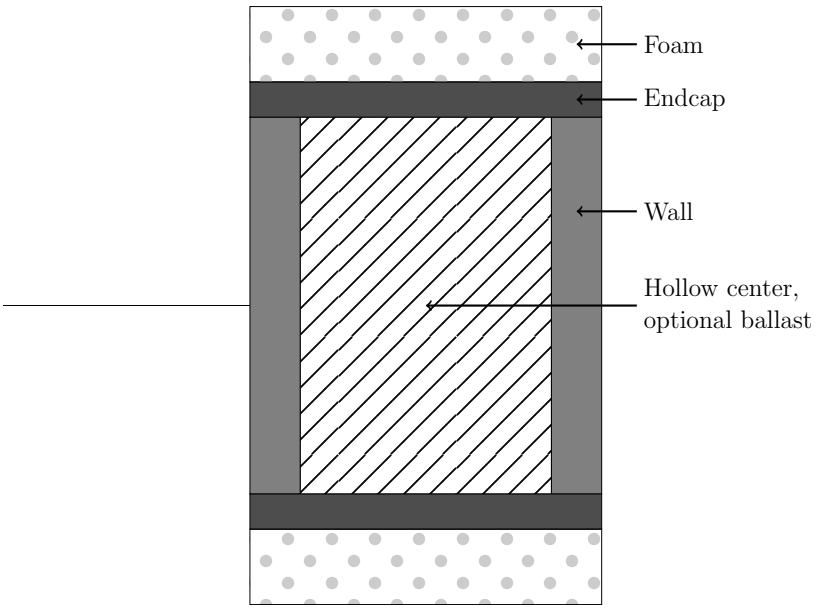

Figure 5.9: Illustration of basic piston geometry.

In this scheme, the gravitational force can be described as:

$$F_g = g\left(v_b\rho_b + v_W\rho_W + 2v_e\rho_e + 2v_f\rho_f\right) \tag{5.14}$$

Where subscripts b, W, e, f denote the ballast, wall, endcap, and foam.

5.4.2 Integrated Generator

For a flooded generator, it is ideal to integrate it into the piston structure. Because it is usually the lighter component and avoids the use of brushes, it is preferable to use the piston as a translator rather than a stator. Two such configurations are shown in figure 5.10.

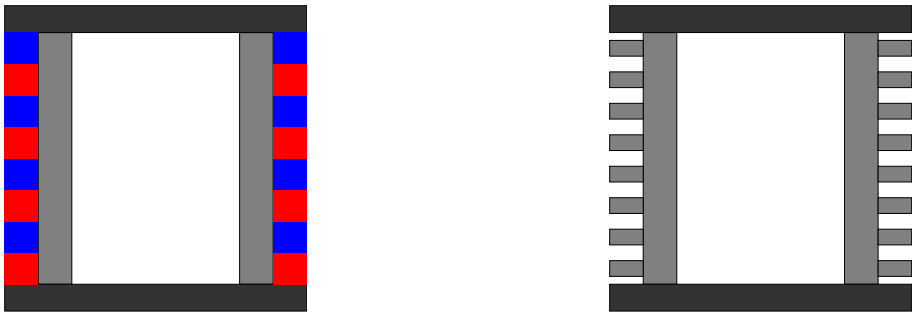

(a) Magnet piston

(b) Slotted piston

Figure 5.10: Example piston configuration cross-sections.

The piston may house a field MMF via permanent magnets, or a slotted translator

such as that used in flux modulation machines. By adopting non-fully pitched magnets, or a slotted structure, the piston mass may be reduced.

The buoyancy force can be given as:

$$F_b = v_{disp}\rho_{water}g \tag{5.15}$$

Where v_{disp} is the volume of water displaced by a body. The gravitational force is then given by:

$$F_g = v_{mat}\rho_{mat}g \tag{5.16}$$

Where the subscripts v_{mat} and ρ_{mat} are the material volume and density respectively. However, it should be noted that this relationship applies to a mono-material body. In actuality, the piston is constructed out of multiple materials, and the equation should be applied to each of them individually. Assuming that no further forces are acting upon the piston, its mechanical motion can be described by:

$$m\ddot{a} = F_g - F_b \tag{5.17}$$

In steady state conditions, there is no acceleration, and neutral buoyancy is achieved when the two forces are equal:

$$0 = F_g - F_b \tag{5.18}$$

Combining equations (5.15) to (5.18), this becomes:

$$m_{mat} = m_{disp} \tag{5.19}$$

Or put in words, the mass of displaced water must equal the piston mass.

5.4.3 Piston Material Mass

The volume of both piston topologies can be described by:

$$\sum v = 2(v_e) + v_w + v_{field} \tag{5.20}$$

Where v_e v_w, and v_{field} are the endcap, wall, and "field provider" volume respectively. The volume of an endcap is:

$$v_e = \pi r_e^2 L_e \tag{5.21}$$

Where r_e and L_e are the endcap radius and axial length. The wall volume is then given as:

$$v_w = \pi L_w(r_w^2 - (r_w - t_w)^2) \tag{5.22}$$

Where L_w, r_w, and t_w are the wall length, outer radius, and thickness respectively.

Lastly, the "field provider" volume is given by:

$$v_{field} = \pi(L_w \tau_f)((r_w + t_{field})^2 - r_w^2) \tag{5.23}$$

Where τ_f is the fill ratio of the magnets or iron teeth, and t_{field} is the height of the magnets/iron teeth.

The mass can then be calculated simply by the following:

$$m_{mat} = g(2v_e\rho_e + v_w\rho_w + v_{field}\rho_{field}) \tag{5.24}$$

5.4.4 Displaced Water Mass

The displaced water mass is defined by the external volume and the density of water as defined in equation (5.15). It is assumed that the slotted topology has its slots filled with epoxy such that it forms a solid cylinder. The epoxy mass is neglected here. The displaced volume is given by:

$$v_{disp} = \pi r_e^2(L_w + 2L_e) \tag{5.25}$$

And the mass is:

$$m_{disp} = v_{disp}\rho_{water} \tag{5.26}$$

5.4.5 Feasible Neutrally Buoyant Dimensions

Hydrostatic models of a neutrally buoyant piston with an integrated electric machine have been developed for the configurations presented in figure 5.10. Geometric properties are used to calculate the point at which the buoyant force and gravitational force cancel out, with the following assumptions made:

- Tooth/magnet height is equal to wall thickness.
- Magnets are fully pitched.
- Slots span half the translator pitched.
- Endcap length fixed to 0.01 m.
- Teeth and back iron are constructed of electrical steel (7650 kg/m^3).
- Endcaps are constructed of marine steel (7500 kg/m^3).
- Magnets are constructed of neodymium (7000 kg/m^3).

The point of neutral buoyancy is presented in figure 5.11, and plotted from 0 to 3 m axial length and 0 to 0.1 m wall thickness, where the surface plot is the precise point of neutral buoyancy. Deviation from the surface along any axis will cause the piston to move towards positively or negatively buoyant.

In both configurations, there is a wide range of feasible neutrally buoyant geometries. There is however an absolute minimum of around 0.148 m axial length, below which, the radius is required becomes unreasonably large. Meanwhile, at very small wall thicknesses, the radius is permitted to reduce as low as 0.05 m; although such a generator may not be feasible.

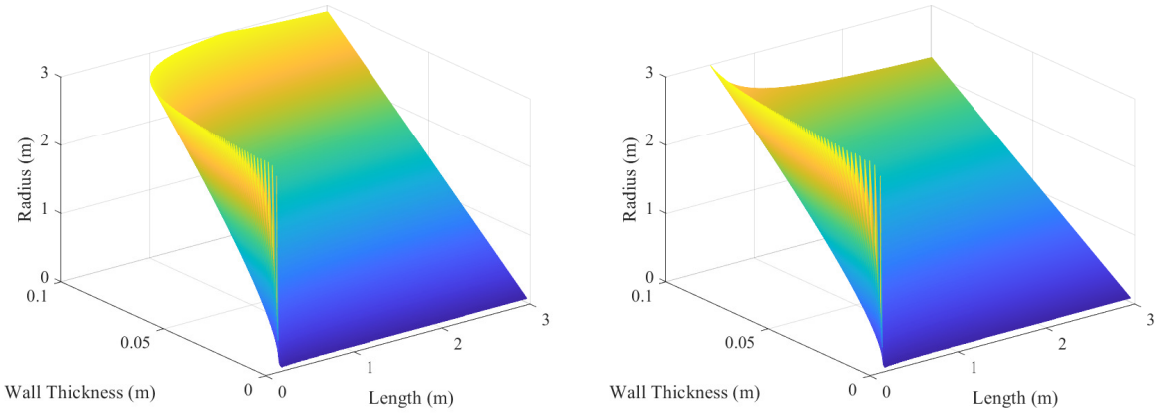

(a) Surface magnets

(b) Slotted piston

Figure 5.11: Feasible external dimensions of the two piston topologies.

Because the endcaps are solid disks of steel, they present a heavy mass, requiring a greater piston length to provide sufficient buoyancy to not sink. Therefore, for any piston radius, there is a minimum required length to produce a valid piston. Once the minimum length is surpassed, further increases to the piston length yield little benefit to the allowable wall thickness. The allowable wall thickness is increased only by increasing the piston radius.

Although the magnets have a lower density than electrical steel, the slotted piston generally allows for a smaller radius for any given piston length. The slotted piston in this configuration, and with these dimensions, is permitted to have a 20 - 25% smaller radius on average.

Across most available geometries, it is possible to achieve neutral buoyancy, although it may result in an infeasible geometry for a direct drive generator. This section does not seek to set hard limitations for design variables, but the following minimum values are set:

5.5 Model Constraints and Calibration

In table 5.1 some minimum dimensions for a neutrally buoyant piston were defined and will be put into practice in this section. In any IPS buoy, but particularly an integrated

Parameter	Value
Axial length	0.148 m
Outer radius	0.05 m

Table 5.1: Minimum acceptable dimensions for a neutrally buoyant piston.

one, the piston is inseparably at the root of all system components. Its outer radius directly defines both the generator size and the volume of water inside the tube. Each of these has a strong impact on the hydrodynamic motion and electrical performance of the device. It is therefore critically important that the piston dimensions be set appropriately. However, for the sake of exploring the model, the generator components are reduced to only damping and radiation forces, with no geometric impact.

5.5.1 Additional Motion Constraints

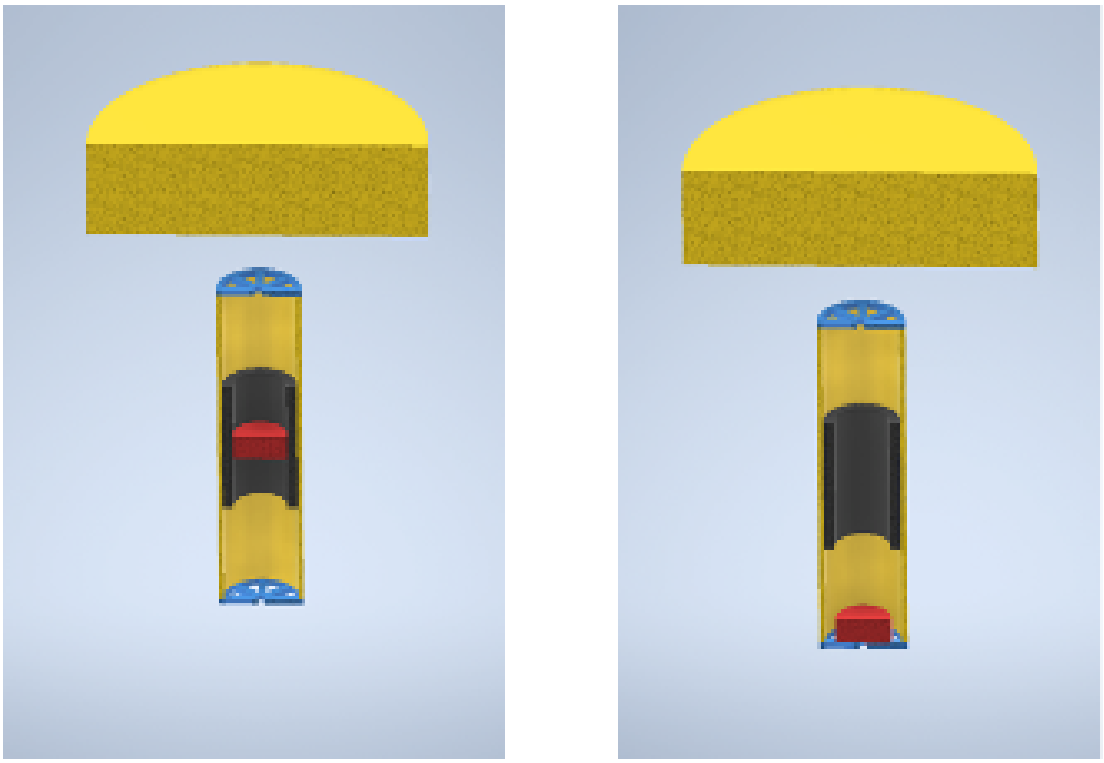

(a) Equilibrium position (b) Large displacement

Figure 5.12: Illustration of an IPS Buoy at its equilibrium condition, and during a large oscillation, where the piston is forced out of the inner tube.

When the piston is driven outside the cylinder during large oscillations, it remains within the wider radius tube in the decoupled state. Although it is decoupled, it is still below water and therefore has an added mass. Along with equation (5.1), [180] also describes the added mass of a drag plate being roughly equal to the volume of a sphere multiplied by water density. As the piston may serve a dual purpose as a generator, it is unlikely to have the aspect ratio necessary to be considered a drag plate. However, it will

be included here for the sake of completeness:

$$m_{aw} = \begin{cases} (v_{tube} - v_{piston})\rho_w & if \quad , \text{ coupled} \\ \frac{2}{3}\pi r^3 \rho_w & if \quad , \text{ decoupled \& cylinder} \\ \frac{4}{3}\pi r^3 \rho_w & if \quad , \text{ decoupled \& drag plate} \end{cases} \tag{5.27}$$

Using this with the dimensions given in table 5.2 yields added masses of 2012 kg, 136 kg, and 272 kg for each case respectively. Although the decoupled states provide a much lower added mass, they are still significant and cannot be neglected; In some cases, they remain a larger mass than the piston itself.

Parameter	Value
Tube length	3 m
Tube radius	0.5 m
Cylinder length	1 m
Cylinder radius	0.4 m
Piston length	0.2 m

Table 5.2: Example IPS tube dimensions

During decoupling, the piston is under the influence of the PTO force only. Because the PTO is an electrical machine, the force upon it is fully controllable and can bring the piston back to the centre or dynamically control it for better performance. However, such a discussion of machine control is outside the scope of this thesis. In this model, it is assumed that during a decoupling, the PTO force is reduced by a factor of 0.9.

As is shown in figure 5.12, the tube allows water to enter but does not allow the piston to exit. In the case of an extreme wave, if the piston reaches the end of the tube, it will be dragged along by the tube until the wave direction changes.

5.5.2 Calibration of Float Damping

In the WEC mechanical model, the interaction between the floating mass and sea is modelled as a damper and two opposing forces: gravitational force down, and the buoyant force restoring. In practice, the two forces act as a spring constant with more realistic constraints on the buoyant force.

The damper is representative of the radiation damping coefficient used in wave theory. It has a strong importance on the hydrodynamic performance of the floating body and is often calculated in simulation packages such as WAMIT [181]. However, as these software packages were not available, other methods were used to estimate the coefficient.

Figure 5.13 shows the influence of radiation damping on an IPS buoy. At time $t = 0$, the float is at its equilibrium depth, and the wave height is raised by 1 m above the mean water level. The displacement profile that the buoy follows is highly variable to the

radiation damping and all values of damping have no impact on the natural frequency of oscillation; 2.396 rad/s in this example.

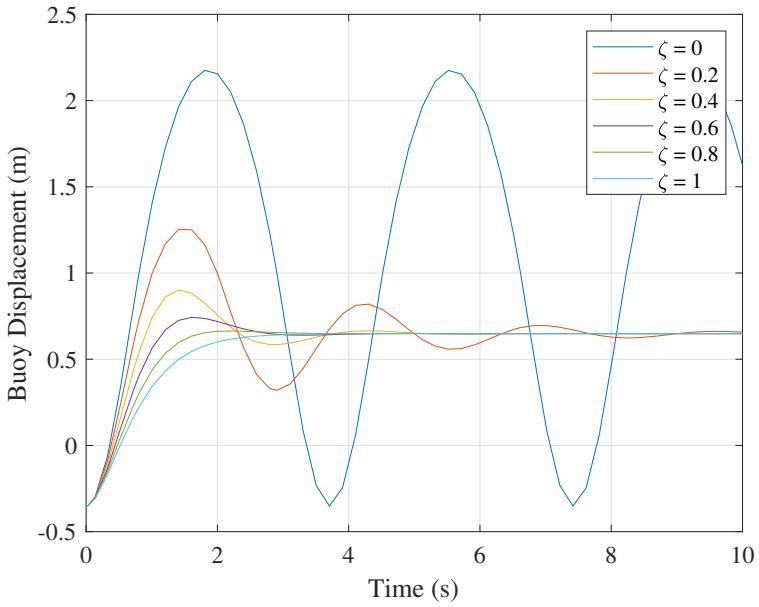

Figure 5.13: Variation of radiation damping on an IPS buoy with inactive power take off.

In the absence of specialized software to calculate the radiation damping of the WEC, and estimation was made based on the settling period of a simulation, ensuring that the device settles to near zero velocity in 10 seconds after disturbance. Therefore, in this chapter, the radiation damping ratio is fixed to a representative value of 0.2 to ensure consistency among results.

These assumptions are true only at the selected wave period and the WEC dimensions specified. Although it can be seen that at this design point, there is not much change up to the critical damping point during a wave event, except for a slight delay and lower magnitude of displacement (figure 5.13). For illustrative purposes, the impact of the damping ratio is also demonstrated for the WEC undergoing displacement from a wave in figure 5.14

5.5.3 Initial Geometry

The initial geometry for comparing the impact of PTO parameters is presented in this section alongside other informative tables of parameters used in the comparison. table 5.3 shows the densities of materials used, table 5.4 contains the WEC dimensions, and table 5.5, the calculated masses of major components and the mass ratio. This initial geometry is not optimised, and because the piston wall thicknesses are set to an anticipated value and the piston is assumed to be neutrally buoyant.

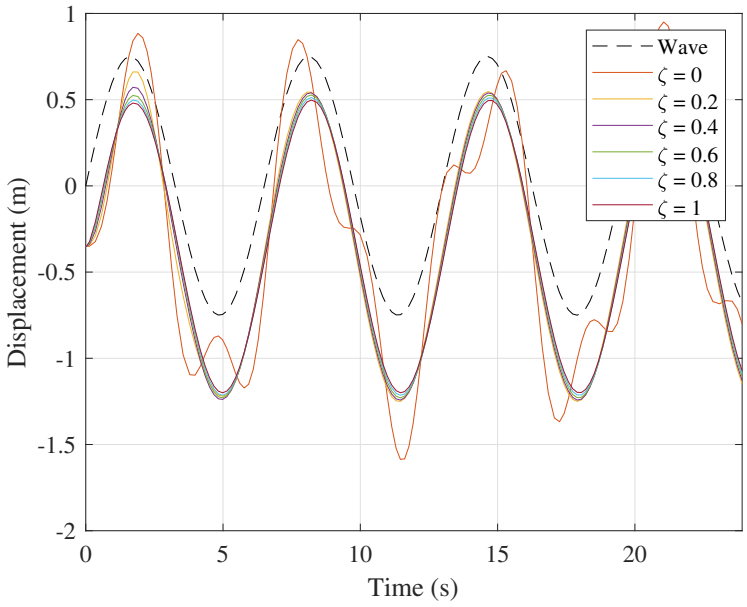

Figure 5.14: Variation of radiation damping on an IPS buoy with inactive power take off undergoing a wave interaction.

Material	Density
Electrical Steel	7650
Marine Steel	7500
Copper	8960
Sea Water	1020
Neodymium	7000

Table 5.3: Assumed material density

Parameter	Value (m)
Float radius	1
Float length	2
Float axial thickness	0.005
Float radial thickness	0.005
Float material	Marine steel
Piston radius	0.5
Piston length	0.2
Piston axial thickness	0.01
Piston radial thickness	0.05
Stator length	1
Stator thickness	0.01
Stator material	Electrical steel
Tube length	1
Tube thickness	0.005
Tube material	Marine steel
Piston $\rightleftharpoons$ stator airgap	0.005

Table 5.4: Initial geometry of IPS Buoy

Parameter	Value (kg)
Float mass	703
Tube mass	243
Stator mass	245
Floating material mass	1191
Piston mass	490
Captured water mass	1504
Floating inertial mass	5478
Captured inertial mass	1993
Mass ratio	0.364

Table 5.5: Calculated variables of initial geometry

5.6 Impact of PTO Parameters

To assess the impact of PTO parameters on the hydrodynamic performance of the WEC, the device was simulated with the radiation damping ratio set to 0.2 N s/m, and PTO damping and spring constants varied from 0 - 1000 N s/m and 0 - 2000 N/m respectively.

The power converted by the PTO is shown in figure 5.15 for the Root Mean Squared (RMS) power and peak power magnitude. figure 5.15a shows that the total power converted reaches the highest level when the damper is inactive and the spring constant is at a high level. However, in practice, the average power across the spring is approximately zero, and useful power is only transferred across the damper, analogous to reactive and real power in an electrical system.

Moreover, in the region of low damping and high spring constant, the PTO take off undergoes displacements larger than the acceleration tube. Following the constraints placed on the model for this study, the added water mass of the piston is penalised when exiting the acceleration tube. However, in a real world IPS buoy, it may not be trivial to reinsert the water-tight piston after a dislocation and can be a failure state. Furthermore, because the power extracted by the damping component is so small, these high spring, low damping configurations offer little to system performance and can largely be discounted.

On the other hand, the spring force does yield some contribution to elevating the system performance. Figure 5.15b shows that at low spring constants, as the damping increases, there is a shallow increase in RMS power which levels off as the system becomes overdamped. It is only when the spring constant is present that more significant power is absorbed by the damper. This is because the damper output depends on rapid motion to generate high power output. The spring component encourages the necessary oscillatory upon which meaningful power can be extracted by the damping component. However, the spring must be near resonance, and spring force must be provided by the PTO. Resonance in WECs is known to give a power yield advantage but requires the drive train to be able to react higher force and power than the rated values.

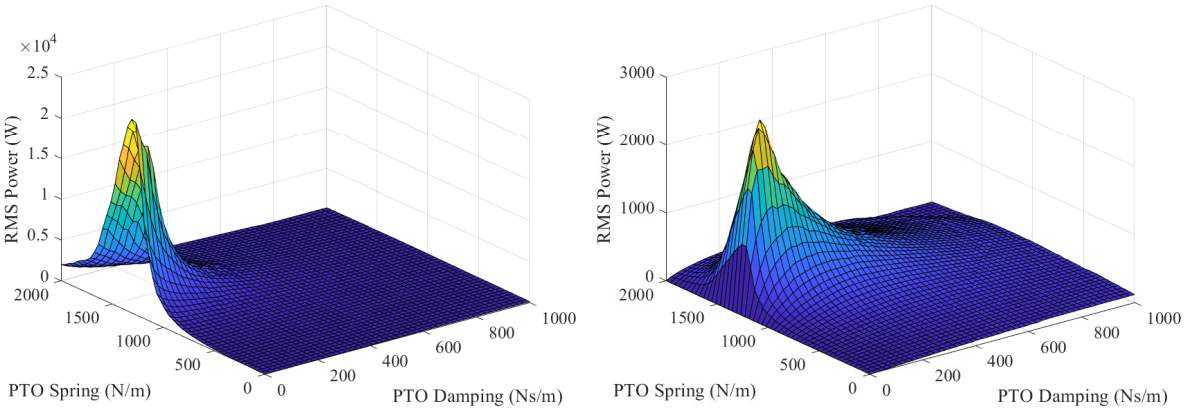

(a) Total (b) Damper

Figure 5.15: RMS power extracted by power take off.

5.6.1 Motion Behaviour at Four Operating Points

To highlight the performance output of the PTO during alteration of the spring and damping coefficients, four characteristic locations within the design space were selected and are stated in table 5.6, and the motion presented in figure 5.16

Damper (N s/m)	Spring (N/m)	Comment
102	1510	Optimal RMS damper power
102	1870	Spring surpasses peak values
755	244	High damping and low spring
755	1510	High damping and high spring

Table 5.6: Selected operating points for motion comparison.

In order topic operate well, WECs require a stable reference point to react force and generate power therefrom; often taking the form of the seabed or a floating body of significantly higher inertia.

Figure 5.16 demonstrates that in an IPS buoy, there is no stable reference point, but rather a lag between bodies.

The mobility of the piston is caused by the mass ratio between the piston/buoy and yields some benefits. In some PTO configurations such as figure 5.16d, the piston displacement becomes partially out of phase with the float, thereby yielding a larger PTO displacement than would be achieved if the piston were static.

At low mass ratios then, it is apparent that the piston is readily accelerated to larger displacements than is experienced by the float. In this configuration, it is advantageous for the spring component of the force to be at or near resonance wherein the largest displacements occur. However, the operating points with the largest damper power output are those that have the largest relative velocity and thereby the largest displacement. In those cases, the displacement vastly exceeds the acceleration tube, likely causing operational difficulties in a physical device in which reinsertion would be more challenging.

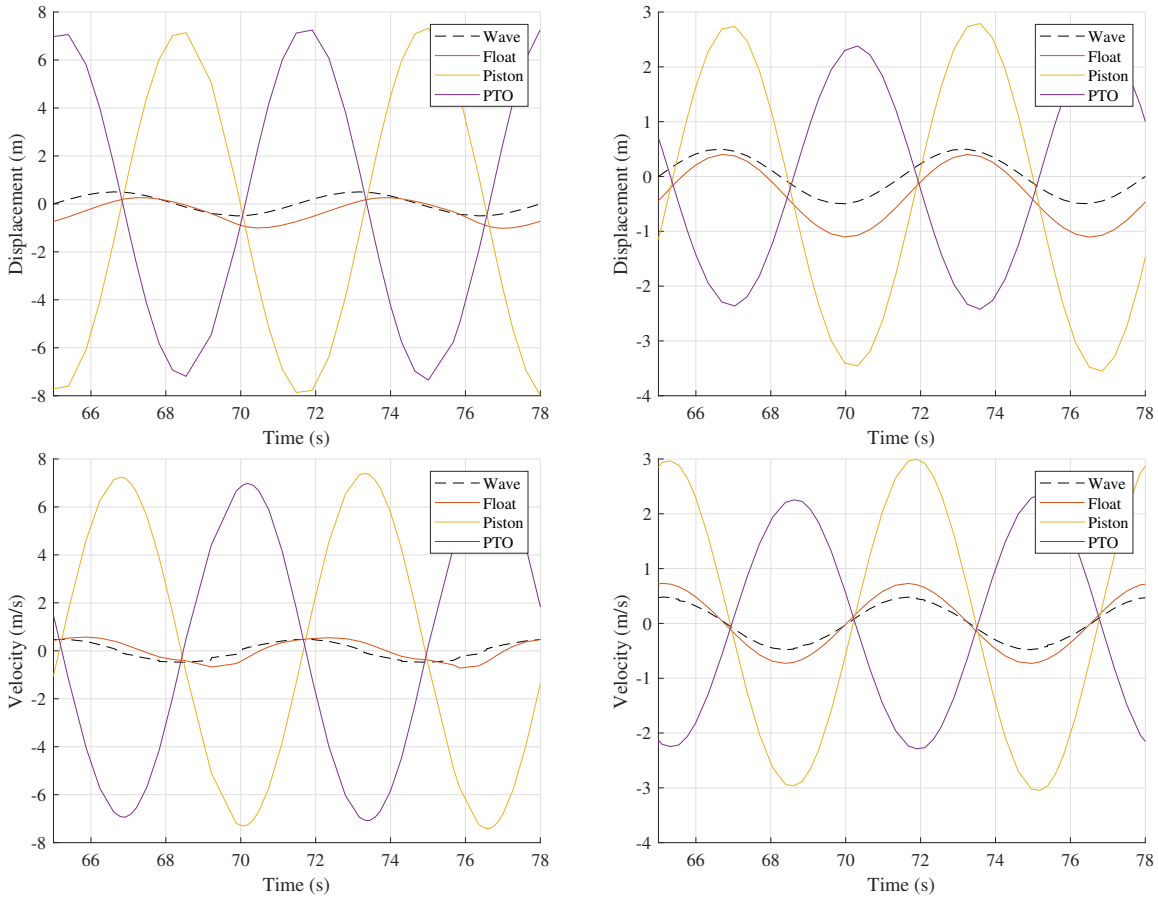

(a) Damping = 102 N s/m, Spring = 1510 N/m(b) Damping = 102 N s/m, Spring = 1870 N/m

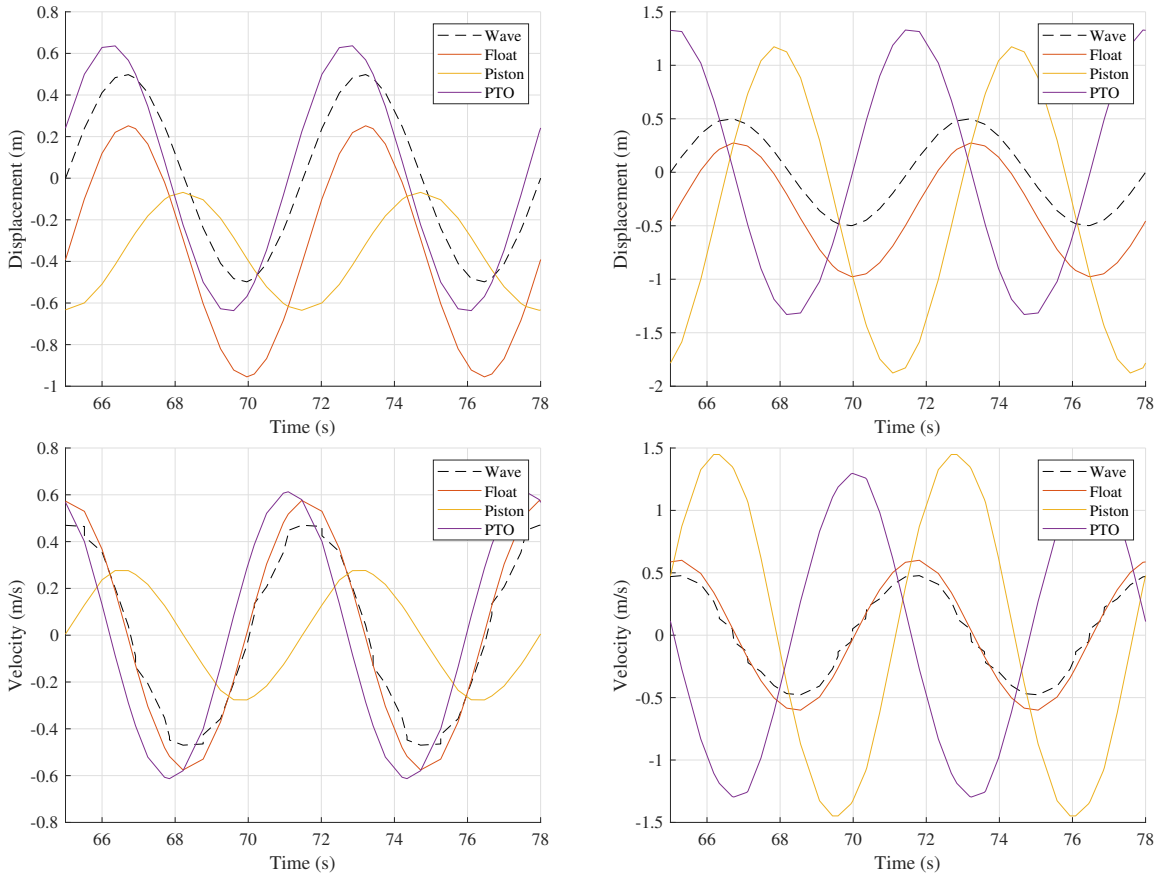

(c) Damping = 775 N s/m, Spring = 244 N/m (d) Damping = 755 N s/m, Spring = 1510 N/m

Figure 5.16: displacement profile of each component at four operating points.

For maximal power output then, it is advantageous to design an IPS Buoy with a long acceleration tube to accommodate the longest piston stroke length possible. Moreover, it is beneficial for WEC operating in heave to have a long, spar-like geometry to provide stability and prevent pitching.

On the other hand, if a direct drive machine is to be used in this WEC, a long stroke length imposes difficult design constraints on the electric machine, likely allowing the active area to cover a fraction of the stroke length without high costs or efficiency losses.

5.7 Impact of Mass Ratio in an Unsprung PTO

Section 5.6 explored the performance impact of making changes to the power take off spring and damping coefficients with a fixed WEC geometry. It was found that a significant peak in damper power occurs around resonant spring conditions. However, an equally large spring power is required to enable the near-resonant spring conditions, which must be supplied externally by the PTO. The additional power requirement for the spring component would greatly increase the PTO rating size and reduce system efficiency; a configuration that would require a much higher ratio of spring/damping power to be a worthwhile investment.

Furthermore, a near resonance spring constant improves damper power absorption by encouraging extreme oscillations and PTO velocity. In a system wherein a directly driven generator is being considered, it would be costly to produce a generator long enough to utilise the full oscillation and lower the lifespan of linear bearings. It is more effective to optimise other machine parameters and eliminate the PTO spring component.

This section aims to investigate the impact of varying the mass ratio of buoy and piston inertial mass on power absorption across the damper. In this comparison, the WEC geometry remains unchanged, and it is assumed that the acceleration tube geometry is extended such that it encompasses a larger water mass without a net impact of buoy mass. This is to compare a wide mass ratio range without the risk of the buoy sinking. Additionally, the IPS Buoy mechanical model remains the same, but the spring constant is set to zero.

Figure 5.17 shows the damper force and power across a range of mass ratio and damping coefficients. In these figures, there is not a discrete peak as was seen in section 5.6, but rather a plateau of high outputs once a minimum mass ratio and damping coefficient is supplied. The RMS force and power imply that for any given mass ratio after the PTO damping exceeds approximately 2×10^4, there are diminishing returns on damper force with further increases to the damping constant. Moreover, there is a reduction in damper power as the coefficient increases, possibly implying that as the PTO becomes overly damped, the force becomes out of phase with velocity. Furthermore, there is a downward trend of power with mass ratio which is more apparent at high damping coefficients.

Across most of the force and power results, the maximum values are approximately twice the RMS values, leading to some power profiles in which there are sharp power

spikes with smaller ripples between. In these cases, the PTO must be rated high enough to react the full force peak, but also have acceptable efficiency.

The key finding from these results is that the IPS Buoy has strict minimum requirements for both the PTO force and the quantity of inertial water contained within the acceleration tube, with a sharp cut-off in performance - particularly for the inertial mass. Once the minimum is met, the WEC comparatively level in its performance. The initial geometry was suboptimal with a mass ratio of 0.364.

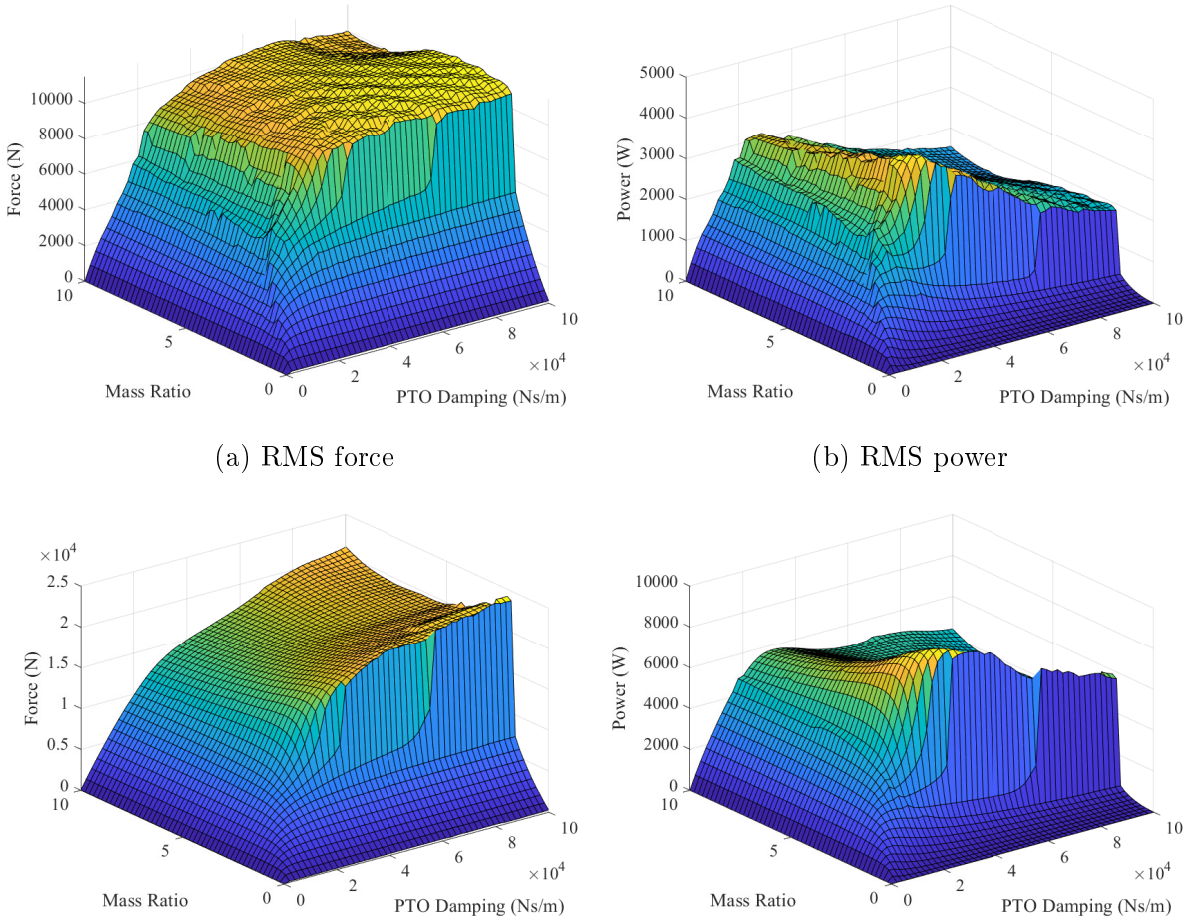

(a) RMS force

(b) RMS power

(c) Peak force

(d) Peak power

Figure 5.17: Force and power across PTO damper.

Figure 5.18 presents the displacements of each system component across a range of mass ratios, with the damping coefficient fixed at 3.16×10^4. These can be considered as the mass ratio "ridge" that can be seen in figure 5.17b.

At low values of mass ratio (figure 5.18a), the piston displays little resistance to displacement of the float, lagging it with minimal delay and a slight reduction in magnitude. Because the difference in displacement and phase is minimal, the PTO experiences equally minimal displacement and little power production; it remains so until the mass ratio reaches approximately 2.

At higher values of mass ratio, the piston shows significantly more resistance to the float displacement, reducing to approximately 50% of the float magnitude in figure 5.18c,

and 10% in figure 5.18d. However, it should be noted that a mass ratio of 50 or more would represent an extremely large mass of confined water, and an equally large acceleration tube to contain it; but this is the extent that must be reached to achieve a completely stable reference mass.

The float displacement is also impacted by the piston inertia. As the mass ratio increases, it has a resistive effect on the float, reducing its magnitude. Therefore, although the piston mass becomes more stationary, it does not necessarily enhance PTO displacement magnitude. Once past a threshold value, any further increase in the mass ratio slightly reduces the PTO displacement magnitude and output power.

Figure 5.19 presents the damping coefficient "ridge" seen in figure 5.17b. Here, the mass ratio is fixed to 2.85, and several points across the range of damping coefficients are plotted.

In the case of these configurations, there is always sufficient reactionary inertia to produce good mechanical motion across the PTO, but the power absorbed, and the mechanical relationship between float and damper is wholly determined, or rather, restricted by the damping coefficient selected. At low levels of damping (figure 5.19a), the piston encounters minimal resistance from PTO forces and oscillates at the highest magnitude possible. However, because the damping is so low, little power is extracted by the PTO.

As the damping coefficient increases, it provides a more significant force between float and piston as more power is extracted from the relative velocity. At moderate damping (figure 5.19b), there is a more significant PTO force, causing the piston to be dragged behind the float with sufficient delay such that there is still a high PTO displacement. This is the region wherein the best power performance is delivered.

When the damping is further increased, the piston delay reduces, leading to a significant reduction of PTO displacement, and becoming almost rigidly linked at extreme damping levels. During some points of the wave cycle at high damping values, the float and piston travel at almost constant velocity, reducing the effective power absorption across the PTO.

In the high damping regions, the extreme damping force pushes the float out of the water, before diving back down below the surface. In a true wave environment, the reentry of a vertical cylinder buoy would be subjected to more dynamic forces and loss of momentum. If such a configuration is to be adopted, the mechanical model must be expanded to include the nonlinear effects, or assumptions made that the float geometry is customised such that the effects are negligible relative to the other system forces.

5.7.1 Feasible Tube Geometry for High Mass Ratio

It is desirable to have a large mass ratio for optimal power output, but because the float provides finite buoyancy, and the mass ratio is linked to tube geometry, there is a maximum achievable mass ratio before the buoy becomes too submerged or sinks. It is decided that the floating body must retain 60% of its vertical length above water to

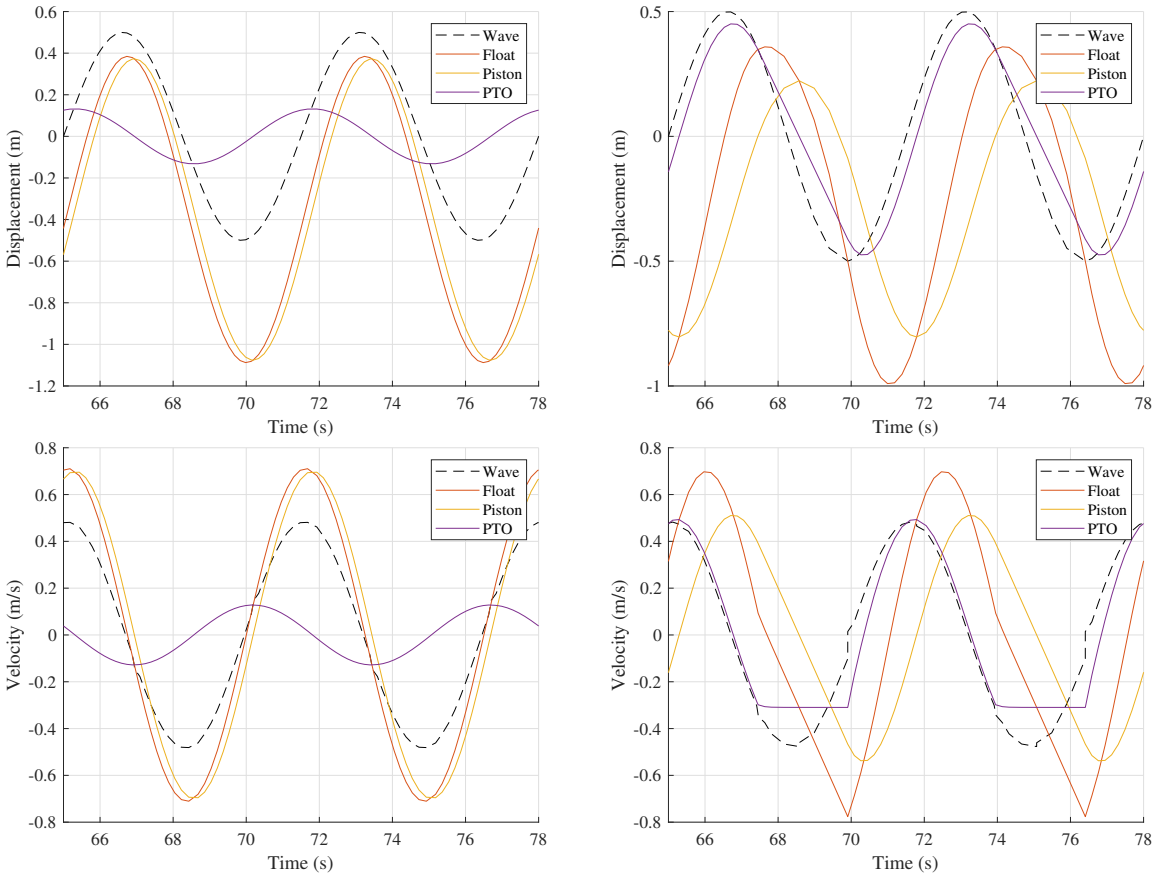

(a) Mass ratio = 1

(b) Mass ratio = 5

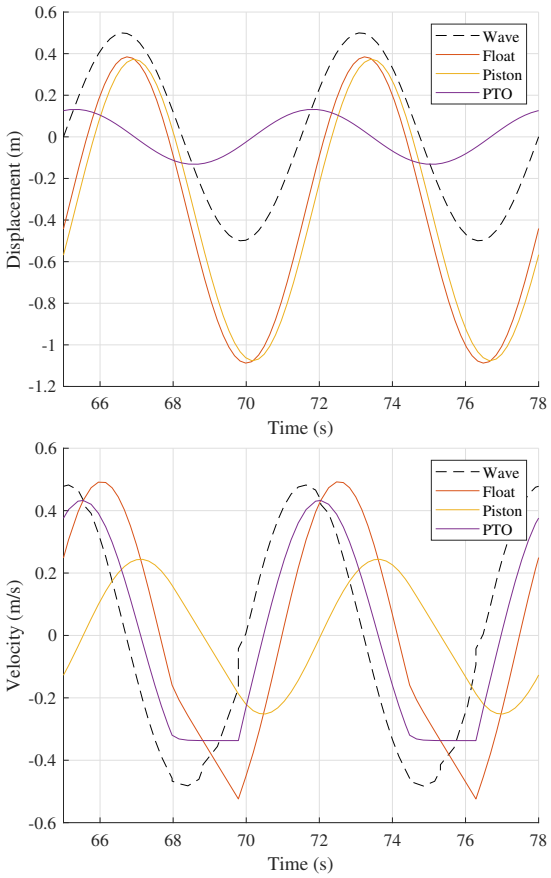

(c) Mass ratio = 10

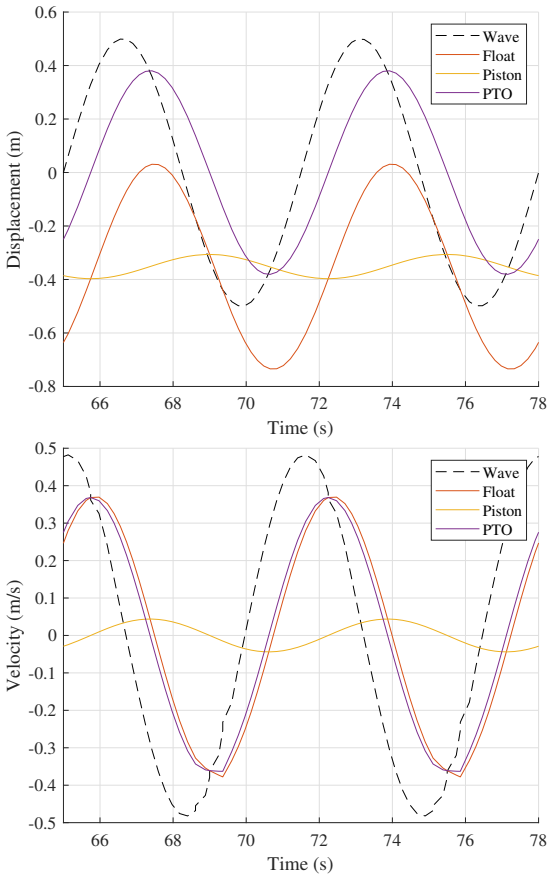

(d) Mass ratio = 50

Figure 5.18: Displacement of WEC at peak damping coefficient (31578) with mass ratio varied.

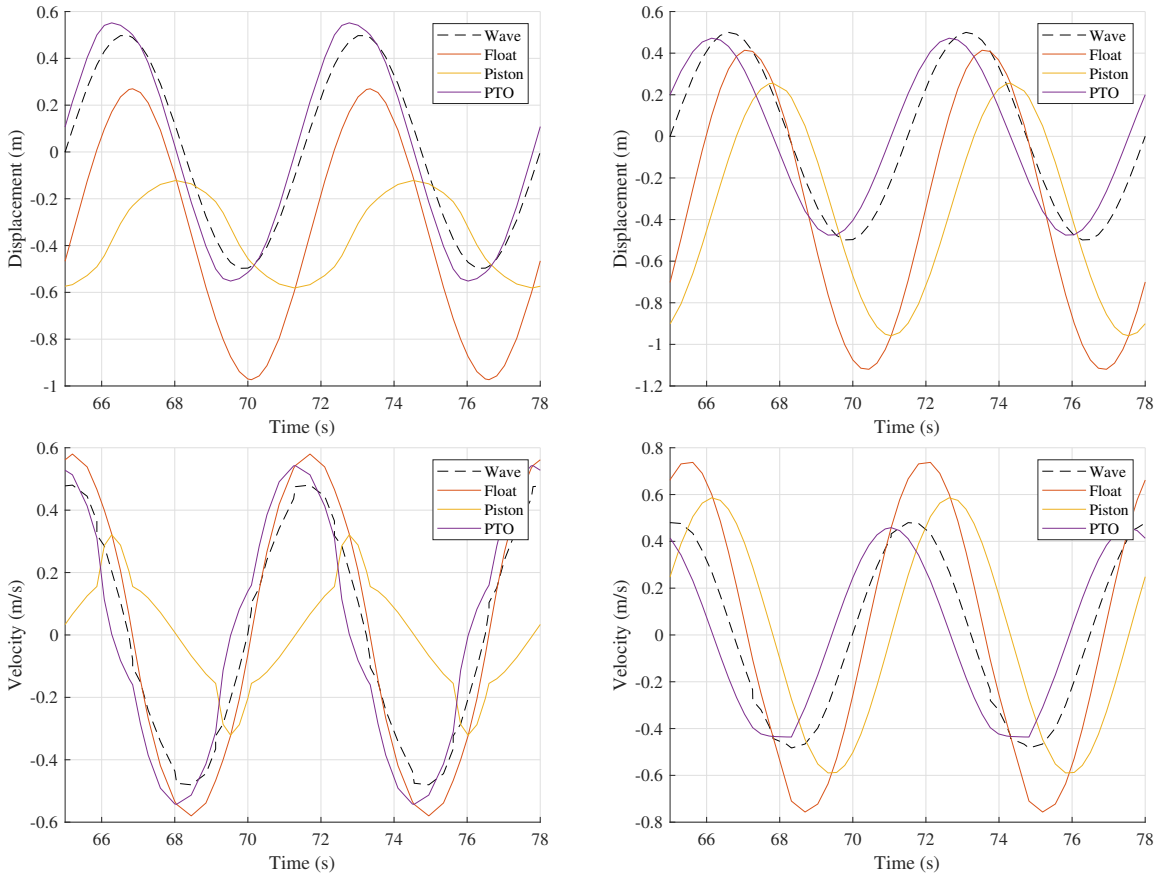

(a) Damping = 0.5e4 N s/m

(b) Damping = 2e4 N s/m

(c) Damping = 4e4 N s/m

(d) Damping = 10e4 N s/m

Figure 5.19: Displacement of WEC at peak mass ratio (2.85) with damping coefficient varied.

ensure visibility at the surface.

The maximum mass ratio for the initial float geometry (table 5.4) is presented in figure 5.20, wherein it can be seen that mass ratios of around 12 are achievable.

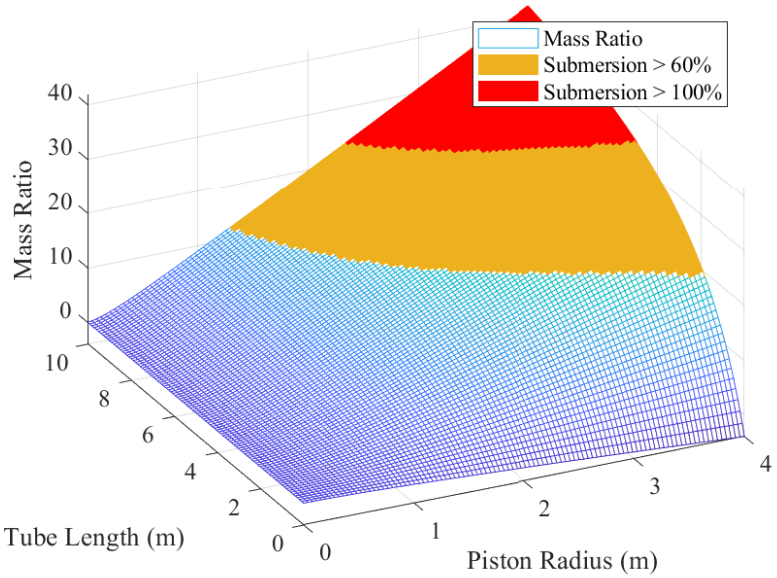

Figure 5.20: Plot of tube dimensions and their resultant mass ratio for the float geometry given in table 5.4.

5.8 WEC and PTO Specifications

Table 5.7 shows the basic WEC and PTO specifications selected for a proposed IPS buoy. The spring component is removed, and the mass ratio and damping component are set such that the minimum RMS power plateau is reached, but the float is not pushed out of the water by the PTO forces.

At this operating point, the PTO is required to be capable of reacting 14.10 kN of force at the peak speed of 0.343 m/s.

Parameter	Value
Mass ratio	8.42
Damping coefficient	31579 N s/m
Peak force	14.10 kN
Peak power	4.83 kW
Peak velocity	0.343 m/s
Airgap length	5 mm
Float radius	1 m

Table 5.7: Initial specification of wave energy converter and power take off.

5.9 Conclusions

In this chapter, the process of designing a heaving WEC from deployment location to PTO specifications has been presented and explored. A 1 m radius IPS Buoy is proposed for deployment in Blyth, UK, capable of yielding 4.83 kW in a sea state of 1 m significant height, and 6.5 s period.

Publicly available data spanning 10 years was taken for a nearby data collection buoy located off the coast of Newbiggin-by-the-Sea and analysed to assess the most suitable wave state for consistent power production with a meaningful magnitude. The site data available had a moderate quantity of poor-quality data, wherein equipment was damaged, lost power, or the buoy was cut loose. The dataset was processed to account for missing values and ensure that the statistics were not negatively impacted.

Several numerical models were derived to assess the hydrodynamic performance of the WEC and the expected power output across a power take off. The hydrodynamic Simulink model was developed using a set of assumptions, and mechanical relationships between WEC bodies, with the inclusion of PTO forces. Additionally, a numerical hydrostatic model was developed for calculating feasible geometries of a neutrally buoyant piston, with the expectation that an electric machine may be integrated; This model was not utilised in this chapter but will be in the following chapter.

In the exploration of the hydrodynamic model, key parameters were adapted to calculate the optimal expected power output from the WEC. The spring force was not strictly necessary and resulted in requiring an overrated system to operate.

Chapter 6. Integrated Design of an IPS Buoy

6.1 Introduction

6.1.1 Scope and Objectives

The previous two chapters of this thesis have stemmed from different fields of research; one being directly driven electromagnetic machines, and the other, hydrodynamic, and hydrostatic design of a Wave Energy Converter (WEC). The main goal of this chapter is to bring together the findings and design a fully marinized Directly Driven (DD) all-electric Power Take-Off (PTO) for an IPS buoy WEC with meaningful power output.

To achieve this objective, this chapter develops a case study wherein an IPS buoy is fully designed, accounting for neutrally buoyant piston geometry, integrated generator size, and linked hydrodynamic behaviour.

Using the case requirements and findings from chapter 4, a tubular Flux Reversal Machine (FRM) is compared to a tubular synchronous generator to assess which is most suitable as PTO.

6.2 Sizing of IPS Buoy and Linear Power Take Off

6.2.1 Sizing Methodology

Sizing the components of an IPS buoy is a complex and interrelated design process. Without concern of PTO, the system's maximum size and performance are underpinned by the floating body; the acceleration tube and hence mass ratio is restricted by the reserve buoyancy of the float, which when exceeded, will cause the device to sink.

The acceleration tube is also restricted by the piston geometry due to the water-tight relationship between them. The piston has strict geometric requirements to ensure it retains neutral buoyancy and directly defines the acceleration tube radius, the most sensitive component in controlling the inertial water mass. Moreover, the piston length occupies volume in the acceleration tube which could have contained water, producing a subtractive effect. However, for large tube dimensions, this has minimal impact on the mass ratio.

When the piston is set to include the translator of an electrical generator, the inter-relations are further compounded. The piston must then contain heavier electromagnetic materials, reducing the range of feasible dimensions, and its geometry additionally defines generator size and force capability. Furthermore, because the PTO force has a strong impact on WEC power output, the hydrodynamic behaviour is doubly affected.

A flow chart for the process is given in figure 6.1.

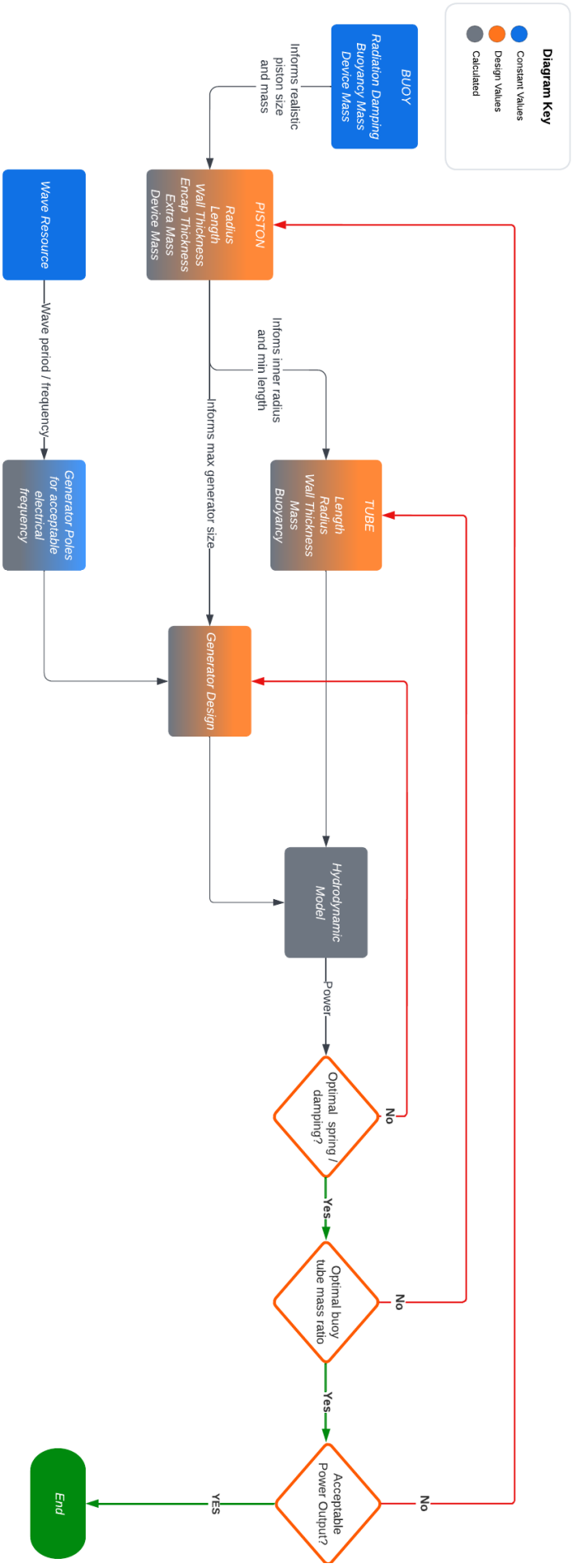

Figure 6.1: Flowchart of IPS buoy design process

Using the specifications for mass ratio and PTO force given in table 5.7, the WEC is sized from the inside out, starting with the piston/generator.

Figure 6.2a shows the required wall thickness to satisfy the neutral buoyancy assumption for a solid piston constructed of electrical steel and magnets of relatively equal density and an endcap thickness of 10 mm. Additionally, figure 6.2b presents the piston geometries giving the minimum active area required to react a 14.10 kN peak force across a range of shear stresses.

A high piston wall thickness whilst maintaining neutral buoyancy is desirable, as the wall thickness is also the translator core. It is mainly driven by the piston's outer radius, with which there is a near-linear increase in allowable thickness. The piston length has an impact only at small lengths where the buoyancy is dominated by the endcap mass; further increases raise the mass and volume at an almost constant rate with little net effect on wall thickness.

Figure 6.2b demonstrates that even at low values of shear stress, it is feasible to construct an electric machine that fits within the constraints set by the piston. Although it should be clarified that the electric machine is not required to occupy the entirety of the piston, it is reasonable for only a central portion of the axial length to be occupied by electromagnetic material, and the remainder by dedicated to buoyancy, or structural support.

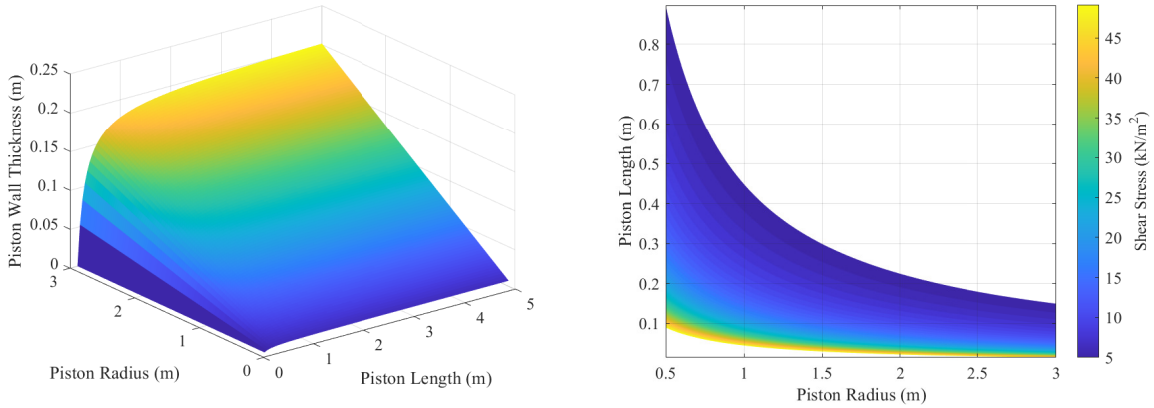

(a) Allowable piston wall thickness to retain neutral buoyancy

(b) Required piston geometry to provide 14.10 kN peak force

Figure 6.2: Geometric relationships used for sizing piston.

As the WEC is sized from the piston outwards, the radial geometry of the cylinder and acceleration tube are driven dimensions, leaving only the tube length as the controlling factor for meeting a required mass ratio. However, the required length is not an independent variable and is slightly altered by piston length and overall WEC geometry. The allowable tube length using dimensions from table 6.1 is shown in figure 6.3 for a target mass ratio of 8.4 and 1 m piston length. The relationship between piston radius and tube length demonstrates that the piston geometry can also have a strong impact on the required tube length, potentially requiring it to be unreasonably long or short.

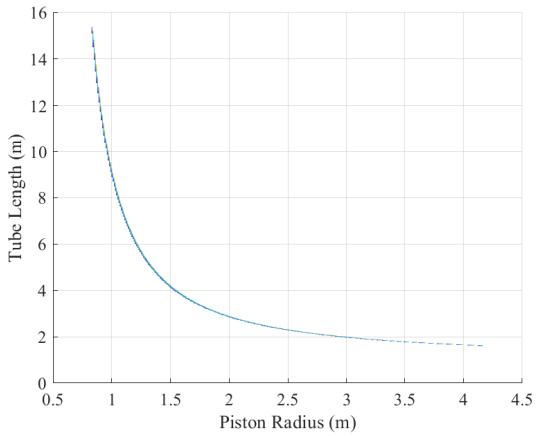

Figure 6.3: Acceleration tube geometry for 8.42 mass ratio and 1 m piston length

The sizing process demonstrated here is strongly intertwined and iterative, as it is quite easy to reach upon an improperly sized generator or acceleration tube, from seemingly reasonable choices for the piston geometry.

6.2.2 Alternative Piston/Generator Configurations

The preceding sections have assumed that the piston and generator are effectively one entity, but this is not necessarily required for a fully marinized generator. Some stator and translator configuration options are shown for the IPS Buoy presenting in figure 6.4 both the long, and short stator variants. In these figures, the piston material is denoted by light grey material, the stator in orange, and the tube and float in yellow.

The previously assumed configuration is shown in figures 6.4a and 6.4b and fully integrates the translator into the neutrally buoyant piston, resulting in an interdependent relationship between WEC geometry and PTO capacity, and imposes strict constraints on the design.

Figures 6.4c and 6.4d have the translator as a solid object rigidly attached to the floating body and the stator is affixed to the neutrally buoyant piston. Although the stator may be heavier than the translator, the neutrally buoyant piston can cover a larger radius allowing more freedom in buoyant volume and decoupling the electric machine from the hydrostatic design.

All variations shown here although presenting varying radii and stator/translator ratios, are assumed to have an equal active area. Moreover, due to the nature of linear machines, the force production can be extrapolated with axial length.

For the FRM simulations to be solved in a reasonable time, and to highlight a method of lower integration, the FRM adopts the configuration in figure 6.4c for this chapter.

6.2.3 Final WEC Geometry

The final proposed geometry is presented in table 6.1, satisfying the target specifications given in table 5.7. The float dimensions are based on typical dimensions for a navigation

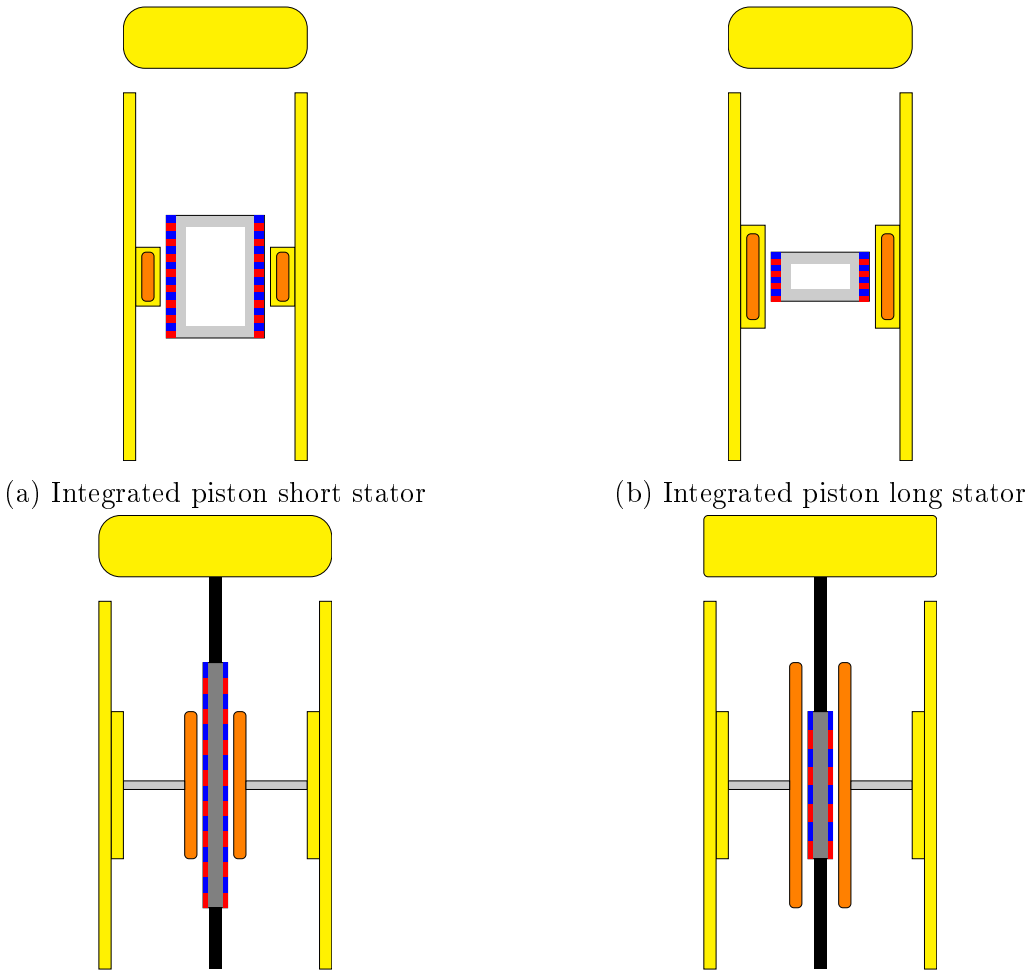

(a) Integrated piston short stator

(b) Integrated piston long stator

(c) Small radius short stator

(d) Small radius long stator

Figure 6.4: Generator configuration options for a fully marinized generator.

buoy, and wall thicknesses are assumed to be reasonable for structural integrity. The cylinder/stator length is selected as 0.2 m to restrict ohmic losses due to the long winding length caused by a large coil radius. The piston geometry is defined using figure 6.2.

Parameter	Value (m)
Float	
Radius	1
Length	2
Wall thickness (axial)	0.005
Wall thickness (radial)	0.005
Tube	
Wall thickness	0.005
Cylinder	
Length	0.2
Wall thickness	0.05
Piston	
Wall thickness (axial)	0.01
Miscellaneous	
Piston/Cylinder airgap	0.005

Table 6.1: Predefined WEC variables

6.2.4 Hydrodynamic Behaviour at Specification

As the piston and tube geometries are somewhat changed from the initial specifications, the hydrodynamic simulation is re-run with updated geometries, and the results are presented in figure 6.5.

With the inclusion of the final geometry, there is a slight reduction in the peak force and an increase in peak velocity, allowing for a larger expected power output and higher velocity. The specifications are restated in table 6.2 and will be used in the assessment of electrical generators. Generator designs must stay true to the geometric parameters otherwise the hydrodynamic performance may no longer be valid, requiring another cycle around the design flow per figure 6.1. The airgap length is set to 5 mm to accommodate antifouling measures as reported in [79], which is at a similar scale to a surface PM synchronous machine reported in [182].

6.3 Conventional Machine Topology

6.3.1 Methodology

This section seeks to compare a Linear Tubular Synchronous Machine (LTSM) in four configurations, to assess their suitability for application in a wave energy converter, the most performant of which will be selected for comparison to the FRM developed in chapter 4 for the Mocean device. The synchronous topology has been selected due to its

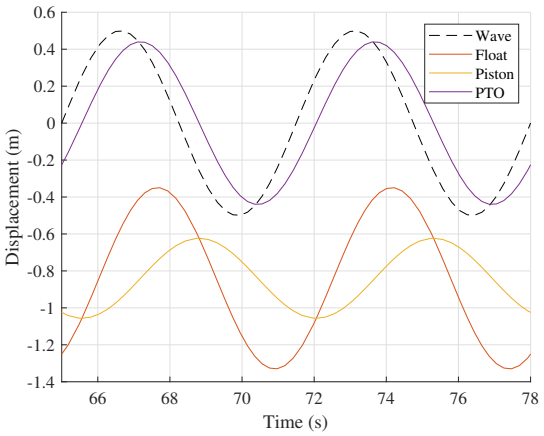

(a) Displacement

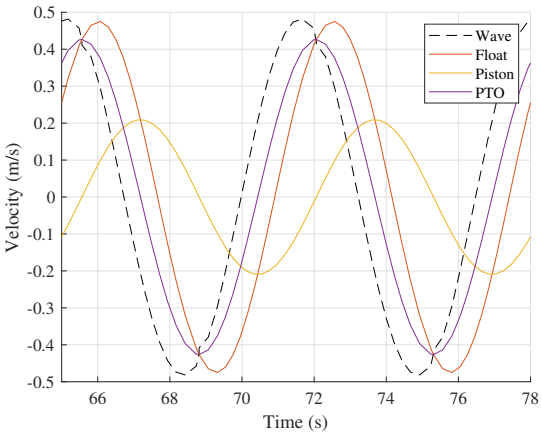

(b) Velocity

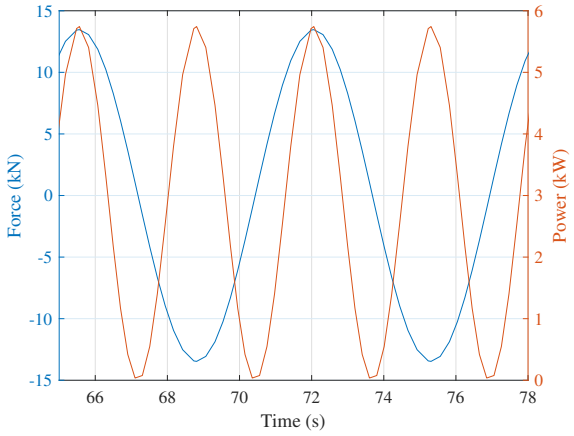

(c) Force and power

Figure 6.5: Hydrodynamic performance of IPS buoy geometry selected with parameters $H_s = 1$ m, $T = 6.5$ s, $C = 31579$ N s/m.

Parameter	Value
Mass ratio	8.42
Damping coefficient	31579 N s/m
Peak force	13.47 kN
Peak power	5.74 kW
Peak velocity	0.427 m/s
Piston outer radius	1250 mm
Cylinder length	200 mm
Airgap length	5 mm

Table 6.2: Final specification of wave energy converter and power take off.

often-favourable comparison in Direct Drive (DD) applications [183], and is made tubular due to its integration into the structure of a hollow piston.

6.3.1.1 Justification

In this comparison, all configurations of LTSM are designed such that there is constant geometry across the translator and stator, and where possible, a constant quantity of electromagnetic materials.

For the translator, the back iron, magnet height, and magnetic poles are kept constant throughout. However, for the Halbach configuration of magnets, the magnets are broken down into smaller pieces to create the Halbach effect.

The stator is the shorter element of the machine and retains a constant coil height, and in the topologies with a back iron, this is constant and in addition to the coil height. The coils have a fixed wire diameter of 1 mm and the number of turns is a function of the coil cross-sectional area and a fill factor of 0.5.

6.3.2 Four Configurations

In the integrated IPS concept, generator mass is critical to ensure the float can support the machine, and that the piston remains neutrally buoyant. For this reason, there is a focus on the generator selection for minimal iron topologies. The four topologies studied here are shown in figure 6.6. Each of the configurations is constructed with three coil phases and simulated using "MagNet".

Each of the variants is fully pitched, wherein each coil phase is wound with one outward and one return side across a single magnet pair, making for 6 coil sides per electrical pitch.

These machines represent the fully integrated piston layout presented in figure 6.4a. The stator contains the magnets, and it is assumed that it is structurally supported by the WEC tube and an epoxy matrix or non-magnetic frame which does not impact the airgap length. The translator holds magnets of alternating polarity and forms a sealed hollow cylinder with non-magnetic endcaps, which are not present in the FEA models.

The considered configurations are:

- Air core.
- Air core with Halbach array magnets.
- Air core with iron teeth.
- Iron core.

Because the airgap must be 5 mm to enable the inclusion of antifouling measures, the air-cored variants have more difficulty in flux crossing the airgap. Therefore, a Halbach magnet arrangement is included to improve airgap crossing behaviour. The Halbach array

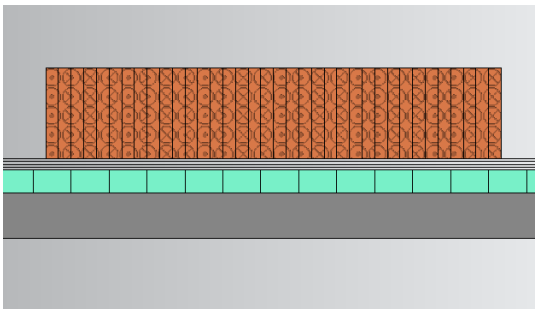

(a) Air core

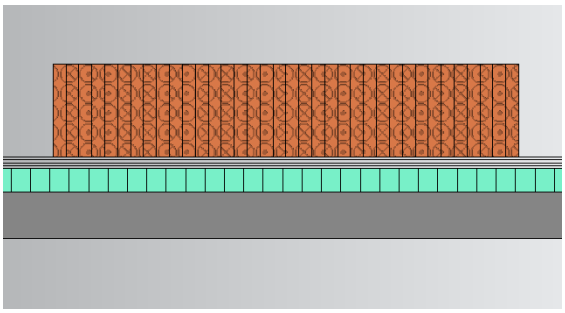

(b) Air core with Halbach magnet arrangement

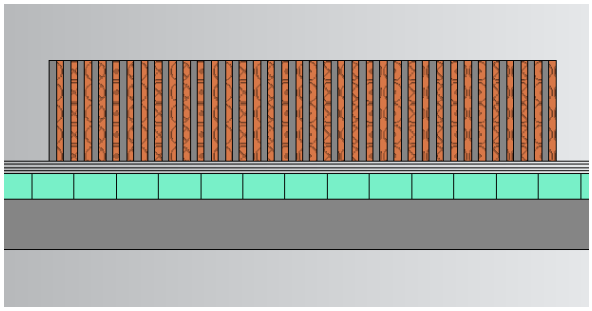

(c) Air core with iron teeth

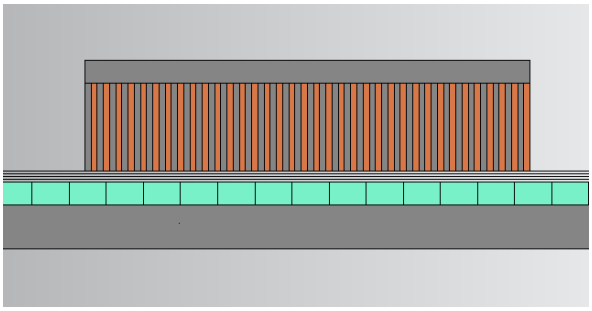

(d) Iron core

Figure 6.6: Four configurations of tubular synchronous machines under consideration. All devices have surface-mounted magnets, magnetised in the radial direction, and presented as 12 pole topologies.

is arranged with alternating magnets of radial and axial magnetisation, and the angle of magnetisation is not optimised in this comparison.

The machines were axis-symmetrically modelled in 2D FEA at full scale and with symmetry about the Z-axis because the simulation time is relatively low, and to ensure that end effects are accounted for.

Figure 6.7b presents the air-cored machine as is modelled, and figure 6.7a shows a close-up of the mesh for an iron-cored variant. Because of the high energy transfer across the airgap, it is split into two remesh regions and two airgap regions between the translator and stator, all four of which are given a fine mesh.

6.3.3 Pole Selection

In conventional rotary generators such as those used in wind turbines, the selection of translator poles is an important consideration. It is often chosen per the rated speed and a variable speed gearbox utilised to maintain the speed. This is done so that a near constant 50-60 Hz power is produced and contributed to the grid.

However, the target wave specification is 6.5 seconds (0.154 Hz), magnitudes lower than the grid power supply. In an electric machine, the electrical frequency can be given by:

$$f = \frac{1}{\tau/u} \tag{6.1}$$

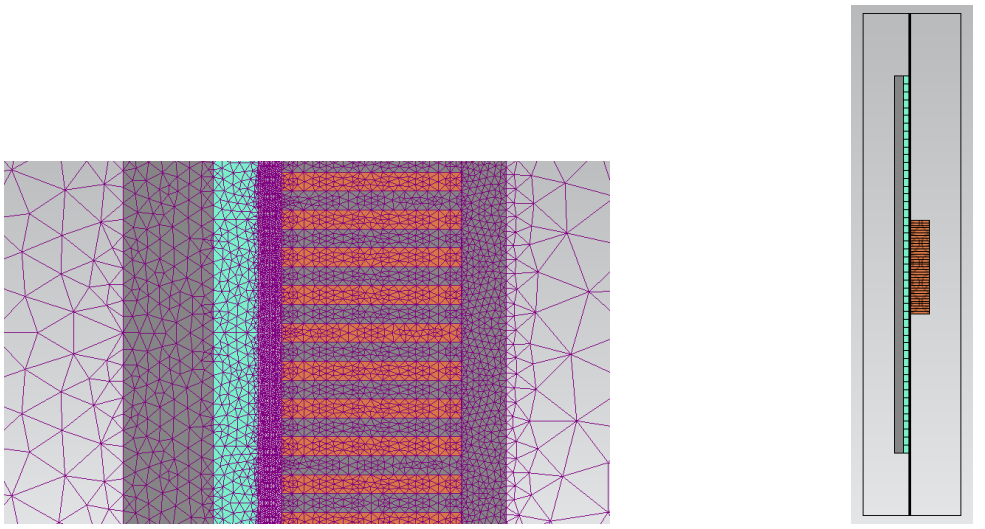

(a) Mesh of iron-cored model. (b) Full air-cored model.

Figure 6.7: FEA model of a linear tubular synchronous machine

Where τ is the pole pitch, and u is the translator velocity.

Because the stator is linear and of fixed length, the pole pitch is a function of the pole number, where L and P are the length and pole number.

$$\tau = \frac{L}{P} \tag{6.2}$$

Figure 6.8 shows the relationship between electrical frequency and resultant pole pitch for the machine dimensions set. When a higher peak frequency is targeted, it requires the stator to be split into smaller pole lengths.

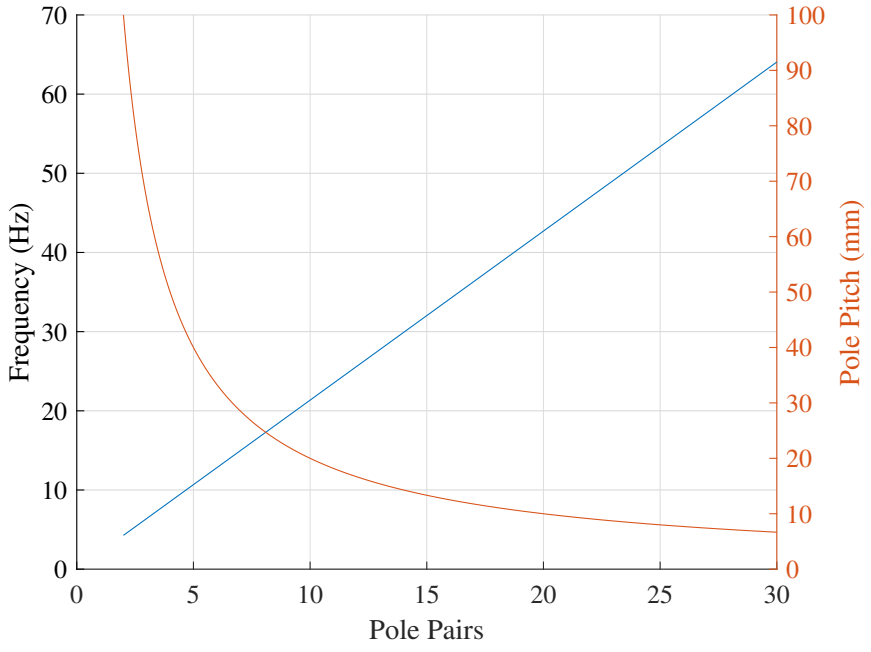

Figure 6.8: Comparison of pole pitch and electrical frequency with varying pole numbers

The increase of pole pairs then becomes a multi-faceted design choice, as a smaller pole

length reduces the available space for coil windings and increases the risk of saturation in iron-cored stators.

6.3.3.1 Unloaded Pole Number Comparison

Unloaded electrical performance of the generators is shown in figure 6.9. It can be seen here that the largest peak amplitudes across all generator variants occur at low magnetic pole numbers and reduce as more poles are added. This is caused partially by wider magnets allowing greater flux linkage across the large airgap, but also the number of turns being linked to coil area. As the stator is divided into more poles, the resulting coil area is reduced, allowing for fewer turns, and therefore lower induced voltage.

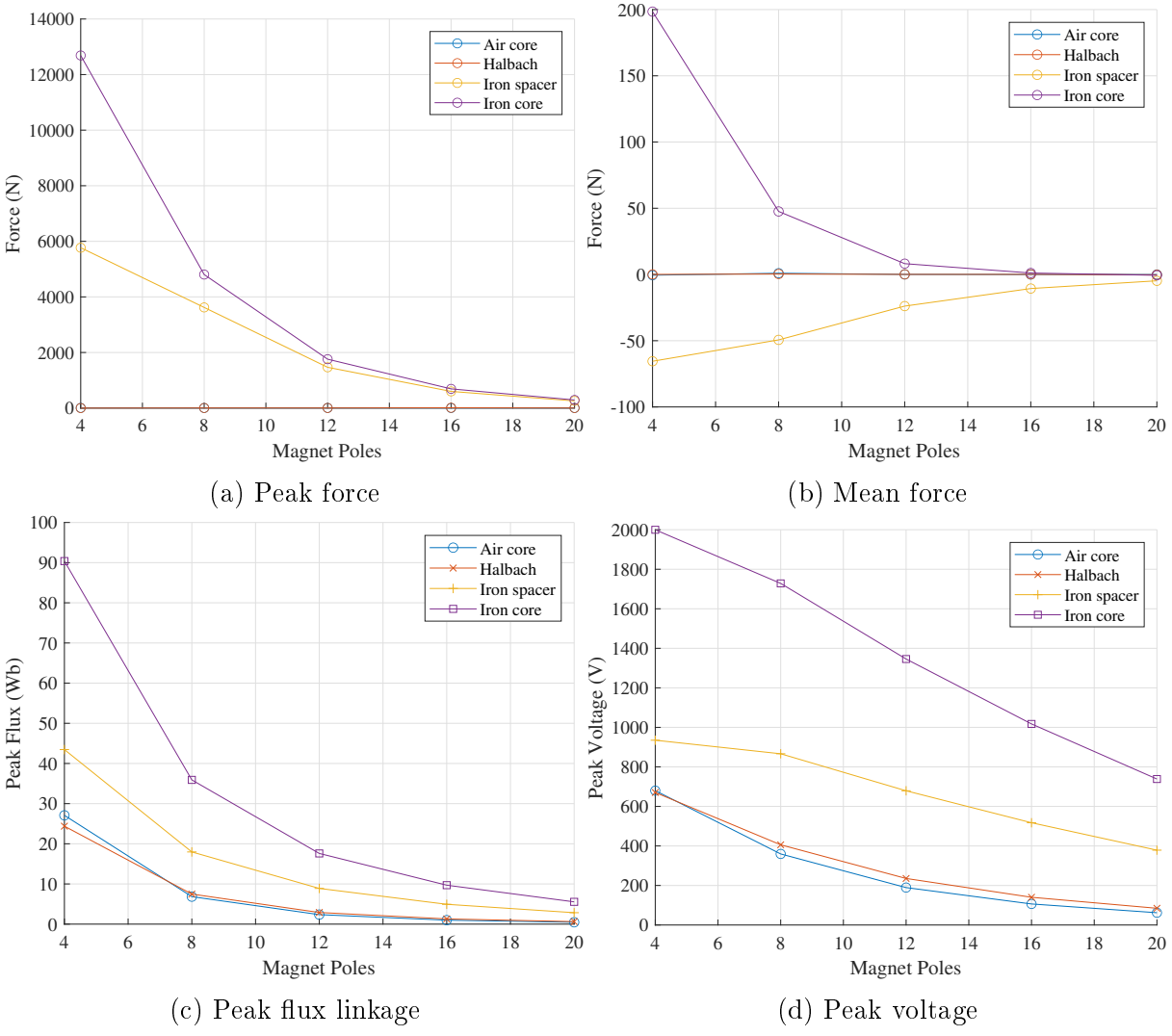

(a) Peak force

(b) Mean force

(c) Peak flux linkage

(d) Peak voltage

Figure 6.9: Generator performance with no electric load.

The reduction of flux magnitude with higher poles is not necessarily a negative impact. Figure 6.9a shows that the generator variants containing iron have extremely high cogging force peaks at low magnetic pole numbers, likely prohibitively large for use in a wave energy converter as the cogging force must be overcome for PTO displacement to occur. The air-cored variants on the other hand have near negligible cogging force as is expected

from the absence of iron in the stator.

Across all magnetic poles, the iron-cored machines are dominant in flux linkage and voltage magnitude, despite the iron teeth reducing the coil area and hence coil turns by half. The air-cored machines have very similar electrical performance, although the Halbach machine tends to yield slightly higher magnitudes. On the other hand, the machine with iron teeth yields higher performance, and the fully iron-cored machine is significantly higher than all, particularly at low pole numbers.

With further increases in the pole numbers outside the range presented, the stator teeth in the iron-cored machines are likely to become so small that saturation becomes a limiting factor, allowing the air-cored designs to be more performant.

6.3.3.2 Loaded Pole Number Comparison

The generator behaviour across the same range of magnet poles is presented in figures 6.10 to 6.12 with a 0.71 A_{rms}/mm^2 electrical load across the coils. Because the wire radius is fixed, the number of turns and wire current is proportional to the coil area; therefore, the wire current magnitude is constant across all magnet poles:

$$turns = \frac{A_{coil}}{A_{wire}}, \qquad I = \frac{JA_{coil}}{turns} = JA_{wire} \tag{6.3}$$

Where J is the current density and A_x represents the area.

As was the case with unloaded results, a low number of magnet poles provides both the greatest benefits and consequences; here the highest voltage and thrust force is generated, but with a high force ripple. Figure 6.10 presents the average force with the upper and lower ripple bounds marked alongside. The iron-cored variants display large ripple amplitudes at low pole numbers, which reduce significantly as magnetic poles increase, whilst also reducing average force output, particularly in the full iron core.

On the other hand, the air core variants have near negligible ripple due to their absence of iron, but also with a much lower mean force. As before, the difference between the two air-cored variants is relatively minor, with a slight improvement in the Halbach array.

In the air-cored machines, there was a turning point in the results at the 12-pole design where the machines create more losses than there is power available, producing misleading results for a design that is infeasible. For this reason, the data for such designs have been removed from the results presented in this section.

6.3.3.3 Power and Losses

In these results, the electrical power is calculated by:

$$P_E = \sum_{i=1}^{3} V_i I_i \cos(\phi_i) \tag{6.4}$$

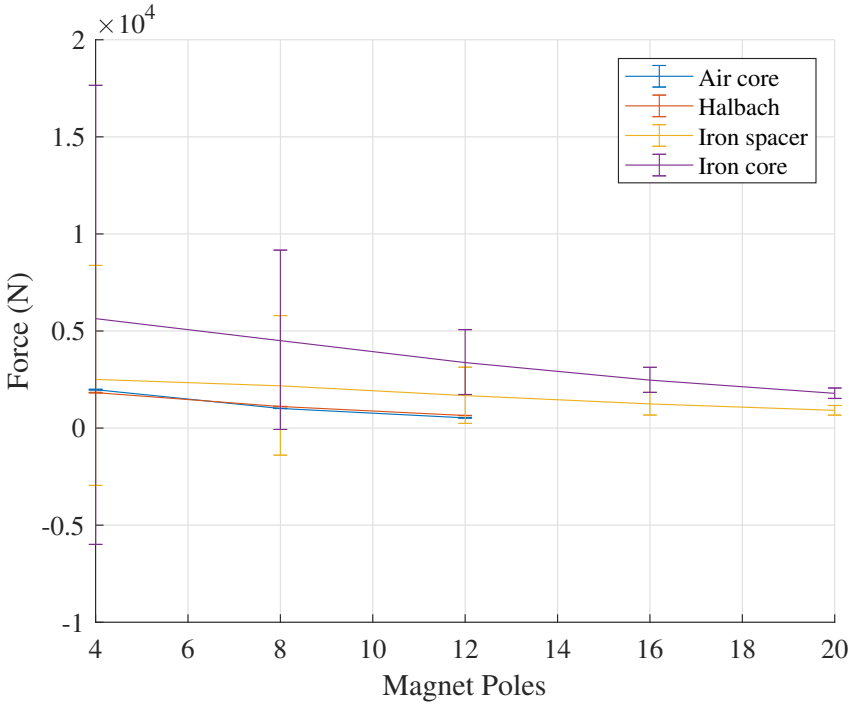

Figure 6.10: Thrust force with 0.71 A_{rms}/mm^2 AC electrical loading.

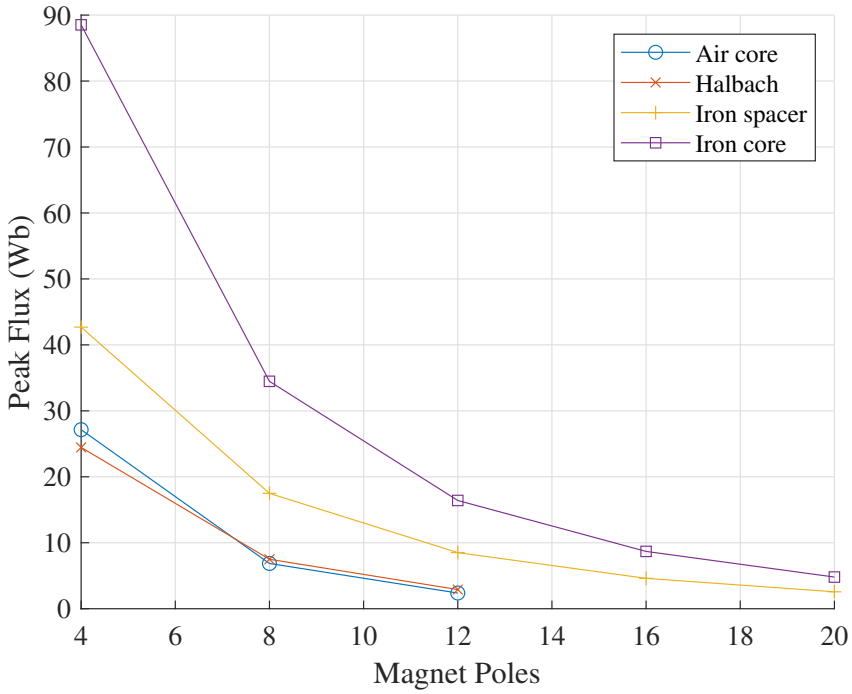

Figure 6.11: Peak flux linkage with 0.71 A_{rms}/mm^2 AC electrical loading.

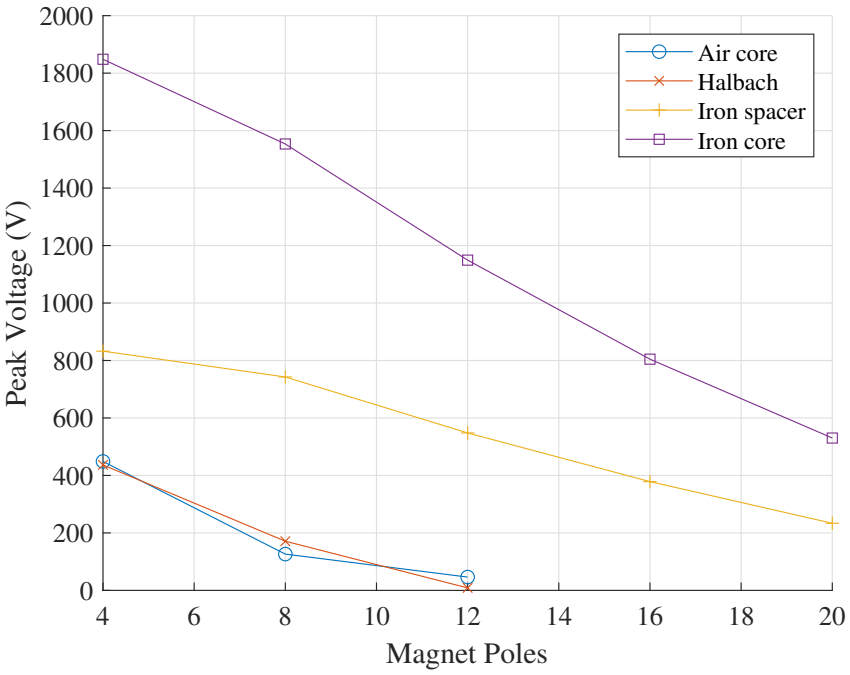

Figure 6.12: Peak voltage with 0.71 A_{rms}/mm^2 AC electrical loading.

Wherein subscript i represents each coil phase, V is the voltage, and ϕ is the phase difference. The efficiency is calculated from the provided losses from FEA in the form of:

$$P_\eta = \frac{P_{out}}{P_{in}} = \frac{P_E}{P_M} = \frac{P_E}{P_E + P_L} \tag{6.5}$$

Where P_M and P_L are the mechanical power and losses respectively.

The power production, losses, and efficiency are presented in figures 6.13 to 6.15. The power production appears similar to the voltage figure; the iron-cored machines achieve the highest electrical power, with all designs reducing in power as the number of magnet poles increases.

Because the designs are tubular, and the radii are large, a very large length of wire is required for each coil, yielding significant ohmic losses. The breakdown of losses in figure 6.14 shows that the total losses are dominated by ohmic loss. In the iron-cored machines, the iron teeth occupy 50% of the coil space, effectively halving the allowable number of turns, thereby enforcing a limit to the ohmic losses. This is apparent in the iron-toothed machine which presents approximately half the ohmic losses encountered by the air cores; the fully iron-core machine, however, introduces new ohmic loss mechanisms by linking the teeth together. At low pole numbers, the iron machines have the greatest iron losses, however, they are much less significant than the ohmic losses.

Overall, the air-cored machines have the highest losses and achieve the lowest efficiency, while the fully iron-cored variant is the most efficient.

To maintain high force production in the air-cored machines, without incurring extreme force ripple from the iron machines, the 12-pole design is selected for further analysis.

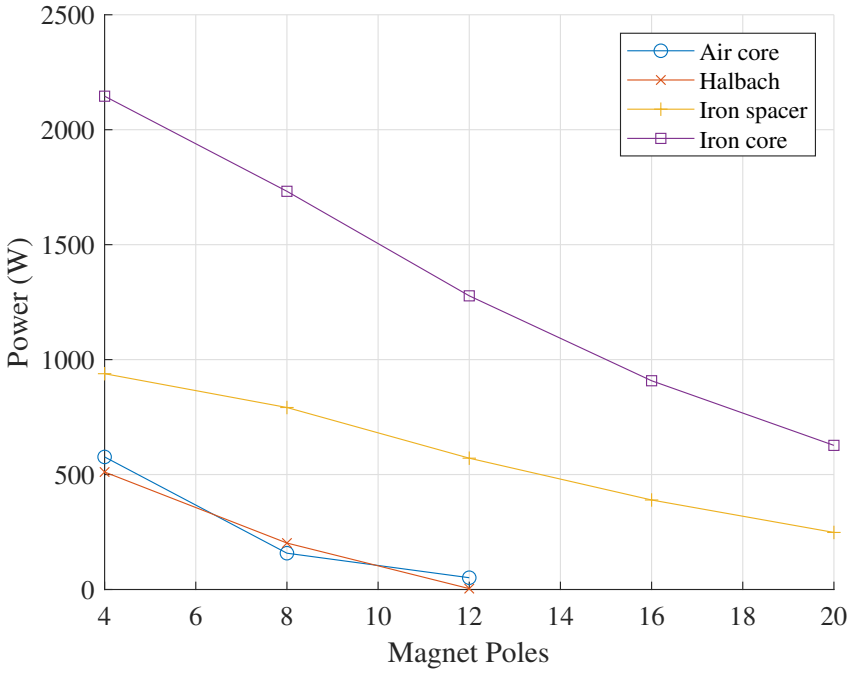

Figure 6.13: Electrical Power with 0.71 A_{rms}/mm^2 AC electrical loading.

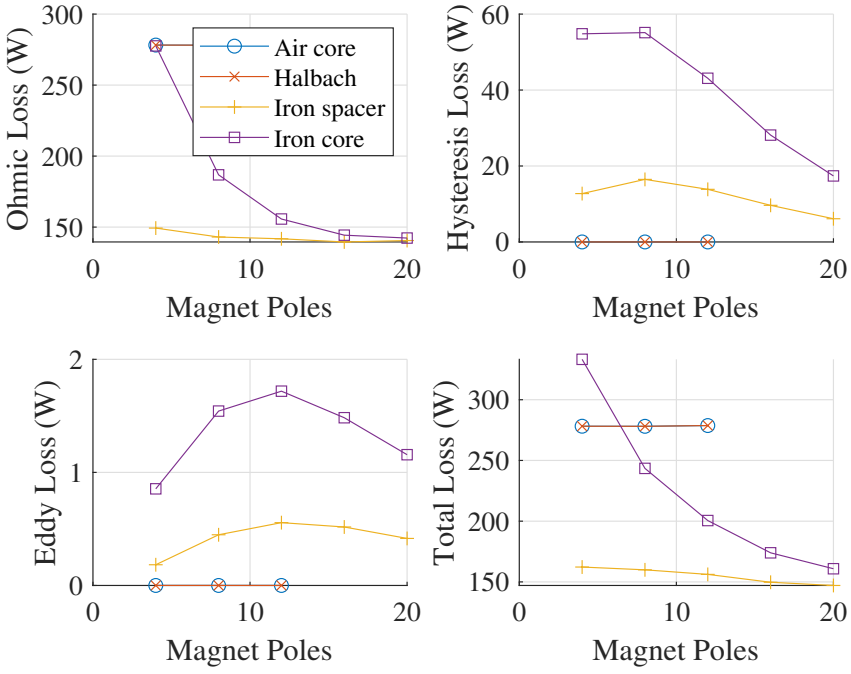

Figure 6.14: Losses with 0.71 A_{rms}/mm^2 AC electrical loading.

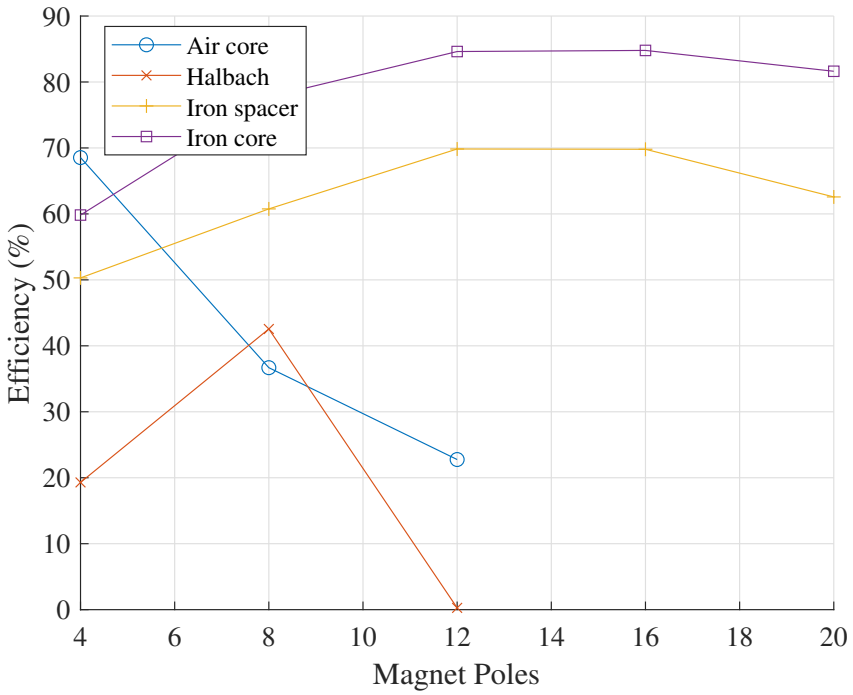

Figure 6.15: Efficiency with 0.71 A_{rms}/mm^2 AC electrical loading.

6.3.4 Current Density Comparison

This section compares the four topologies in the 12-pole variant across a range of current densities. Here the current density is varied from 0.7 - 2.1 A_{rms}/mm^2 with no alteration to the model geometry. Following equation (6.3), the current is constant across all topologies and increases linearly with current density. The results are shown in figure 6.16

With a fixed geometry, the torque ripple in the iron-cored machines holds fairly constant across the range of current densities, increasing gradually with higher currents, and lowest as the current approaches zero. The air core machines remain without force ripple, but lower in magnitude. Additionally, the thrust force of all machines increases approximately linearly in the presented current density range.

The flux linkage remains moderately constant, but a gradual decline in voltage is present among all topologies.

6.3.4.1 Power and Losses

The power and losses are shown in figures 6.17 to 6.19; with no variation of geometric parameters, the relationship between current density and the loss modes is quite simple. Iron losses are naturally only present in the iron-containing topologies and are relatively unaffected by increases to current density. Except at very low current density, the iron losses are insignificant, and the losses are again driven majorly by the ohmic losses. Because the losses are given by $P_\Omega = I^2R$, the loss component increases roughly to the square of the current, although with a smaller gradient for the iron-cored machines, due to their lower number of turns.

Figure 6.17 shows that all machines except the fully iron-cored design have difficulty in

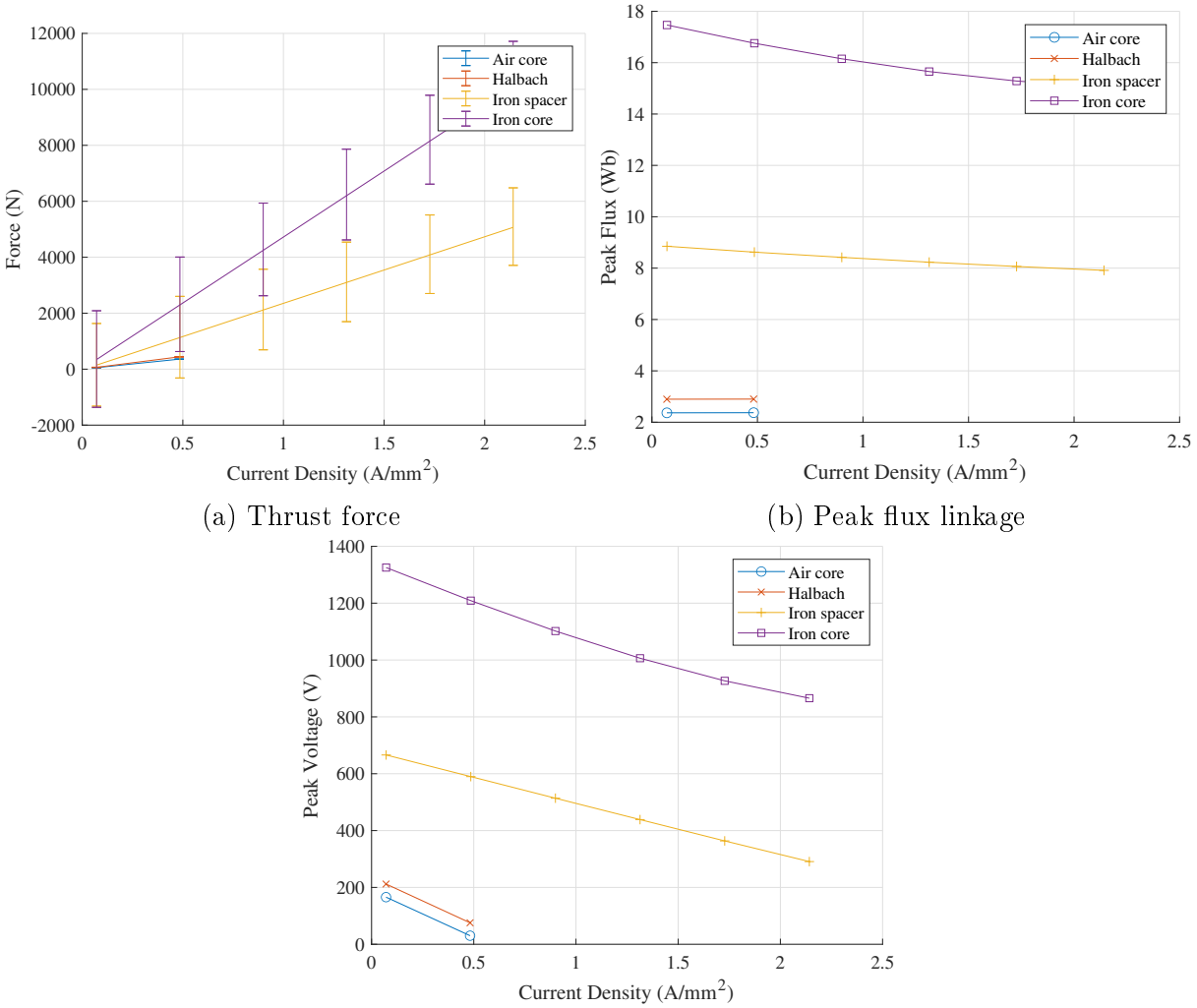

(a) Thrust force

(b) Peak flux linkage

(c) Peak voltage

Figure 6.16: Generator performance with variable AC electrical load in RMS phase values.

producing sufficient power to outpace the rapidly increasing ohmic losses. The air-cored machines cease to function at around 0/7 A_{rms}/mm^2, and the iron-toothed variant has visibly diminished returns on electrical power, with efficiency rapidly falling after around 0.5 A/mm^2.

On the other hand, the iron-cored machine gains healthy electrical power with increases in current density and retains fairly high efficiency in the presented data.

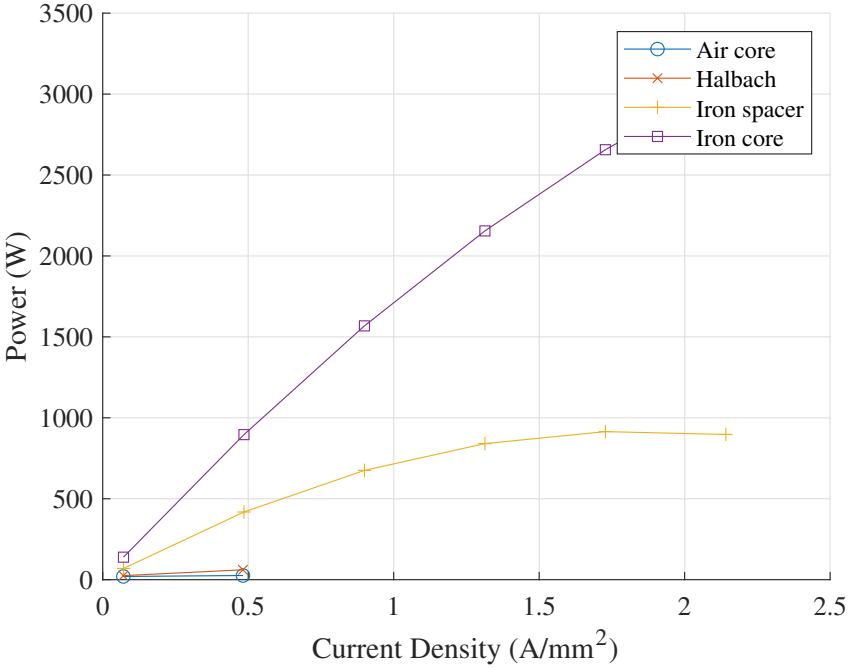

Figure 6.17: Electrical power with variable AC load in RMS phase values.

6.3.5 Discussion

In the past sections, 4 configurations of an LTSM have been sized for a WEC of fixed specifications and constraints. It was required for the generators to be capable of reacting 13.47 kN at 0.427 m/s.

The requirement for a 5 mm airgap poses difficulty for air-cored topologies; without further optimisation or relaxation of allowed airgap, it is not feasible for an air-cored machine to react with sufficient force. Moreover, with a higher translator velocity, there would be higher mechanical power in the generators, thereby increasing the allowable electrical load. However, the air core designs are simply not suitable for slow-speed applications in their current configuration.

The fully iron-cored machine is the best-performing variant in terms of force production and is the only one capable of meeting the rated force, as such it will be selected for further comparison to an FRM.

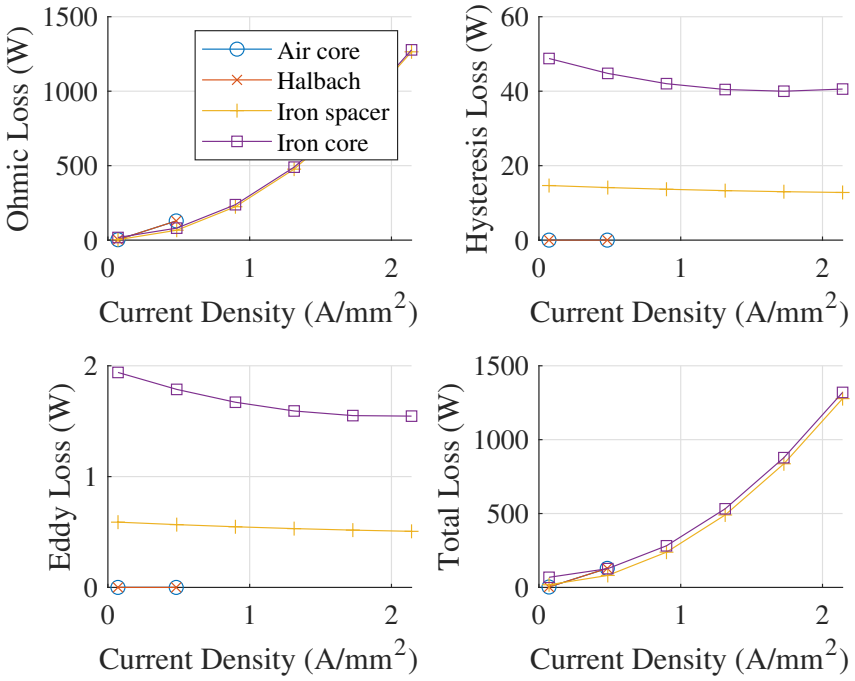

Figure 6.18: Peak current with variable AC load in RMS phase values.

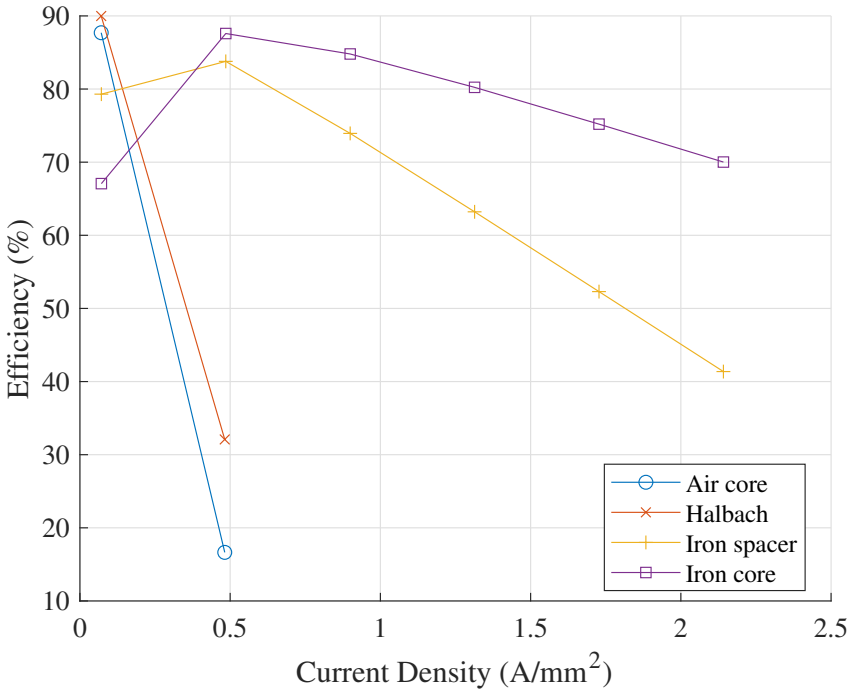

Figure 6.19: Efficiency with variable AC load in RMS phase values.

6.4 Flux Reversal Machine

6.4.1 Introduction to Topology

The FRM was introduced in chapter 4 in the form of a rotary machine and was found to be advantageous over a Vernier Hybrid Machine (VHM) for its slight advantage in electromagnetic performance.

It is presented in this section in its configuration for linear motion. For linear motion FRMs, the design is much less constrained geometrically and conceptually. The magnet width for example can be increased to any required length, not constrained as a portion of the machine radius, as is the case with rotary machines. Additionally, the translator or stator may have one or multiple sides, becoming similar to a tubular machine when sufficient sides are used [184].

A concern in linear DD wave energy is the sealing requirements of the electrical generator. In multi-sided topologies of FRM, the translator has a non-circular cross-section, imposing greater difficulty and cost on the machine water seals.

As with the synchronous machine, the generator is intended for a flooded application and is independent of sealing concerns, but also adopts a tubular topology for integration into a neutrally buoyant cylinder.

Although unconventional in design, it has been shown that any flat topology can be converted into a tubular scheme with some customisation and a 3-dimensional flow of flux [185, 186].

The tubular topology is effectively achieved by taking a flat double-sided FRM, rotating the magnets 90° and wrapping the machine about its axis of motion with each stator side connected as one yoke, such that it appears similar to the rotary design. The resultant machine, first proposed in [185, 186], is shown in figure 6.20.

6.4.1.1 Stator Tooth Position and Cogging Shift

It can be seen in figure 6.20a that each of the phases is equally spread around the stator circumference as would be seen in a rotary topology. However, because the direction of motion is along the axis, there must be a mechanical shift between the translator teeth to provide the 120° spacing between phases. The gap required between stator teeth of differing phases is given by:

$$\tau_p = \tau_t \cdot \frac{120}{360} \tag{6.6}$$

Where τ_t is the mechanical pole width of the translator.

Figure 6.21 shows the FRM in a flattened state, as though it were cut between tooth *B1* and *A1* in figure 6.20a and unrolled. Each stator phase has two teeth around which the flux links, with 120° between each phase (figure 6.21a), but there is also the option to introduce a pole shift within each phase. By shifting one side of each pole (figure 6.21b)

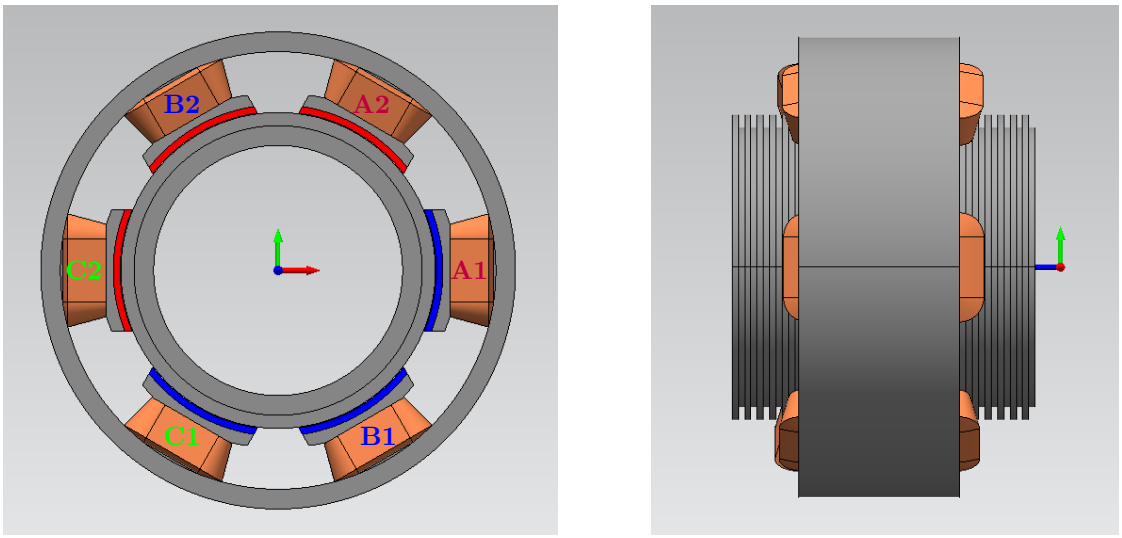

(a) Front

(b) Side

(c) Isometric

Figure 6.20: Tubular FRM concept

cogging forces may be manipulated at the cost of peak back EMF and manufacturing complexity. It was demonstrated in [185] that a 30° cogging shift is ideal for low cogging forces at a minimal cost.

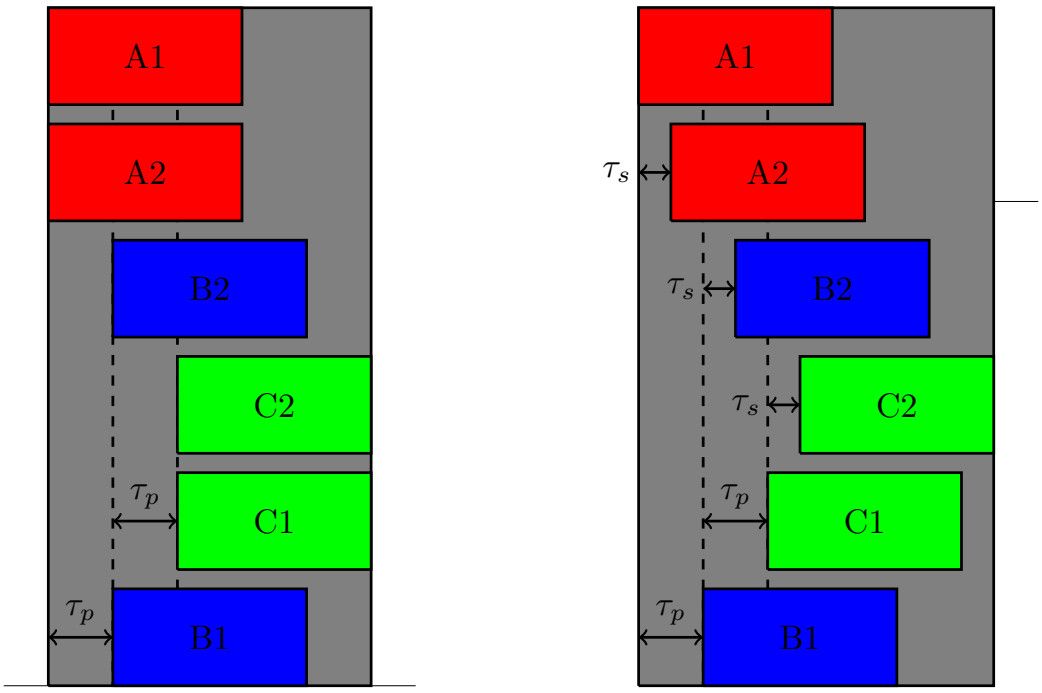

(a) No shifting (b) Shifted

Figure 6.21: Unrolled tubular FRM shown with and without cogging shift.

The cogging shift is given by:

$$\tau_{shift} = \tau_t \cdot \frac{30}{360} \tag{6.7}$$

6.4.1.2 Mode of Operation

The tubular FRM operates much the same as the rotary or flat variants; the stator magnetic field is modulated by the translator iron teeth, achieving rapid flux reversal across short pole pitches. However, because the magnets and stator teeth are located along the axis of motion, the machine flux paths are inherently three-dimensional.

Although the machine operates with three-dimensional flux does not do so in the same way as a machine like the Transverse Flux Machine (TFM) wherein the flux travels in three dimensions. At any displacement, each phase of the tubular FRM can be thought to be a slice of the machine with a 2D path where the flux loop links two corresponding magnets of a single phase with a single translator tooth. There is some linkage of flux in the axial direction, but it is not significant to the machine's performance.

The flux paths for each machine are shown as a lamination slice for each phase in figure 6.22 where the dashed red line is the flux path. Each phase comprises two stator teeth and forms a flux path linking a slice of translator and stator. Ideally, there is

complete isolation between the phases and no axial leakage, however, in a full structure there is interphase overlap (figure 6.21) and intra-phase overlap in shifted designs.

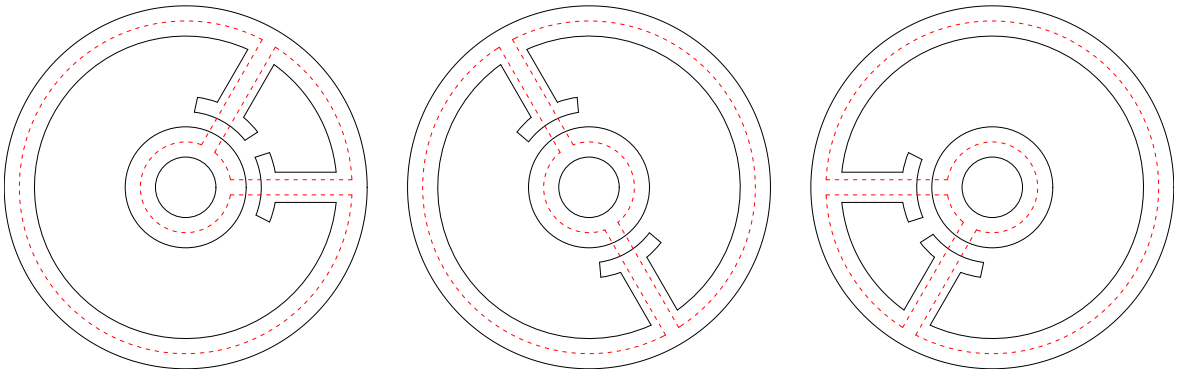

(a) Phase A (b) Phase B (c) Phase C

Figure 6.22: Simplified flux paths for each phase in isolation.

6.4.1.3 Challenges

Because the tubular FRM does not have a true 3D flux path, it can be constructed from laminations in the transverse direction, but this would require multiple lamination cross-section shapes for the stator.

At smaller scales it can be simpler and more cost-effective to construct the machine out of a solid block of Soft Magnetic Composite (SMC), producing a more robust construction due to independence from laminations. Although this may require modular design or a bespoke manufacturing process as the author in [185] was required to glue together multiple 20 mm long SMC blocks to form a stator.

6.4.2 FEA Model

In this research, the tubular FRM is modelled via FEA to address its electromagnetic performance at a suitable scale for comparison to the synchronous machine. To account for any interphase leakage and end effects, the machine must be simulated in full 3D FEA, incurring long solution times, hardware limitations, and a strict limit on the maximum model size. This is a limiting factor to the scale of comparison and restricts the model to prototype scale. The FEA software used is the same as in previous chapters.

6.4.2.1 Mesh Density

The chosen mesh density of the model is shown in figure 6.23 without the mesh density of the air regions shown. This mesh was selected as a compromise between accuracy and solution time and has a tight mesh around the airgap, magnets, and teeth, which loosens up at the stator and translator cores where the rate of change is lower. It was found for the model that increasing the polynomial order of the solver had a greater impact than tighter meshing on solver time.

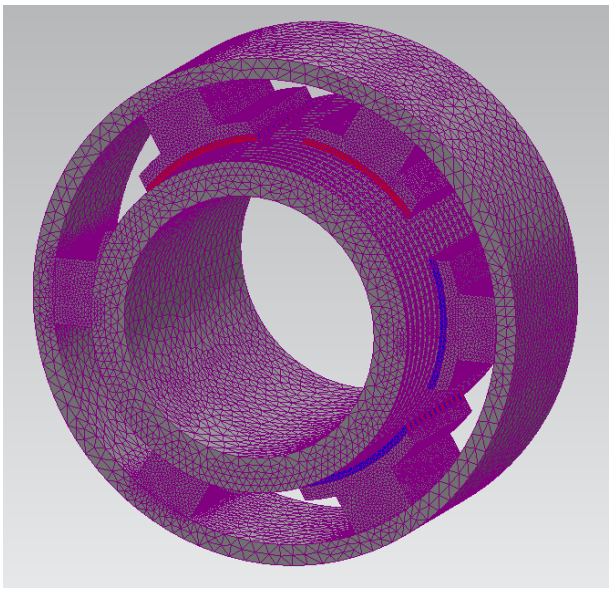

Figure 6.23: Mesh utilised in the study.

6.4.2.2 Winding Considerations

Because this topology is constructed of six discrete stator poles, each with a single concentrated coil encompassing all magnetic occupying the tooth, it is possible to have a much larger number of turns per stator pole. The winding can theoretically occupy the full area between stator poles, but they were restricted to occupy 50% of the available space (figure 6.20a) with an addition assumption that the fill factor is 0.5.

6.4.2.3 Geometry

The geometry of the FRM is presented in table 6.3. Due to the salient design of the FRM stator, it is required that it have a more complex geometry and occupy sufficient space such that the pole arms are long enough to fit coil windings, and the core depth can handle the transfer of flux without saturating.

The translator tooth ratio, that is, the width of translator teeth relative to its pitch was found to be 0.2 in chapter 4 for a rotary FRM and is also adopted here.

6.5 FRM Coil Turns and Inductance

The electrical circuit of phase in the generator is given in figure 6.24.

In this circuit, the power factor is influenced by the impedance triangle:

Where θ is the phase angle. Incorporating Ohm's law, and assuming the current is supplied in phase with the back EMF, the vector diagram becomes:

In this circuit, the inductive reactance is given by:

$$X_L = \omega L \tag{6.8}$$

Where ω is the angular frequency and L is the inductance, given by:

Parameter	Value
Constraint Driven	
Stator Axial length	200 mm
Airgap length	5 mm
Design Variables	
Translator radius	200 mm
Translator tooth ratio	0.2
Stator magnet poles	12
Stator tooth angle	45°
Stator arm attachment angle	22.5°
Magnet height	10 mm
Coil turns	20
Driven Variables	
Translator pitch (τ_t)	16.7 mm
Translator tooth height	τ_t
Translator tooth width	3.34 mm
Translator core height	$\tau_t \cdot \frac{3}{2}$
Stator core height	$\tau_t \cdot \frac{3}{2}$
Stator arm height	$3\tau_t$

Table 6.3: Constraint driven variables

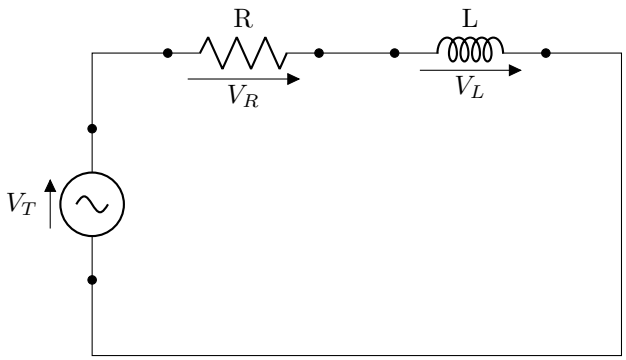

Figure 6.24: Generic phase circuit of a generator.

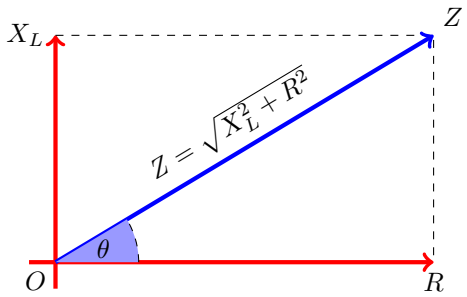

Figure 6.25: Impedance triangle of an RLC circuit.

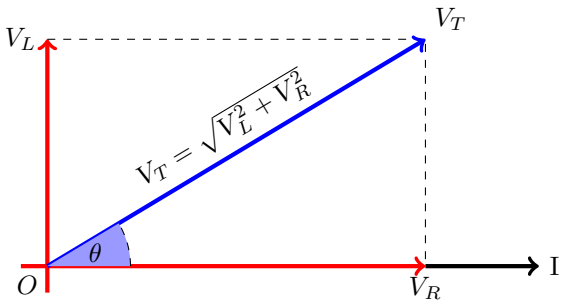

Figure 6.26: Ohms triangle of an RL circuit.

$$L = \mu_0 \frac{N^2 A}{l} \tag{6.9}$$

Where μ_0 is the permeability of N is the number of turns, A is the core cross-sectional area, and l is the coil sinusoidal length.

From figure 6.25 and figure 6.26 the power factor is calculated as:

$$PF = \cos(\theta) \tag{6.10}$$

The power factor is therefore largely driven by the relative difference between circuit resistance and reactance. The machines presented in this thesis consist of inductance and internal resistance, with no capacitance present. With no capacitance, current lags voltage and power factor is most influenced by inductance as defined in equation (6.9). The inductance is proportional to the square of the number of turns, suggesting that this parameter should be restricted to maintain an acceptable power factor, due to the FRM reputation of low power factor.

The power factor of a Variable Reluctance Permanent Magnet (VRPM) machine was given in equation (3.2) and is repeated here:

$$PF = \frac{1}{\sqrt{1 + \left(\frac{L_s I}{\Psi_M}\right)}} \tag{6.11}$$

The power factor here is also improved through the reduction of inductance, but also current restriction or improvement of flux utilisation. It was found that across a range of current densities and without alteration of the geometry, turns higher than 20 yielded a very low power factor, and would require a significant power electric converter to correct it.

6.6 FRM FEA Simulations

6.6.1 Cogging Shift

The flux linkage with coils separated is shown in figure 6.27. Here the shift between coil sides can be seen, with the shifted side lagging. It can also be noted that in phases A and

C there is a magnitude difference of 23% between phase sides. In the proceeding results, the coil sides are joined together and presented in three-phase form.

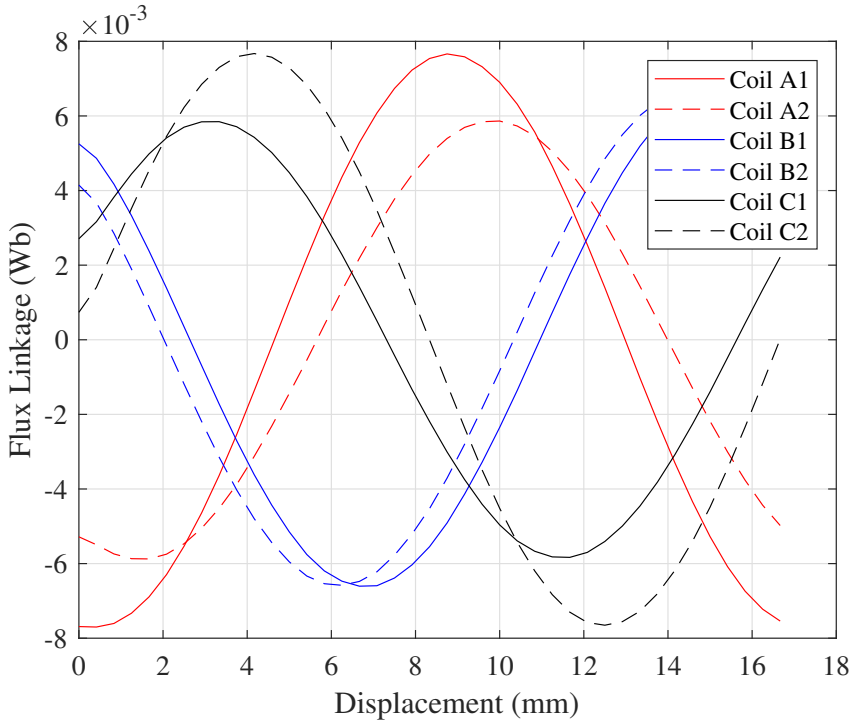

Figure 6.27: Flux linkage with coil phases separated.

6.6.2 Unloaded Simulations

6.6.2.1 Flux Linkage and Voltage

The flux linkage and voltage are presented in figure 6.28. At this scale, and geometry, the voltage and flux linkage magnitude are relatively small due to the small number of turns and unoptimized flux concentration.

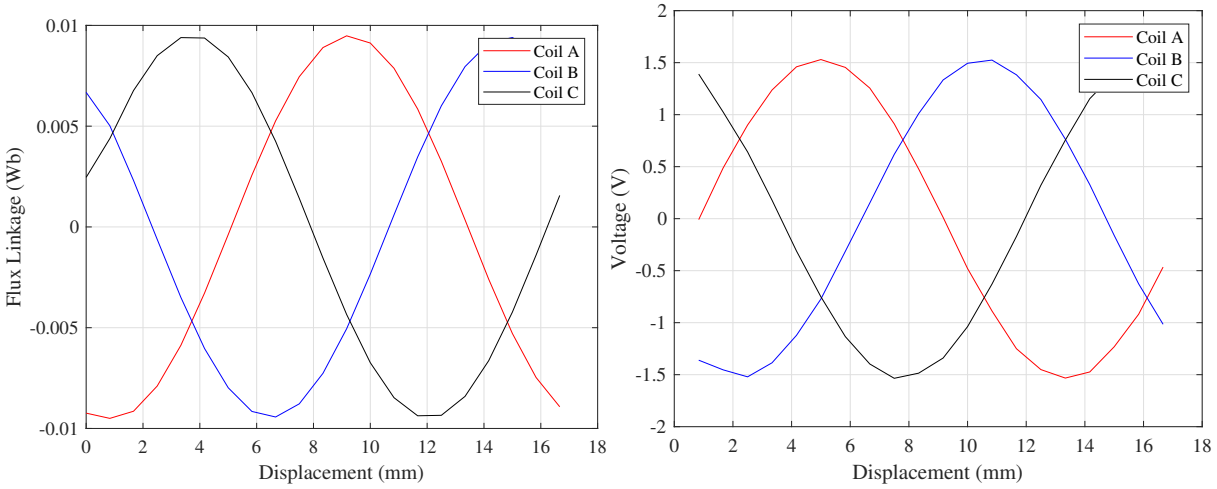

(a) Flux Linkage (b) Voltage

Figure 6.28: Generator performance with no electrical load

6.6.2.2 Flux Distribution

The flux distribution and direction of flow are presented in figure 6.29. Here it can be seen that the flux concentration in unloaded conditions, the flux density is fairly low throughout the machine. This suggests that the machine is at low risk of saturation, and the stator and translator cores could be further optimised to reduce their mass.

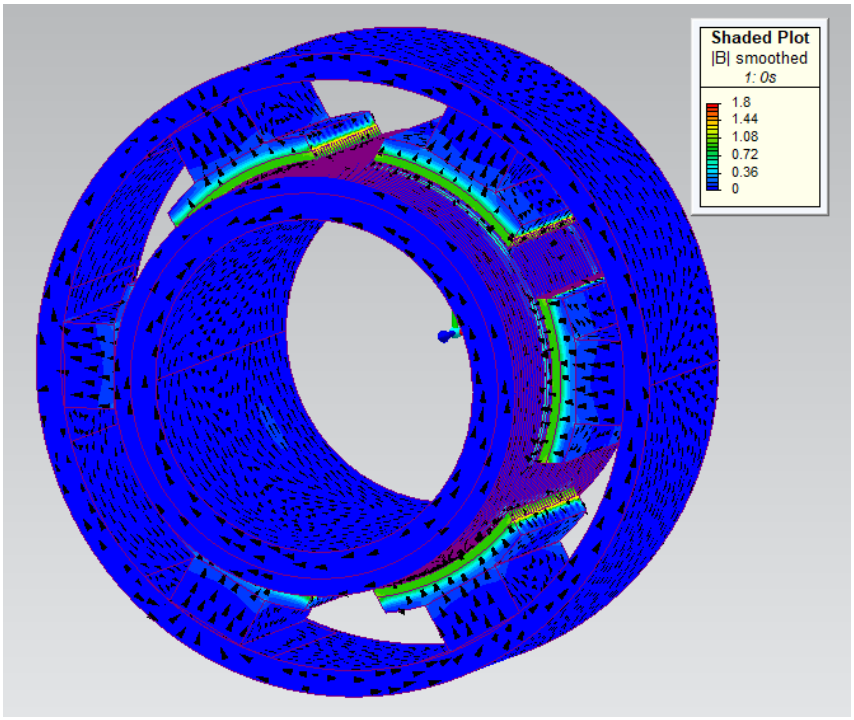

Figure 6.29: Flux density plot with arrows showing flux direction.

6.6.3 Loaded Simulations

6.6.3.1 Current Density Comparison

The generator was simulated with an AC current load, where the current density is varied from 1 to 2 A_{rms}/mm^2 and the results are presented here. Figure 6.30 shows the electromagnetic behaviour across this range. As with the LTSM results, the flux linkage and voltage increase are approximately proportional to the square of the current density. The thrust force has a fixed ripple magnitude and increases linearly to the current density for the range plotted where there are few non-linear effects from saturation.

6.6.3.2 Power and Losses

The powers and losses present in the generator are shown in figure 6.31. It can be seen from figure 6.31b that the iron losses are proportionally low, with the ohmic losses broadly dominating the total. The generator achieves a low efficiency of 30% - 40% decreasing with current. The power factor on the other hand is near unity at low power levels, but quickly drops off to 0.5 at 2 A_{rms}/mm^2.

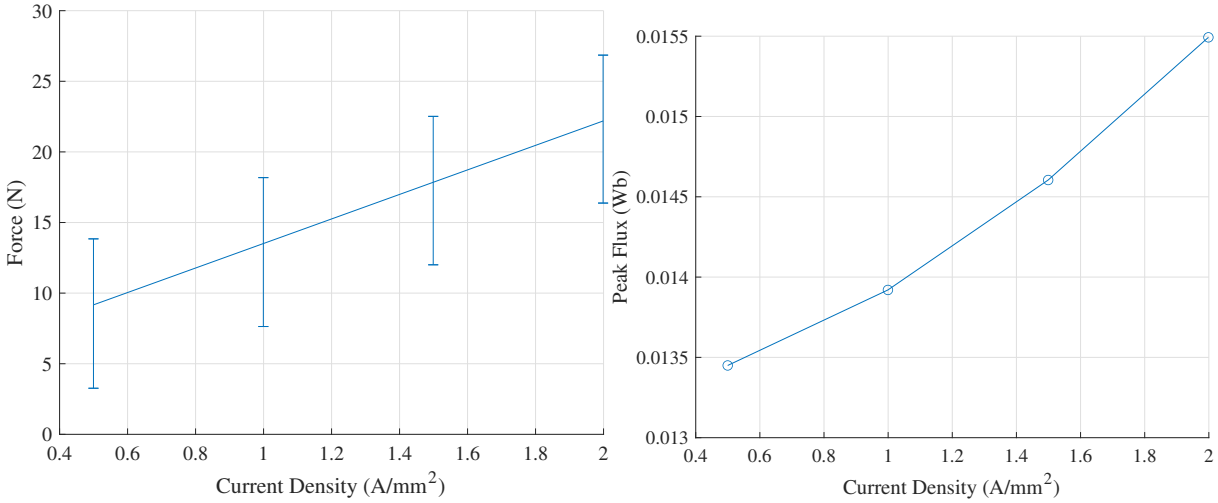

(a) Thrust force

(b) Peak flux linkage

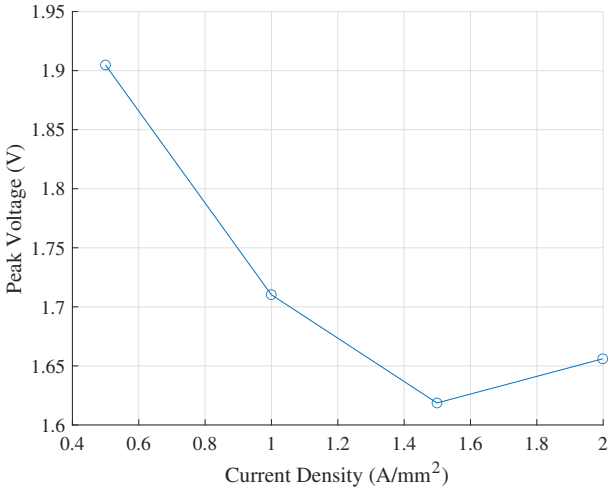

(c) Peak voltage

Figure 6.30: Generator performance with variable current load.

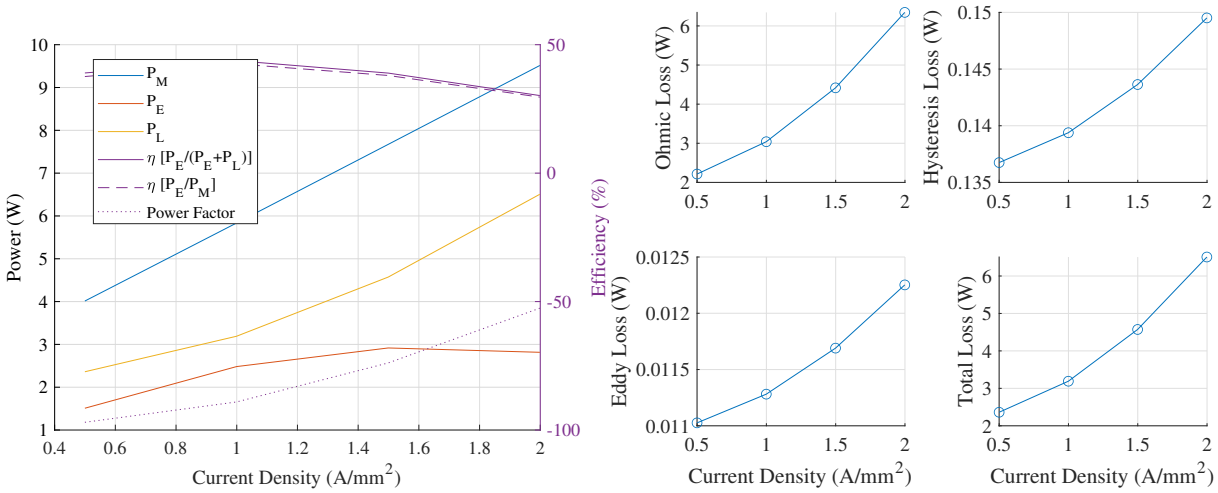

(a) Electrical power

(b) Peak current

Figure 6.31: Power and losses with variable current load.

6.6.3.3 Flux Distribution

The distribution of flux within the generator at zero displacement is presented in figure 6.32 and displays little change from the unloaded state, confirming minimal saturation in the machine.

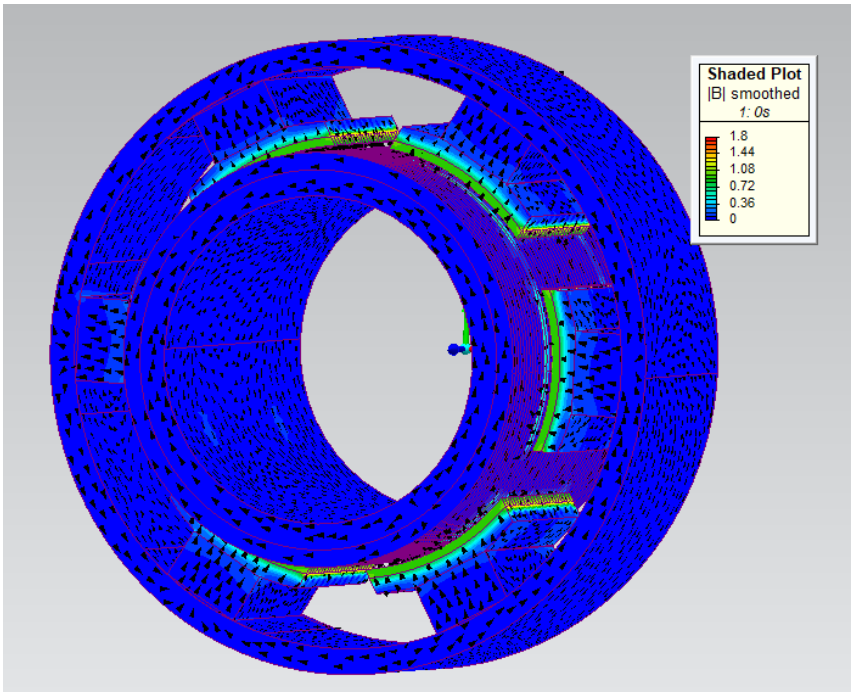

Figure 6.32: Flux density plot with arrows showing flux direction at 3 A/mm^2.

6.7 Reduction of FRM Airgap

6.7.1 Challenged to large airgap VRPMs

Machines from the VRPM family operate by flux transferring from the stator magnet to the translator tooth. As such, they perform best with a small airgap with minimal leakage. A simple reluctance network is shown in figure 6.33.

For an ideal power factor, a high proportion of the flux is expected to transfer through the tooth, and not leak to nearby magnets; this is generally the case when the magnet width or height is larger than the airgap. In this scheme, the reluctance can be approximated as:

$$R_g = \frac{L_g}{\mu_0 A} \tag{6.12}$$

And

$$R_L = \frac{\tau_m}{\mu_0 A} \tag{6.13}$$

Because the area and permeability are equal, the reluctances are proportional to the length component. Hence, the most favourable flux path into another magnet rather than

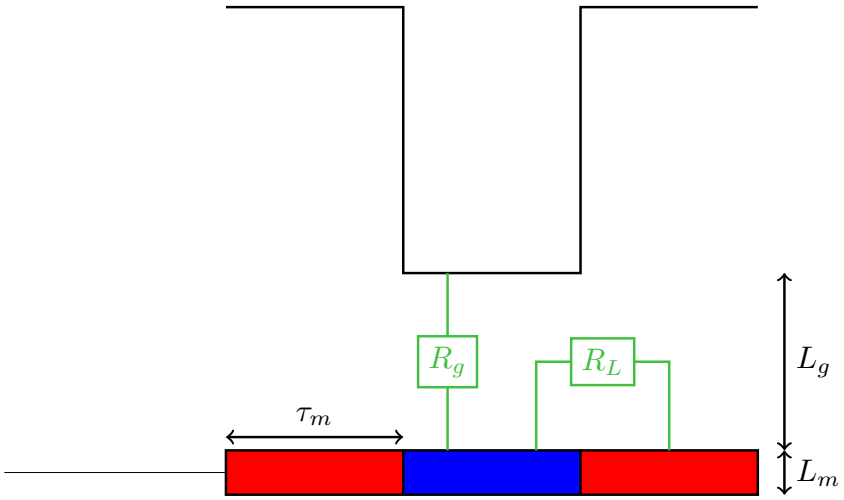

Figure 6.33: Reluctance network of a VRPM pole pair.

across the tooth at large airgap lengths. Because this machine is not operating near the level reported in literature [185], the impact of airgap is investigated by setting the airgap to 1 mm in this section.

6.7.2 Unloaded

6.7.2.1 Electrical

With the airgap reduced to 1 mm, in unloaded conditions, the flux and voltage shown in figure 6.34 are magnified by a factor of 6.

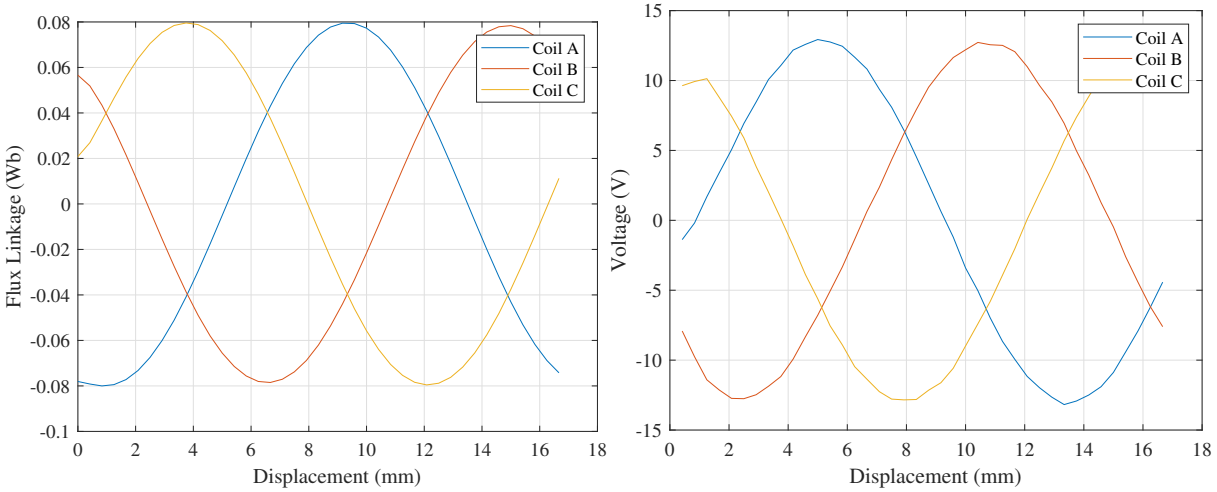

(a) Flux linkage (b) Voltage

Figure 6.34: Electromagnetic results with no electrical load.

6.7.2.2 Cogging Forces

The cogging forces are shown in figure 6.35 and display that the X and Y axis forces are of similar magnitude, but the Y axis forces oscillate at a higher frequency and contain more complicated harmonics.

The Z force highlights that the Z force in figure 6.35, was not numerical error, but implies that there is a near-constant axial force with displacement.

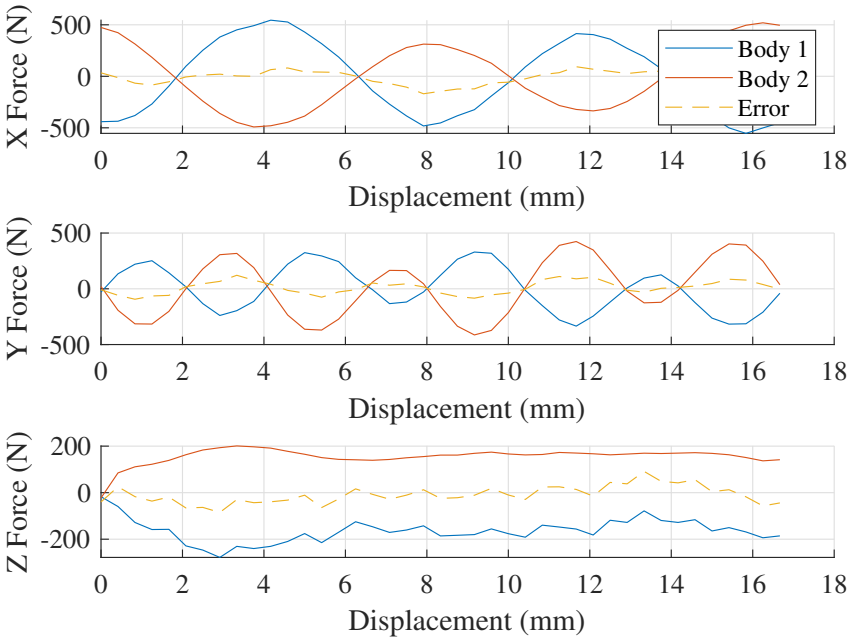

Figure 6.35: Forces with no electrical load.

6.7.2.3 Flux Distribution

In the FEA flux distribution it can be seen that with a reduced airgap, there is a greater level of flux transferring into the stator in figure 6.36.

6.7.3 Loaded

The machine was simulated at 2 A/mm^2 of AC load and the results are presented here.

6.7.3.1 Electrical

At the given load, there is minimal difference in flux linkage and voltage as compared to the unloaded conditions (figure 6.37).

6.7.3.2 Force and Power

The force and power are shown in figure 6.38. There is also little difference in the magnitude of force production, but there is a clear thrust force with a 210 N peak value; a similar magnitude to that presented in [185]. At this level of loading, a modest efficiency of 32.8% is achieved.

6.7.3.3 Flux Distribution

The flux distribution (figure 6.39) when loaded shows that there is flux flowing through the machine, but it is still far from saturation or heavy loading.

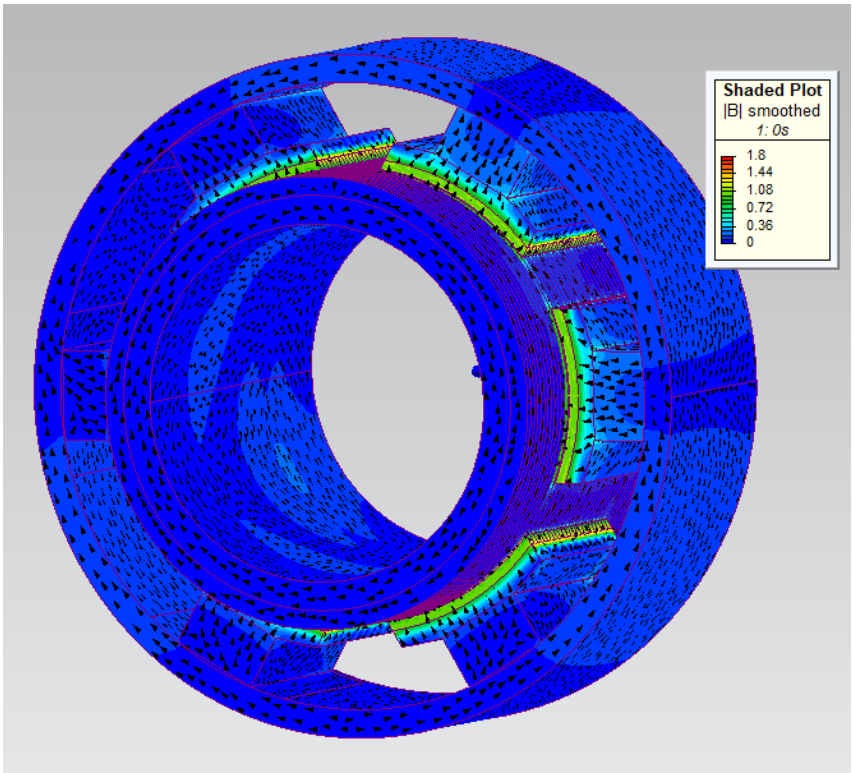

Figure 6.36: Flux density plot with arrows showing flux direction, with no electrical load.

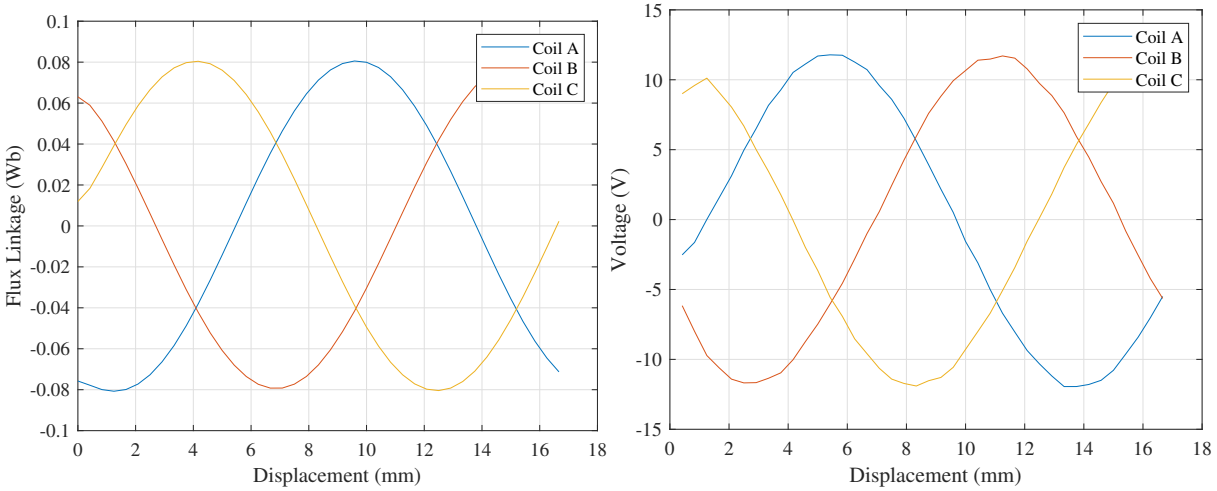

(a) Flux linkage (b) Voltage

Figure 6.37: Electromagnetic results with 2 A_{rms}/mm^2.

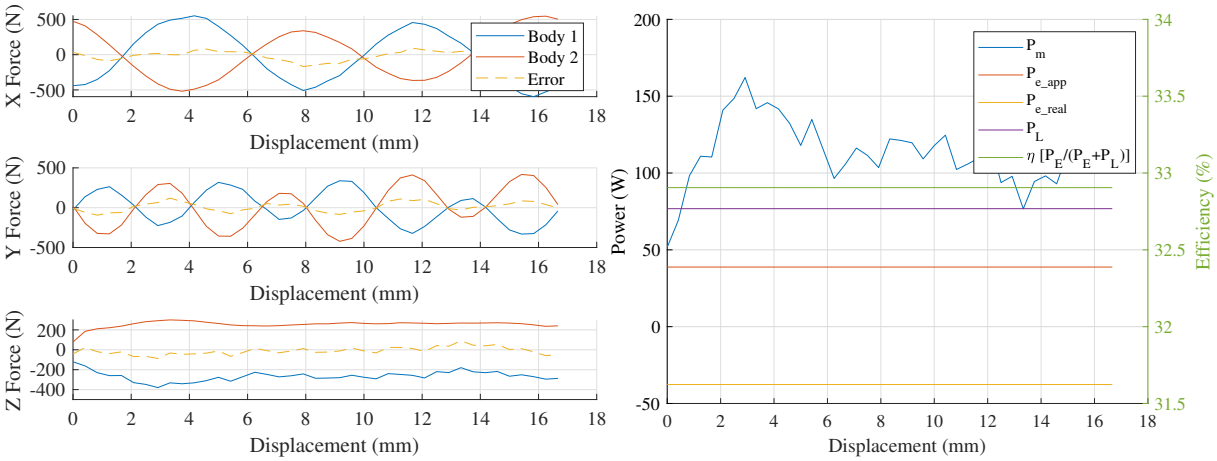

(a) Directional forces (b) Power

Figure 6.38: Power performance at 2 A_{rms}/mm^2.

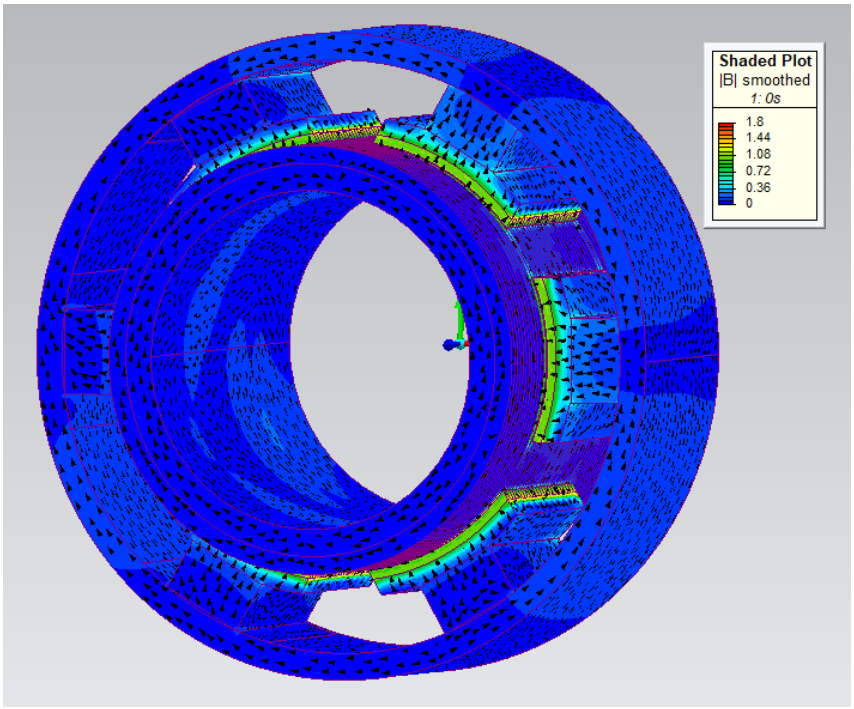

Figure 6.39: Flux density plot with arrows showing flux direction, with 2 A_{rms}/mm^2 AC current.

6.8 Discussion of Comparison

In the preceding sections, two configurations of integrated pistons were presented: a wide radius fully integrated LTSM and a small radius tubular FRM. The results of each are presented here.

6.8.1 Geometry

The FRM is much freer in terms of geometric design. The stator's slotted and salient nature presents a great opportunity for magnetic and mass optimisation. On the other hand, the LTSM has a stator that is fixed as a solid steel and copper tube. Furthermore, because the FRM adopts concentrated pole windings in the axial direction, lower ohmic losses are achieved by using shorter windings overall. This factor also means that the FRM is better suited to larger device radii while restricting winding length. Additionally, because the FRM has much more space between stator poles, it is possible to have a larger number of coil turns around each tooth as compared to the LTSM, further increasing performance potential.

However, the FRM also has the most complex geometry out of the two, requiring a well-thought-out and costly manufacturing process, or acceptance of lower-performing SMC materials.

A tabulated comparison of the two designs is shown in table 6.4. Here it can be seen that the volumetric and mass difference between the two machines is approximately half, despite the large difference in radius. The translator and stator of the PMSM have thin walls relative to the radius, which for the difference. Due to the large radius and small thickness, this may imply a firmer requirement for structural materials.

6.8.2 Electrical Performance

The LTSM far outperforms the FRM in terms of all electrical performance parameters, achieving much greater flux linkage and thrust force for comparable current density, even when comparing them as a function of force density or active area. Furthermore, the efficiency of the FRM is much lower than the iron cored LTSMs across all values of current density.

The major cause for the difference in electrical performance is the poor power factor inherent to the FRM design, made worse in tubular form through multiple end effects and leakage flux around the small magnet poles. The FRM topology presented here has not been optimised for power factor, and is in critical need of geometric optimisation, either in the form of optimising coil geometry for inductance reduction (equation (6.9)), or by enhancing the magnetic circuit through geometric adjustments or the inclusion of flux concentration (equation (6.11)). Additionally, the VHM would likely require a significant power converter to overcome the low power factor in practice, increasing system costs.

Parameter	Iron Core PMSM	Tubular FRM
Geometry (m)		
Stator length	0.2	
Translator radius	1.25	0.2
Magnet height	0.01	
Volume (m^3)		
Translator	0.0093	0.0107
Stator	0.0402	0.0147
Magnets	0.03129	0.0003
Coils	0.032	0.02123
Total	0.113	0.047048
Mass (kg)		
Translator	71.436	82.17
Stator	307.62	112.12
Magnets	219.03	13.854
Coils	287.12	191.08
Total	885.21	399.18

Table 6.4: Tabulated comparison of the two designs. The airgaps used are 5 mm and 1 mm for the PMSM and FRM respectively.

Parameter	Iron Core PMSM	Tubular FRM	Rotary FRM
Open circuit voltage (V)	1350	12	187.8
Flux linkage (Wb)	18	0.08	2.8
Average thrust force (N) @$2A_{rms}/mm^2$	9520	210	2548 (N m)
Thrust force ripple (%)	37.82	40	11.48
Cogging force (N)	1900	1850	30 (N m)
Shear stress (kN/m^2)	6.06	0.37	42.99
Power density (kW/m^3)	23.92	1.39	
Force density (kN/m^3)	84.33	4.47	

Table 6.5: Tabulated comparison of electric machines. The airgaps used are 5 mm and 1 mm for the PMSM and FRM respectively.

Inside the context of this case study, the FRM is subject to several geometric and conceptual constraints. It would achieve a better power factor if it were permitted longer stator pole height or focused magnet arrays. It is also likely that the topology performs better at full scale.

6.9 Conclusions

In this chapter, a case study has been conducted for selecting a directly driven power take-off for a fully rated and specified IPS Buoy. Two machine topologies and several variants have been selected for analysis, optimisation, and comparison in terms of their suitability in the wave energy converter.

First, the terms, constraints, and goals of the case study were laid out using the findings from previous chapters. An IPS buoy was sized and rated from a selected wave resource location with the methodology of sizing fully explained, and the hydrodynamic motion of the device presented. The required parameters of the power take-off were also highlighted here. Possible configurations of integrating a generator into a neutrally buoyant piston with different levels of integration were also explained along with their impacts on the design requirements.

Two types of direct drive electric machines were considered as the power take-off mechanism, a baseline synchronous machine (LTSM), and a Flux Reversal Machine (FRM), both of which are tubular and required to fit into the geometric constraints of the IPS buoy. The LTSM is applied to the fully integrated piston, and the FRM into a lesser integrated design. For each machine and variant considered, simulations were conducted in FEA for both loaded and unloaded conditions, with the electrical performance discussed afterwards.

For the LTSM, four variants were considered, two air-cored designs, one hybrid core, and one fully iron core. Each variant was simulated at varying pole numbers, and current densities to find the most performant variation. It was found that the variants containing iron achieved higher induced voltage, and higher thrust force when loaded. However, at lower stator pole numbers, they experience large cogging force amplitudes and force ripple. Moreover, it was found that the large radii and tubular windings led to uncommonly large ohmic losses under loaded conditions. The high losses excluded the air-cored variants from being feasible options as they were incapable of producing sufficient force without low efficiency. The hybrid core and iron core performed much better, meeting the design specification with acceptable efficiency, particularly in the fully iron-cored machine.

The tubular FRM was introduced as a comparison to the LTSM under the same design requirements as a 3D FEA model. The FRM was simulated under loaded and unloaded conditions and the results were discussed in the same manner as above. It was found that the FRM suffered from a very low power factor in its unoptimized state. A high inductance restricted the coils to around 20 turns to avoid a dropping power factor, thereby limiting the back EMF to low values.

Ultimately, the tubular FRM was not able to compete with the LTSM at this scale and design requirements.

Chapter 7. Conclusions and Future Work

7.1 Contribution to Knowledge

The key contribution of this research is the development of an integrated design flow for the design of an all-electric heaving IPS Buoy. This includes the development of hydrodynamic and hydrostatic models, wave state analysis tools, simulated model, and a codebase for rapid design and organised FEA simulations in MATLAB.

The contributions of this thesis are summarised here as:

- Developed an approach to the co-design of a direct drive power take off and an IPS buoy wave energy converter.
- Co-designed a marinized IPS buoy with two methods of generator integration, highlighting the challenges involved in each method.
- Carried a wave energy concept from wave resource location to a fully designed device proposition.
- Compared a rotary Flux Reversal Machine (FRM) and VHM for application in an existing hinged wave energy converter. Investigating the impact of rotor tooth width on cogging harmonics content and revealed options for cogging torque minimisation.
- Developed a hydrodynamic model for the transient simulation of an IPS Buoy oscillating in heave, and an analytical model for the design of a neutrally buoyant IPS Buoy piston. Applied the models to aid in the co-design and uncovered the implications of fully integrating a generator into an IPS Buoy piston.
- Compared a tubular VHM against a baseline synchronous generator to ascertain its suitability for use in an IPS Buoy with strict performance and geometric constraints. Found that in the synchronous topologies it can be better for an iron core to be used despite the added mass due to in increased performance across large airgaps.

7.2 Suggestions for Future Work

This thesis is a combination of several fields of research brought together as one and hopes to encourage further integration for the design of wave energy converters. The recommendations for future work are:

- Incorporate a marinized generator into the IPS Buoy with less coupling to the IPS Buoy piston geometry. When integrated into the piston, the generator creates a cyclical constraint and is unlikely to scale well with radii.

- Integrate the optimisation of structural mass into the combined design approach. Direct-drive electric machines are highly dependent on strong structures to hold their shape, and it may have an impact on hydrodynamic performance.
- Inclusion of the antifouling mechanisms into the hydrodynamic model.
- Optimisation of antifouling devices to reduce minimum airgap clearance required.
- It would be interesting to extend this research without the aim of marinized generators, instead considering placing the generator inside the device's float.
- Power electric converters should also be included in the design study to address conversion costs for a complete system.

7.3 Conclusion

In this research, a multidisciplinary design study has been conducted for a real wave energy converter, incorporating hydrodynamic and electric machine analysis.

A Vernier Hybrid Machine (VHM) was compared against a Flux Reversal Machine (FRM) in a case study for application in a Mocean Blue Star hinged wave energy converter. It was found that the electrical performance and cogging torque are highly dependent on rotor tooth width, allowing the FRM to achieve 5% higher induced voltage with acceptable cogging torque.

Analytical hydrodynamic models were developed for an IPS buoy operating in heave and a 1 m radius device proposed for deployment in Blyth, UK, using historical wave data as a guide.

The FRM was compared against a Permanent Magnet Synchronous Machine (PMSM) for integration into the IPS buoy as a fully integrated and marinized generator. Both topologies were designed to integrate into the IPS buoy piston and were tubular machines. It was found that the tubular FRM performed poorly due to a large airgap required for the antifouling mechanisms and the PMSM was shown as a more suitable generator.

It has been found in this research that co-designing a wave energy converter and power take off is a challenging task with cyclical and occasionally conflicting dependencies. But the task is of critical importance to field of wave energy so that developers can quickly find out which topologies are promising devices that can be prototypes and build confidence in the field, without spending too much time on topologies that have no realistic power take off options.

References

[1] UK Government. *Climate Change Act c.27*. 2008. URL: https://www.legislation.gov.uk/ukpga/2008/27/contents.

[2] Council of European Union. *Paris Agreement*. 2015. URL: https://eur-lex.europa.eu/legal-content/EN/TXT/?uri=CELEX:22016A1019(01).

[3] The London School of Economics and Political Science. *Grantham Research Institute on climate change and the environment*. Oct. 2022. URL: https://www.lse.ac.uk/granthaminstitute/explainers/what-is-climate-change-legislation/.

[4] Wencong Su et al. "A survey on the electrification of transportation in a smart grid environment". In: *IEEE Transactions on Industrial Informatics* 8.1 (2011), pp. 1–10.

[5] Hannah Ritchie, Max Roser, and Pablo Rosado. *CO_2 and Greenhouse Gas Emissions*. 2020. URL: https://ourworldindata.org/co2-and-green%5C-house-gas-emissions.

[6] National Grid. *Uk electricity generation in 2023*. Apr. 2023. URL: https://www.energy-uk.org.uk/insights/electricity-generation/.

[7] *Wave and tidal energy: part of the UK's energy mix*. Jan. 2013. URL: https://www.gov.uk/guidance/wave-and-tidal-energy-part-of-the-uks-energy-mix.

[8] TV Heath. "A review of oscillating water columns". In: *Philosophical Transactions of the Royal Society A: Mathematical, Physical and Engineering Sciences* 370.1959 (2012), pp. 235–245.

[9] Richard Yemm et al. "Pelamis: experience from concept to connection". In: *Philosophical Transactions of the Royal Society A: Mathematical, Physical and Engineering Sciences* 370.1959 (2012), pp. 365–380.

[10] Jens Peter Kofoed et al. "Prototype testing of the wave energy converter wave dragon". In: *Renewable energy* 31.2 (2006), pp. 181–189.

[11] Diego Vicinanza and Peter Frigaard. "Wave pressure acting on a seawave slot-cone generator". In: *Coastal Engineering* 55.6 (2008), pp. 553–568.

[12] T Miyazaki and Y Masuda. "Tests On The Wave Power Generator "Kaimei"". In: *Offshore Technology Conference*. OTC. 1980, OTC–3689.

[13] K Budar and Johannes Falnes. "A resonant point absorber of ocean-wave power". In: *Nature* 256.5517 (1975), pp. 478–479.

[14] DV Evans. "A theory for wave-power absorption by oscillating bodies". In: *Journal of Fluid Mechanics* 77.1 (1976), pp. 1–25.

[15] Blair Kinsman. *Wind waves: their generation and propagation on the ocean surface*. Courier Corporation, 1984.

[16] Alex DD Craik. "The origins of water wave theory". In: *Annu. Rev. Fluid Mech.* 36 (2004), pp. 1–28.

[17] RL Wiegel and JW Johnson. "Elements of wave theory". In: *Coastal Engineering Proceedings*. 1951.

[18] Andrew M Cornett. "A global wave energy resource assessment". In: *ISOPE International Ocean and Polar Engineering Conference*. ISOPE. 2008, ISOPE–I.

[19] Johannes Falnes. "A review of wave-energy extraction". In: *Marine structures* 20.4 (2007), pp. 185–201.

[20] Thomas B Johannessen. "Nonlinear superposition methods applied to continuous ocean wave spectra". In: *Journal of Offshore Mechanics and Arctic Engineering* (2012).

[21] Christian Kharif and Efim Pelinovsky. "Physical mechanisms of the rogue wave phenomenon". In: *European Journal of Mechanics-B/Fluids* 22.6 (2003), pp. 603–634.

[22] ZhengShun Cheng et al. "Frequency/time domain modeling of a direct drive point absorber wave energy converter". In: *Science China Physics, Mechanics and Astronomy* 57 (2014), pp. 311–320.

[23] Eugen Rusu and Florin Onea. "A review of the technologies for wave energy extraction". In: *Clean Energy* 2.1 (2018), pp. 10–19.

[24] Royal society of London. *Philosophical Transactions of the Royal Society of London*. W. Bowyer and J. Nichols, 1864.

[25] Albert W Stahl. "The utilization of the power of ocean waves". In: *Journal of Fluids Engineering* 13 (1892), pp. 438–494.

[26] Michael T Morris-Thomas, Rohan J Irvin, and Krish P Thiagarajan. "An investigation into the hydrodynamic efficiency of an oscillating water column". In: *Journal of Offshore Mechanics and Arctic Engineering* (2007), pp. 273–278.

[27] F de O Antonio. "Wave energy utilization: A review of the technologies". In: *Renewable and sustainable energy reviews* 14.3 (2010), pp. 899–918.

[28] JCC Henriques et al. "Design of oscillating-water-column wave energy converters with an application to self-powered sensor buoys". In: *Energy* 112 (2016), pp. 852–867.

[29] JM Leishman and George Scobie. *The development of wave power: a techno-economic study*. 1976.

[30] Stephen H Salter. "Wave power". In: *Nature* 249.5459 (1974), pp. 720–724.

[31] PJ Rance. "The Development of the HRS Rectifier". In: *Wave Energy Conference, London-Heathrow 22-23 November 1978* (1978).

[32] C Cockerell, MJ Platts, and R Comyns-Carr. "The Development of the Wave-Contouring Raft". In: *Wave Energy Conference, London-Heathrow 22-23 November 1978* (1978).

[33] David Ross. *Energy from The Waves 2nd Edition Revised & Enlarged*. New York: Pergamon Press, 1980.

[34] M Goden de Sousa Prado et al. "Modelling and test results of the Archimedes wave swing". In: *Proceedings of the Institution of Mechanical Engineers, Part A: Journal of Power and Energy* 220.8 (2006), pp. 855–868.

[35] MJ Hannon, R van Diemen, and J Skea. "Lost at sea or a new wave of innovation? Examining the effectiveness of the UK's wave energy innovation system since 2000". In: *International Sustainability Transitions* 20 (2018), pp. 1–35.

[36] L Cameron et al. "Design of the next generation of the Oyster wave energy converter". In: *3rd international conference on ocean energy*. Vol. 6. ICOE Bilbao, Spain. 2010, 1e12.

[37] L Claeson. "Recent wave energy research in Sweden". In: *OCEANS'88.'A Partnership of Marine Interests'. Proceedings*. IEEE. 1988, 1638–vol.

[38] SH Salter. "The development of the duck concept". In: *Proc. Wave Energy Conference*. 1978, pp. 17–27.

[39] AC Mendes et al. "Performance assessment of the ANACONDA WEC in regular waves at 1: 50 model scale". In: *International Conference on Offshore Mechanics and Arctic Engineering*. Vol. 57786. American Society of Mechanical Engineers. 2017, V010T09A016.

[40] Mahbubur Rahman Kiran et al. "Progress in piezoelectric material based oceanic wave energy conversion technology". In: *IEEE Access* 8 (2020), pp. 146428–146449.

[41] Mark Leybourne et al. "Preliminary design of the OWEL wave energy converter pre-commercial demonstrator". In: *Renewable energy* 61 (2014), pp. 51–56.

[42] Even Mehlum. "Tapchan". In: *Hydrodynamics of Ocean Wave-Energy Utilization: IUTAM Symposium Lisbon/Portugal 1985*. Springer. 1986, pp. 51–55.

[43] Vincenzo Franzitta et al. "The desalination process driven by wave energy: A challenge for the future". In: *Energies* 9.12 (2016), p. 1032.

[44] Álvaro Serna and Fernando Tadeo. "Offshore hydrogen production from wave energy". In: *International journal of hydrogen energy* 39.3 (2014), pp. 1549–1557.

[45] Mocean Energy. *Mocean Energy Homepage*. July 2023. URL: `https://www.mocean.energy/`.

[46] Baba Tamim. *"Archimedes Waveswing": 20 years of research leads to successful trials of this wave energy converter*. Nov. 2022. URL: https://interestingengineering.com/innovation/archimedes-waveswing-successful-trail.

[47] Iain McLeod and John V Ringwood. "Powering data buoys using wave energy: a review of possibilities". In: *Journal of Ocean Engineering and Marine Energy* 8.3 (2022), pp. 417–432.

[48] Rasmus Lema, Ambuj Sagar, and Yuan Zhou. "Convergence or divergence? Wind power innovation paths in Europe and Asia". In: *Science and Public Policy* 43.3 (2016), pp. 400–413.

[49] Ralf Bucher et al. "Creation of investor confidence: The top-level drivers for reaching maturity in marine energy". In: *Renewable Energy* 88 (2016), pp. 120–129.

[50] Simon Ambuhl et al. "Operation and maintenance strategies for wave energy converters". In: *Proceedings of the Institution of Mechanical Engineers, Part O: Journal of Risk and Reliability* 229.5 (2015), pp. 417–441.

[51] Sharay Astariz and Gregório Iglesias. "The economics of wave energy: A review". In: *Renewable and Sustainable Energy Reviews* 45 (2015), pp. 397–408.

[52] Sofia Patrício, André Moura, and Teresa Simas. "Wave energy and underwater noise: State of art and uncertainties". In: *OCEANS 2009-EUROPE* (2009), pp. 1–5.

[53] Lan Lin and Haitao Yu. "Offshore wave energy generation devices: Impacts on ocean bio-environment". In: *Acta Ecologica Sinica* 32.3 (2012), pp. 117–122.

[54] Cigdem Ozkan, Kelsey Perez, and Talea Mayo. "The impacts of wave energy conversion on coastal morphodynamics". In: *Science of the Total Environment* 712 (2020), p. 136424.

[55] Rahman Saidur et al. "Environmental impact of wind energy". In: *Renewable and sustainable energy reviews* 15.5 (2011), pp. 2423–2430.

[56] SH Salter. "Changing the 1981 spine-based ducks (wave power generation)". In: *International Conference on Renewable Energy-Clean Power 2001, 1993.* IET. 1993, pp. 121–132.

[57] Benjamin Frieske and Sylvia Stieler. "The "semiconductor crisis" as a result of the COVID-19 pandemic and impacts on the automotive industry and its supply chains". In: *World Electric Vehicle Journal* 13.10 (2022), p. 189.

[58] Sabine Langkau and Martin Erdmann. "Environmental impacts of the future supply of rare earths for magnet applications". In: *Journal of Industrial Ecology* 25.4 (2021), pp. 1034–1050.

[59] SH Salter. "Recent progress on ducks". In: *IEE Proceedings A (Physical Science, Measurement and Instrumentation, Management and Education, Reviews)* 127.5 (1980), pp. 308–319.

[60] Stephen Salter. "Wave energy: Nostalgic Ramblings, future hopes and heretical suggestions". In: *Journal of Ocean Engineering and Marine Energy* 2 (2016), pp. 399–428.

[61] Lewis Chambers and Nick J Baker. "Developing a direct drive generator for a heaving IPS buoy". In: *11th International Conference on Renewable Power Generation - Meeting net zero carbon*. IET, 2022.

[62] Matt Folley. *Numerical modelling of wave energy converters: state-of-the-art techniques for single devices and arrays*. Academic Press, 2016.

[63] Toshiaki Setoguchi and Manabu Takao. "Current status of self rectifying air turbines for wave energy conversion". In: *Energy conversion and management* 47.15-16 (2006), pp. 2382–2396.

[64] Tom Heath. *Islay Limpet Project Monitoring Final Report*. Technological report. Wavegen, 2001.

[65] Offshore Energy. *Mutriku Wave Plant Hits 2GWh Mark*. 2020. URL: `https://www.offshore-energy.biz/mutriku-wave-plant-hits-2gwh-mark`.

[66] Owen M Phillips. *The dynamics of the upper ocean*. Cambridge University Press, 1977.

[67] Ieuan Collins et al. "Flexible membrane structures for wave energy harvesting: A review of the developments, materials and computational modelling approaches". In: *Renewable and Sustainable Energy Reviews* 151 (2021), p. 111478.

[68] Andrea Bucchi and Grant E Hearn. "Analysis of the SEA-OWC-Clam wave energy device part B: structural integrity analysis". In: *Renewable energy* 99 (2016), pp. 253–269.

[69] Emanuele Quaranta et al. "The Very Low Head Turbine for hydropower generation in existing hydraulic infrastructures: State of the art and future challenges". In: *Sustainable Energy Technologies and Assessments* 51 (2022), p. 101924.

[70] The Liquid Grid. *Wave energy techonology brief*. Oct. 2022. URL: `https://theliquidgrid.com/marine-clean-technology/wave-energy-converters/`.

[71] K Budal and J Falnes. "Optimum operation of improved wave-power converter". In: *Mar. Sci. Commun.;(United States)* 3.2 (1977).

[72] AM Muzathik et al. "Planning and development of ocean wave energy conversion". In: *7th UMT International Symposium on Sustainability Science and Management held at Malaysia, UMTAS-2-14*. 2008.

[73] *OPT PowerBuoy Tested at DeepStar's "Zero Carbon Power for Electric Subsea Operations" Project*. Oct. 2020. URL: https://www.oedigital.com/news/483271-opt-powerbuoy-tested-at-deepstar-s-zero-carbon-power-for-electric-subsea-operations-project.

[74] Paul Stansell and David J Pizer. "Maximum wave-power absorption by attenuating line absorbers under volume constraints". In: *Applied Ocean Research* 40 (2013), pp. 83–93.

[75] Masato Sagawa et al. "New material for permanent magnets on a base of Nd and Fe". In: *Journal of Applied Physics* 55.6 (1984), pp. 2083–2087.

[76] Sheng Xu, Shan Wang, and C Guedes Soares. "Experimental study of the influence of the rope material on mooring fatigue damage and point absorber response". In: *Ocean Engineering* 232 (2021), p. 108667.

[77] Tom W Thorpe et al. *A brief review of wave energy*. A report produced for The UK Department of Trade and Industry. Didcot, United Kingdom, 1999.

[78] António FO Falcão et al. "Hydrodynamics of the IPS buoy wave energy converter including the effect of non-uniform acceleration tube cross section". In: *Renewable energy* 41 (2012), pp. 105–114.

[79] Lewis Chambers and Nick J Baker. "Designing an Integrated Generator for a Wave Energy Converter". In: *2023 IEEE International Electric Machines & Drives Conference (IEMDC)*. IEEE. 2023, pp. 1–7.

[80] Johannes Palm and Claes Eskilsson. "On end-stops and snap loads for taut moored wave energy converters". In: *Proc. 14th European Wave and Tidal Energy Conference, Plymouth, UK*. 2021.

[81] Tianzhi Zhou. *Damping profile research for CorPower Ocean's wave energy converter*. 2016.

[82] Jonas Sjolte et al. "Exploring the potential for increased production from the wave energy converter lifesaver by reactive control". In: *Energies* 6.8 (2013), pp. 3706–3733.

[83] Dara O'Sullivan et al. *DYNAMIC CHARACTERISTICS OF WAVE AND TIDAL ENERGY CONVERTERS & A RECOMMENDED STRUCTURE FOR DEVELOPMENT OF A GENERIC MODEL FOR GRID CONNECTION*. Research Report. Ocean Energy Systems-Implementing Agreement (OES-IA), International Energy Agency, 2010. URL: https://hal.science/hal-01265981.

[84] Benjamin Drew, Andrew R Plummer, and M Necip Sahinkaya. *A review of wave energy converter technology*. 2009.

[85] Morten Kramer, Laurent Marquis, and Peter Frigaard. "Performance evaluation of the wavestar prototype". In: *9th ewtec 2011: Proceedings of the 9th European Wave and Tidal Conference, Southampton, UK, 5th-9th September 2011*. University of Southampton. 2011.

[86] Shafiqur Rehman, Luai M Al-Hadhrami, and Md Mahbub Alam. "Pumped hydro energy storage system: A technological review". In: *Renewable and Sustainable Energy Reviews* 44 (2015), pp. 586–598.

[87] Deping Cao, Jie He, and Hao Chen. "Empirical Predictions on Wave Overtopping for Overtopping Wave Energy Converters: A Systematic Review". In: *Processes* 12.9 (2024), p. 1940.

[88] Henk Polinder et al. "Comparison of direct-drive and geared generator concepts for wind turbines". In: *IEEE Transactions on energy conversion* 21.3 (2006), pp. 725–733.

[89] Chunyuan Liu. "Current research status and challenge for direct-drive wave energy conversions". In: *IETE Journal of Research* (2021), pp. 1–13.

[90] Benedikt Kaiser and Nejila Parspour. "Transverse flux machine—a review". In: *IEEE Access* 10 (2022), pp. 18395–18419.

[91] I Boldea et al. "Analysis and design of flux-reversal linear permanent magnet oscillating machine". In: *Conference Record of 1998 IEEE Industry Applications Conference. Thirty-Third IAS Annual Meeting (Cat. No. 98CH36242)*. Vol. 1. IEEE. 1998, pp. 136–143.

[92] SA Nasar and I Boldea. "Three-phase flux reversal machine (FRM)". In: *IEE Proceedings - Electric Power Applications* 146.2 (1999), pp. 139–146.

[93] Xiaofeng Zhu et al. "Analysis of back-EMF in flux-reversal permanent magnet machines by air gap field modulation theory". In: *IEEE Transactions on Industrial Electronics* 66.5 (2018), pp. 3344–3355.

[94] E Spooner and L Haydock. "Vernier hybrid machines". In: *IEE Proceedings-Electric Power Applications* 150.6 (2003), pp. 655–662.

[95] Nick J Baker et al. "Evaluating alternative linear vernier hybrid machine topologies for integration into wave energy converters". In: *IEEE Transactions on Energy Conversion* 33.4 (2018), pp. 2007–2017.

[96] Judicael Aubry. "Optimisation du dimensionnement d'une chaîne de conversion électrique directe incluant un système de lissage de production par supercondensateurs: application au houlogénérateur SEAREV". PhD thesis. École normale supérieure de Cachan-ENS Cachan, 2011.

[97] Deok-je Bang et al. "Review of generator systems for direct-drive wind turbines". In: *European wind energy conference & exhibition, Belgium*. Vol. 31. 2008, pp. 1–11.

[98] Deok-je Bang et al. "Promising direct-drive generator system for large wind turbines". In: *2008 Wind Power to the Grid-EPE Wind Energy Chapter 1st Seminar*. IEEE. 2008, pp. 1–10.

[99] PRM Brooking and MA Mueller. "Power conditioning of the output from a linear vernier hybrid permanent magnet generator for use in direct drive wave energy converters". In: *IEE Proceedings-Generation, Transmission and Distribution* 152.5 (2005), pp. 673–681.

[100] David Elwood et al. "Numerical modeling and ocean testing of a direct-drive wave energy device utilizing a permanent magnet linear generator for power take-off". In: *International conference on offshore mechanics and arctic engineering*. Vol. 43444. 2009, pp. 817–824.

[101] Ergo Kannikka and Nadia Kanwal. "Control of Overload Safety in Wind Turbines Through Blade Pitch Control Implementing Artificial Intelligence". In: *2021 International Conference on Electrical, Computer and Energy Technologies (ICECET)*. IEEE. 2021, pp. 1–6.

[102] Roxana Tiron et al. "The challenging life of wave energy devices at sea: A few points to consider". In: *Renewable and Sustainable Energy Reviews* 43 (2015), pp. 1263–1272.

[103] Brian Polagye and Jim Thomson. *Screening for biofouling and corrosion of tidal energy device materials: in-situ results for admiralty inlet, puget sound, Washington*. Technical Report. 2010. URL: `https://ir.library.oregonstate.edu/concern/technical_reports/b5644r91j`.

[104] Karin Sauer et al. "The biofilm life cycle: expanding the conceptual model of biofilm formation". In: *Nature Reviews Microbiology* 20.10 (2022), pp. 608–620.

[105] Tiina Mattila-Sandholm and Gun Wirtanen. "Biofilm formation in the industry: a review". In: *Food reviews international* 8.4 (1992), pp. 573–603.

[106] Bryan Field. "Marine biofouling and its control: history and state-of-the-art review". In: *OCEANS 81* (1981), pp. 542–544.

[107] KT Chau, Ching Chuen Chan, and Chunhua Liu. "Overview of permanent-magnet brushless drives for electric and hybrid electric vehicles". In: *IEEE Transactions on industrial electronics* 55.6 (2008), pp. 2246–2257.

[108] Federico Caricchi, Fabio Crescimbini, and O Honrati. "Modular axial-flux permanent-magnet motor for ship propulsion drives". In: *IEEE Transactions on Energy Conversion* 14.3 (1999), pp. 673–679.

[109] Xiaowei Song et al. "Commissioning of the world's first full-scale MW-class superconducting generator on a direct drive wind turbine". In: *IEEE Transactions on Energy Conversion* 35.3 (2020), pp. 1697–1704.

[110] MA Mueller. "Electrical generators for direct drive wave energy converters". In: *IEE Proceedings-generation, transmission and distribution* 149.4 (2002), pp. 446–456.

[111] H Weh. "New permanent magnet excited synchronous machine with high efficiency at low speeds". In: *Proceedings of the International Conference on Electrical Machines, 1988*. 1988.

[112] Sung-Il Kim et al. "Investigation and experimental verification of a novel spoke-type ferrite-magnet motor for electric-vehicle traction drive applications". In: *IEEE Transactions on Industrial Electronics* 61.10 (2014), pp. 5763–5770.

[113] Mohammad Kimiabeigi et al. "High-performance low-cost electric motor for electric vehicles using ferrite magnets". In: *IEEE Transactions on Industrial Electronics* 63.1 (2015), pp. 113–122.

[114] Alasdair McDonald and Nurul Azim Bhuiyan. "On the optimization of generators for offshore direct drive wind turbines". In: *IEEE Transactions on Energy Conversion* 32.1 (2016), pp. 348–358.

[115] Elaheh Taherian-Fard et al. "Wind turbine drivetrain technologies". In: *IEEE Transactions on Industry Applications* 56.2 (2020), pp. 1729–1741.

[116] Henk Polinder et al. "Conventional and TFPM linear generators for direct-drive wave energy conversion". In: *IEEE Transactions on energy conversion* 20.2 (2005), pp. 260–267.

[117] Kun Zhao et al. "Induction motors lifetime expectancy analysis subject to regular voltage fluctuations". In: *2017 IEEE Electrical Power and Energy Conference (EPEC)*. IEEE. 2017, pp. 1–6.

[118] ER Laithwaite et al. "Linear motors with transverse flux". In: *Proceedings of the Institution of Electrical Engineers*. Vol. 118. 12. IET. 1971, pp. 1761–1767.

[119] H Weh and H May. "Achievable force densities for permanent magnet excited machines in new configurations". In: *Proc. Int. Conf. Electrical Machines*. Vol. 3. 1986, pp. 1107–1111.

[120] Bo Zhang et al. "A comparison of the transverse, axial and radial flux PM synchronous motors for electric vehicle". In: *2014 IEEE International Electric Vehicle Conference (IEVC)*. IEEE. 2014, pp. 1–6.

[121] Iago Martinez-Ocaña et al. "Transverse flux machines as an alternative to radial flux machines in an in-wheel motor". In: *The Journal of Engineering* 2019.17 (2019), pp. 3624–3628.

[122] Baoping Gan, Bingyi Zhang, and Guihong Feng. "Design and analysis of modular permanent magnet fault-tolerant motor for ship direct-drive propulsion". In: *IEEJ Transactions on Electrical and Electronic Engineering* 16.9 (2021), pp. 1260–1278.

[123] R Saou, ME Zaïm, and K Alitouche. "Optimal designs and comparison of the doubly salient permanent magnet machine and flux-reversal machine in low-speed applications". In: *Electric Power Components and Systems* 36.9 (2008), pp. 914–931.

[124] NJ Baker et al. "Developing a direct drive power take off for the mocean wave energy converter". In: *11th International Conference on Power Electronics, Machines and Drives*. IET, 2022.

[125] Kangkang Du et al. "Analysis and design of a fault-tolerant permanent magnet vernier machine with improved power factor". In: *IEEE Transactions on Industrial Electronics* 69.5 (2021), pp. 4353–4363.

[126] Dawei Li, Ronghai Qu, and Thomas A Lipo. "High-power-factor vernier permanent-magnet machines". In: *IEEE transactions on industry applications* 50.6 (2014), pp. 3664–3674.

[127] Dave Latimer. "MAGSPLIT®-a magnetic CVT". In: *The Newsletter, Business Development Manager, Magnomatics, Spring* (2014).

[128] Alexei Winter et al. "Robotic placement of high-strength permanent magnets for a wind turbine generator". In: *2021 11th International Electric Drives Production Conference (EDPC)*. IEEE. 2021, pp. 1–8.

[129] Li Ran, JR Bumby, and PJ Tavner. "Use of turbine inertia for power smoothing of wind turbines with a DFIG". In: *2004 11th International Conference on Harmonics and Quality of Power (IEEE Cat. No. 04EX951)*. IEEE. 2004, pp. 106–111.

[130] Jacobus Daniel Van Wyk and Fred C Lee. "On a future for power electronics". In: *IEEE Journal of Emerging and Selected Topics in Power Electronics* 1.2 (2013), pp. 59–72.

[131] Arindam Chakraborty. "Advancements in power electronics and drives in interface with growing renewable energy resources". In: *Renewable and Sustainable Energy Reviews* 15.4 (2011), pp. 1816–1827.

[132] Galina Mirzaeva, Khalid Imtiaz Saad, and Mohsen Ghaffarpour Jahromi. "Comprehensive diagnostics of induction motor faults based on measurement of space and time dependencies of air gap flux". In: *IEEE Transactions on Industry Applications* 53.3 (2016), pp. 2657–2666.

[133] Vincenzo Delli Colli et al. "A tubular-generator drive for wave energy conversion". In: *IEEE Transactions on Industrial Electronics* 53.4 (2006), pp. 1152–1159.

[134] DPM Cahill and B Adkins. "The permanent-magnet synchronous motor". In: *Proceedings of the IEE-Part A: Power Engineering* 109.48 (1962), pp. 483–491.

[135] Eric R Laithwaite. "Linear electric machines—A personal view". In: *Proceedings of the IEEE* 63.2 (1975), pp. 250–290.

[136] Nabeel A Mancheri et al. "Effect of Chinese policies on rare earth supply chain resilience". In: *Resources, Conservation and Recycling* 142 (2019), pp. 101–112.

[137] Jelle H Rademaker, René Kleijn, and Yongxiang Yang. "Recycling as a strategy against rare earth element criticality: a systemic evaluation of the potential yield of NdFeB magnet recycling". In: *Environmental science & technology* 47.18 (2013), pp. 10129–10136.

[138] Simon M Jowitt et al. "Recycling of the rare earth elements". In: *Current Opinion in Green and Sustainable Chemistry* 13 (2018), pp. 1–7.

[139] Md Rabiul Islam, Youguang Guo, and Jianguo Zhu. "A review of offshore wind turbine nacelle: Technical challenges, and research and developmental trends". In: *Renewable and Sustainable Energy Reviews* 33 (2014), pp. 161–176.

[140] Anoop Jassal, Henk Polinder, and JA Ferreira. "Literature survey of eddy-current loss analysis in rotating electrical machines". In: *IET Electric Power Applications* 6.9 (2012), pp. 743–752.

[141] AS McDonald, MA Mueller, and Henk Polinder. "Structural mass in direct-drive permanent magnet electrical generators". In: *IET Renewable Power Generation* 2.1 (2008), pp. 3–15.

[142] Jawad Faiz and Alireza Nematsaberi. "Linear electrical generator topologies for direct-drive marine wave energy conversion-an overview". In: *IET Renewable Power Generation* 11.9 (2017), pp. 1163–1176.

[143] Reza Jafari et al. "Linear Permanent Magnet Vernier Generators for Wave Energy Applications: Analysis, Challenges, and Opportunities". In: *Sustainability* 14.17 (2022), p. 10912.

[144] Danilo Riquelme et al. "Impact of static and dynamic eccentricity on the performance of permanent magnet synchronous machines with modular stator core". In: *2021 IEEE Energy Conversion Congress and Exposition (ECCE)*. IEEE. 2021, pp. 3775–3780.

[145] CA Oprea et al. "Permanent magnet linear generator for renewable energy applications: Tubular vs. four-sided structures". In: *2011 International conference on clean electrical power (ICCEP)*. IEEE. 2011, pp. 588–592.

[146] Irina A Ivanova et al. "Simulation of wave-energy converter with octagonal linear generator". In: *IEEE Journal of Oceanic Engineering* 30.3 (2005), pp. 619–629.

[147] Nick J Baker et al. "Marinisation of direct drive generators for wave energy converters". In: *11th International Conference on Renewable Power Generation-Meeting net zero carbon (RPG 2022)*. Vol. 2022. IET. 2022, pp. 23–27.

[148] Joseph Prudell et al. "A permanent-magnet tubular linear generator for ocean wave energy conversion". In: *IEEE Transactions on Industry Applications* 46.6 (2010), pp. 2392–2400.

[149] NP Gargov and AF Zobaa. "Multi-phase air-cored tubular permanent magnet linear generator for wave energy converters". In: *IET Renewable Power Generation* 6.3 (2012), pp. 171–176.

[150] M Mueller and NJ Baker. "A low speed reciprocating permanent magnet generator for direct drive wave energy converters". In: *2002 International Conference on Power Electronics, Machines and Drives* (2002).

[151] Víctor Ballestín-Bernad, Jesús Sergio Artal-Sevil, and José Antonio Domínguez-Navarro. "A review of transverse flux machines topologies and design". In: *Energies* 14.21 (2021), p. 7173.

[152] Nick J Baker et al. "Experimental comparison of two linear machines developed for the free piston engine". In: *The Journal of Engineering* 2019.17 (2019), pp. 4406–4410.

[153] Gianmario Pellegrino and Chris Gerada. "Modeling of flux reversal machines for direct drive applications". In: *Proceedings of the 2011 14th European Conference on Power Electronics and Applications*. IEEE. 2011, pp. 1–10.

[154] MR Harris, GH Pajooman, and SM Abu Sharkh. "The problem of power factor in VRPM (transverse-flux) machines". In: *1997 Eighth International Conference on Electrical Machines and Drives* (1997).

[155] TW Ching, KT Chau, and Wenlong Li. "Power factor improvement of a linear Vernier permanent-magnet machine using auxiliary DC field excitation". In: *IEEE Transactions on Magnetics* 52.7 (2016), pp. 1–4.

[156] Lewis Chambers et al. "Comparison of the Flux Reversal and Vernier Hybrid Machine for a Hinged Wave Energy Converter". In: *2021 IEEE Energy Conversion Congress and Exposition (ECCE)*. IEEE. 2021, pp. 4016–4023.

[157] Rieghard Vermaak and Maarten J Kamper. "Construction and control of an air-cored permanent magnet linear generator for direct drive wave energy converters". In: *2011 IEEE International Electric Machines & Drives Conference (IEMDC)*. IEEE. 2011, pp. 1076–1081.

[158] Nick J Baker, MA Mueller, and E Spooner. "Permanent magnet air-cored tubular linear generator for marine energy converters". In: *Second International Conference on Power Electronics, Machines and Drives (PEMD 2004)*. Vol. 2. IET. 2004, pp. 862–867.

[159] AS McDonald, MA Mueller, and JG Jeffrey. "Development of a novel permanent magnet linear generator topology for direct-drive wave energy converters". In: *2008 4th IET Conference on Power Electronics, Machines and Drives*. IET. 2008, pp. 81–85.

[160] Yinye Yang et al. "Thermal management of electric machines". In: *IET Electrical Systems in Transportation* 7.2 (2017), pp. 104–116.

[161] Richard Crozier and Markus Mueller. "Integrated structural and electromagnetic design of direct-drive linear machines for wave energy". In: *IET Renewable Power Generation* 6.3 (2012), pp. 137–148.

[162] AS McDonald et al. "Integrated design of direct-drive linear generators for wave energy converters". In: *2009 International Conference on Sustainable Power Generation and Supply*. IEEE. 2009, pp. 1–7.

[163] Markel Penalba and John V Ringwood. "A review of wave-to-wire models for wave energy converters". In: *Energies* 9.7 (2016), p. 506.

[164] Jonas Sjolte. "Marine renewable energy conversion: Grid and off-grid modeling, design and operation". PhD thesis. Norges teknisk-naturvitenskapelige universitet, 2014.

[165] Rico Hjerm Hansen. "Design and control of the powertake-off system for a wave energy converter with multiple absorbers". PhD thesis. Aalborg Universitet, 2013.

[166] Elisabetta Tedeschi et al. "Effect of control strategies and power take-off efficiency on the power capture from sea waves". In: *IEEE Transactions on Energy Conversion* 26.4 (2011), pp. 1088–1098.

[167] Feng Wu et al. "Modeling and control of AWS-based wave energy conversion system integrated into power grid". In: *IEEE Transactions on Power systems* 23.3 (2008), pp. 1196–1204.

[168] Adrian O'Sullivan and Gordon Lightbody. "Wave to wire power maximisation from a wave energy converter". In: *Proceedings of the European Wave and Tidal Energy Conference* (2015).

[169] Markel Penalba and John V Ringwood. "Systematic complexity reduction of wave-to-wire models for wave energy system design". In: *Ocean Engineering* 217 (2020), p. 107651.

[170] *Mocean Blue X concept art*. Mar. 2023. URL: `https://www.mocean.energy/wave-energy-converter`.

[171] J Cameron McNatt and Christopher H Retzler. "The performance of the Mocean M100 wave energy converter described through numerical and physical modelling". In: *International Marine Energy Journal* 3.1 (2020), pp. 11–19.

[172] Yuting Gao et al. "Consequent-pole flux-reversal permanent-magnet machine for electric vehicle propulsion". In: *IEEE Transactions on Applied Superconductivity* 26.4 (2016), pp. 1–5.

[173] Byungtaek Kim and Thomas A Lipo. "Operation and design principles of a PM vernier motor". In: *2013 IEEE Energy Conversion Congress and Exposition*. IEEE. 2013, pp. 5034–5041.

[174] Jamie G Washington, Glynn J Atkinson, and Nick J Baker. "Reduction of cogging torque and EMF harmonics in modulated pole machines". In: *IEEE Transactions on Energy Conversion* 31.2 (2016), pp. 759–768.

[175] Infologic Design. *MagNet*. 2021. URL: https://www.infologicdesign.co.uk/magnet.

[176] Yubo Yang et al. "Analytical Electromagnetic Performance Calculation of Vernier Hybrid Permanent Magnet Machine". In: *IEEE Transactions on Magnetics* 54.6 (2018), pp. 1–12. DOI: 10.1109/TMAG.2018.2818069.

[177] EPSRC. *MU-EDRIVE*. 2021. URL: https://gow.epsrc.ukri.org/NGBOViewGrant.aspx?GrantRef=EP/V040758/1.

[178] EPSRC. *USMART - smart dust for large scale underwater wireless sensing*. 2017. URL: https://gow.epsrc.ukri.org/NGBOViewGrant.aspx?GrantRef=EP/P017975/1.

[179] National Network of Regional Coastal Monitoring Programmes. *NNRCMP Homepage*. 2023. URL: http://coastalmonitoring.org.

[180] S Nallayarasu and Kirti Bairathi. "Hydrodynamic response of spar hulls with heave damping plate using simplified approach". In: *Ships and Offshore Structures* 9.4 (2014), pp. 418–432.

[181] WAMIT, inc. *WAMIT*. 2021. URL: https://www.wamit.com.

[182] Lei Huang et al. "Design and experiment of a direct-drive wave energy converter using outer-PM linear tubular generator". In: *IET Renewable Power Generation* 11.3 (2017), pp. 353–360.

[183] Maxime R Dubois and Henk Polinder. "Comparison between TFPM generator with toothed rotor and Conventional PM Synchronous generator for direct-drive wind turbines". In: *Proceedings of ICEM 2004*. Institute of Mechatronics and Information Systems, 2004, p. 228.

[184] Azza A Faiad and IA Gowaid. "Linear generator technologies for wave energy conversion applications: A review". In: *2018 53rd International Universities Power Engineering Conference (UPEC)*. IEEE. 2018, pp. 1–6.

[185] Mohammad Abdul Hakim Raihan. "Development of high force dense linear generators for wave energy converters". PhD thesis. Newcastle University, 2020.

[186] Mohammad AH Raihan et al. "Development and testing of a novel cylindrical permanent magnet linear generator". In: *IEEE Transactions on Industry Applications* 56.4 (2020), pp. 3668–3678.